

Magmatic processes by U-Th disequilibria method.

Comparison of two Andean systems:

El Misti Volcano (S. Peru) and Taapaca Volcanic Center (N. Chile).

Dissertation

zur Erlangung des Doktorgrades

der Mathematisch-Naturwissenschaftlichen Fakultäten

der Georg-August-Universität zu Göttingen

vorgelegt von

Aneta Kiebała

aus Rzeszów (Polen)

Göttingen 2008

D 7

Referent: Prof. Dr. G. Wörner

Korreferent: Prof. Dr. B. Hansen

Tag der mündlichen Prüfung: 03.04.2008

Abstract

El Misti Volcano (South Peru) and Taapaca Volcanic Complex (North Chile) both located in the Central Andean Volcanic Zone in South America have been studied in order to place constraints on the evolution of their distinct magmatic systems. Although both volcanic centers are located in similar general geological settings (CVZ) they show very contrasting magmatic evolution. El Misti volcano is a single stratocone (<112ka, Thouret et al., 2001), which erupted magmas ranging between 58 and 68wt% SiO₂. By contrast Taapaca is a long-lived dome cluster (1.27 Ma to Holocene, Wörner et al., 2004a; Clavero et al., 2004), which erupted magmas ranging between 60 and 71wt% SiO₂. However the majority (69%) of samples fall into the narrow range of 63 to 67wt% SiO₂.

The radiogenic Sr-isotopic compositions are slightly higher for El Misti (0.7075-0.7078) than for Taapaca (0.7063-0.7067). Pb isotopic compositions are different, most likely reflecting the composition of assimilated continental crust (e.g. ²⁰⁶Pb/²⁰⁴Pb=17.68-17.84 for El Misti and 18.10 for Taapaca (Mamani et al., 2004)).

The two studied volcanic systems are very different in their U-Th disequilibria measured by TIMS. In fact Th/U isotopic compositions define end-members of the whole of CVZ: Misti volcanic rocks have very low (²³⁰Th/²³²Th) activity ratios of 0.33-0.5 possibly the lowest measured in volcanic rocks. (²³⁰Th/²³²Th) at Taapaca is 1.02-1.36 for dacites and at upper bound of CVZ. The mafic inclusions at Taapaca (basaltic andesites) have lower (²³⁰Th/²³²Th) values of 0.66. Misti rocks are also enriched in ²³⁸U with surprisingly high (²³⁸U/²³⁰Th) of up to 1.4 one of the highest measured of CVZ. Samples from Taapaca system all fall close to the equiline with (²³⁸U/²³⁰Th)=0.93-1.06.

The major elements of erupted rocks at El Misti and Taapaca volcanic centers point to mineral fractionation (10.08 %) of olivine and orthopyroxene deep in the mantle followed by assimilation and fractionation processes in the crust.

The radiogenic isotopic data suggest that magmas at both volcanoes suffered significant up to 15% (El Misti) and 10% (Taapaca) of assimilation during the passage through 70km continental crust. However the source of the magmas at El Misti and at Taapaca was contaminated as well. Source contamination at El Misti magma is controlled by the Arequipa crust and fluids, while at Taapaca additional role play sediments.

Taapaca evolved over the long time and this is also shown by the absence of significant U-series disequilibria in the youngest rocks. Taapaca system stayed undisturbed with respect to the U/Th for up to 350ka and potential enrichment from fluid addition decayed away over hundreds of thousand years. Taapaca is thus a “slow“ system where magma evolution may take more than hundred thousand years. In contrast at El Misti it is surprising to still see such of U-isotopic enrichment that usually is attributed in arc volcanism to slab-fluids in the mantle wedge. Additionally melting, ascent, assimilation and eruption all occurred within 350ka as estimated by U-series isotopes.

The differences in compositions and thus the rates and styles of magma evolution between the two Andean volcanic centers can be caused by different magma production rates in the mantle, different depth of magma evolution, different composition of the crust and different structure of the basement. The structure of basement may cause an easy and rapid magma

ascent resulting in frequent magma mixing events and large range of erupted compositions (like at El Misti) or make conditions at which magma is stored and evolves at depth in relatively undisturbed reservoirs for longer time (Taapaca).

Content:

Abstract	3
1 Introduction	7
1.1 Timescales of magmatic processes	7
1.2 Geological background	10
1.2.1 The Andes	11
1.2.2 Central Andean evolution	12
1.2.3 The CVZ	13
1.3 Principles and methods employed	15
1.3.1 U-series disequilibrium	15
1.3.2 The radioactivity background	16
2 El Misti Volcano, South Peru	17
2.1 Geologic and eruptive history	17
2.2 Basement under El Misti volcano	18
2.3 Sampling	18
2.4 Geochemistry – major and trace elements	25
2.4.1 Spider diagram	26
2.4.2 Rare earth elements	27
2.4.3 Sr, Nd, Pb isotopes	27
2.5 U-Th isotopes	28
3 Taapaca Volcanic Complex, North Chile	30
3.1 Geological settings	30
3.2 Basement under Taapaca Volcanic Complex	31
3.3 Sampling	31
3.4 Geochemistry	38
3.4.1 Major and trace elements	38
3.4.2 Spider	39
3.4.3 Rare earth elements	40
3.4.4 The isotopes (Nd, Sr, Pb)	40
3.5 Ar-Ar data	41
3.6 U-Th isotopes	42
3.6.1 Whole rock data	42
3.6.2 Mineral separates	43
4 Discussion	46
4.1 Whole rock U-Th signatures of El Misti, Taapaca and other CVZ volcanics	46
4.2 The U-Th fractionation in subduction zones as recent event	47
4.3 Crustal involvement	48
4.4 Fluid addition	49
4.5 Components involved in magma genesis at the CVZ.	49
4.5.1 Mass balance calculation	54
4.5.2 Magma petrogenesis - major elements	57
4.5.3 Magma genesis - trace elements	61
4.5.4 Magma genesis – isotopes	64
4.6 Timescales of magmatic processes at Taapaca	65
4.7 Constrains on timescales of magmatic processes at El Misti	66
4.8 Different magmatic systems	66
5 Conclusions	68
6 Appendix	71
6.1 Analytical techniques	71

6.1.1	Sample preparation.....	71
6.1.2	Whole rock powders.....	71
6.1.3	Mineral separation.....	71
6.2	XRF analyses.....	71
6.3	ICP-MS analyzes.....	72
6.4	Procedure for U-Th isotopes	72
6.4.1	Chemical separation	73
6.4.2	TIMS analyzes.....	73
6.5	Ar/Ar analyzes.....	74
6.6	Modelling	75
7	Literature	78
Acknowledgements		

1 Introduction

Lava and pyroclastic flows, lahars and debris flows resulting from sector collapse and tephra falls are the most common hazards associated with the Andean volcanoes.

The rate of volcano construction, as well as how and when magmatic processes generate explosive eruption or edifice collapse, is one part of better predicting hazards, which are concentrated in subduction zones. Ascent rates, crustal storage and differentiation times characterize the kind of arc magmatic processes. The contemporaneous and closely spaced occurrence of two different types of volcanic edifices is an interesting feature, which allows placing constraints on the size of magma reservoirs under the volcanic centers as well as on rates of ascent and magmatic activity. Effusive and explosive eruption characterizes activity of El Misti volcano, which is located about 20km away from Arequipa, the second largest city of Peru. A large eruption is the most hazardous for Arequipa citizens due to the canyon and gullies, which are directed toward the city. The last big eruption occurred about 2000 years ago (Thouret et al., 2001). However, the fumarolic activity suggests that magmatic system is still potentially active.

The second studied centre, the Taapaca Volcanic Complex, consists mostly of lava flows and block and ash flows. The last eruption took place about 8000 years ago; however, the growing dome in the inner crater also inclines the potential of eruption. The activity centre of the Taapaca edifice moves toward the south since the beginning of the volcanic history, where the city of Putre is located. Therefore similarly to El Misti, it constitutes potential hazard to the citizens of that area.

The increasing interest in timescales of magma formation, transfer and storage beneath volcanoes provide important insights into the physical processes of magma formation and may ultimately allow for better prediction of eruptive hazards.

1.1 Timescales of magmatic processes

Magmatic processes and their timescales are key problems for understanding the nature of volcanic products and the type of volcanic activity. This study is dedicated to processes and timescales of subduction-related volcanic activities at a convergent plate margin, the South American Andes. The goal of this work is to study two contrasting Andean volcanic centers: El Misti (South Peru) and Taapaca (North Chile) both located in the Central Volcanic Zone of the Andean Cordillera to gain insight into the processes and their time scales of recent calc-alkaline magma genesis and evolution in the CVZ. The focus of this work on the Central Volcanic Zone (CVZ) is unusual due to its unique end-member tectonic settings, very thick crust (70km) and magma crust interaction.

In the Andean volcanic chain, subduction occurs beneath the South American plate along the entire Mountain Range. Volcanic centres along the active Andean continental margin represent variable styles and patterns of igneous evolution. Eruption patterns and eruptive styles of active and potentially dangerous volcanoes seem to change in the course of tens to thousands of years (e.g. Parinacota, Bourdon et al. 2000). Important questions, which are still to be answered, concern the evolutionary stages of individual Andean volcanoes, their transitions from young to mature systems and the time of achieving particular stages of magma evolution. Studies on timescales of individual processes including magma generation in the mantle, magma ascent through the mantle wedge, storage in lower and upper crustal reservoirs (magma chambers), fractional crystallization and assimilation of wall rocks,

tapping/replenishment of magma chambers, magma-mixing and eruption patterns give significant clues for quantitative modelling of magma evolution.

Such timescales of magmatic processes can be studied by several methods, which give different kinds of age information: absolute and relative ages. The first can be estimated by short-lived U-series isotope compositions of whole rocks and mineral separates (e.g. Condomines et al., 2003; Turner et al., 2003). The relative ages are studied by mineral in situ analyses of major and accessory mineral phases with trace element and Sr isotope profiles in phenocrysts (e.g. Gerlach and Grove 1982; Nakamura, 1995, Zellmer et al., 1999; Ginibre et al., 2002; Costa et al., 2003; Zellmer et al., 2003b), and crystal size distributions (CSD; e.g. Marsh, 1988, Higgins 1996a, 1996b, 2000; Turner et al., 2003c). The present work focuses on the first approach and tries to reveal the evolution of two distinct volcanic edifices of the Andean volcanic arc from their source in the mantle to their eruption utilising disequilibrium within the short-lived U-series.

The principle mechanism that produces ^{238}U - ^{230}Th disequilibrium in magmas is the melting process in the mantle wedge. The time needed for such melt generation is thought to be similar in magnitude to the half life of ^{230}Th (Peate and Hawkesworth 2005) so much of the information of melt generation comes from application of short-lived U-series disequilibrium method.

It is commonly believed that the individual components of source region (peridotite, mafic slab, sediment-derived slab sections) are in secular equilibrium and therefore the initial activity ratios of the source will be known. Different physical models of melt generation include “batch melting” (melt produced stays in equilibrium with the residual solids until it is extracted) and “fractional melting” (amounts of melt are extracted as soon as they are produced). These models treat U series nuclides like any other trace elements, and disequilibrium between these nuclides is attributed to net element fractionation due to differences in partitioning between melt and residual solid.

However, chemical modification of the source, e.g. fluids expelled from a slab component to the peridotite may cause disequilibrium in the bulk source. At subduction zone settings, addition of fluids is supposed to be the major trigger of melting; these fluids are supposed to be U-enriched relative to Th. Therefore, subduction zones probably represent the most complex melting environment and the primary controls on melting are poorly established. In these tectonic settings melt generation are controlled largely by the amount and composition of the slab derived fluid and to a minor degree by the thermal structure of the mantle wedge. Thus, the slab-derived fluids play a major role in generating subduction zone magmas. This fluid introduction dominates the extent and the sense of disequilibria between U series nuclides. A comprehensive recent review of the origin and interpretation of U series disequilibria in the subduction zone environment is presented by Turner et al. (2003, 2003c). For the interpretation of U series disequilibrium data measured in erupted subduction-related magmas it is of crucial importance to distinguish between elemental fractionation during mantle source enrichment, the partial melting process, and fractional crystallisation/contamination. In the latter process, U series disequilibria can be used to study the timescales of crystallisation and differentiation processes utilising U-series isotope composition on separated minerals and whole rocks.

The crystal residence ages in the melt of tens of years up to 100years have been indicated by the Sr isotope profiles in phenocrysts. The residence time of plagioclase from dacitic rocks based on Sr profiles of 100 years and 450 years have been indicated by Zellmer et al., 1999

Modelling of Mg-Fe diffusion in olivine suggest that the crystals have a residence time of 13-150 days, which is in accordance with Li isotope profiles (Parkinson et al., 2007). However it is important to keep in mind that diffusion profiles on minerals bring time information of how long the crystal spent in particular temperature, but it does not give absolute crystallization age information.

The present data for magma differentiation are consistent with long time scales 10^5 years for basanitic magmas deep in the crust, and with very much shorter periods of up to a few thousand years at shallower depths. In contradiction to this statement, short magma residence time has been reported for basaltic volcanoes from oceanic islands (Marion, Mauna Kea, and Piton de la Fournaise; Newman et al., 1984; Condomines et al., 1988). The samples have nearly constant ratios of ($^{230}\text{Th}/^{238}\text{U}$) and ($^{230}\text{Th}/^{232}\text{Th}$) suggesting short residence time of magmas in continuously replenished magma chambers. One of the pioneering studies on Etna applying ^{230}Th - ^{226}Ra systematics to magma chamber processes suggests that magma differentiation from hawaiites to mugearites and estimated magma residence time in a steady-state deep reservoir (~20km depth) took place over <1500yr (Condomines et al., 1995). Crystallization ages determined on ^{230}Th - ^{226}Ra and model calculation for 1978 AD lavas of Ardoukoba volcano, Djibouti, seem to be 1880 and 870 years for open- and closed-system models (Viegiere et al., 1999). Other studies on basaltic eruptions Lanzarote in Canary Islands (Sigmarsson et al., 1998), Karthala volcano from Comores (Claude-Ivanaj et al., 1998), and Asal Rift (Vigier et al., 1999) negligible transfer times of the magma. However, the whole rock ^{226}Ra - ^{230}Th data suggest that the final feldspar-dominated differentiation to the most evolved phonolites took place within a thousand years before eruption. For three lavas from Tenerife significant ^{226}Ra excesses, which span wide range of composition from 9 to 2 wt% MgO (Lundstrom et al., 2003) require much shorter time than suggested by ^{230}Th - ^{238}U system, implying that ^{230}Th - ^{238}U disequilibria could have been affected by open system processes. In open system processes, the times span of differentiation will be overestimated because the reduction in measured disequilibrium in the evolved magmas is due to combination of radioactive decay and addition of material in secular equilibrium. Such an example has been suggested for Socorro Island, Mexico (Bohrson and Reid, 1998). The rhyolites were related to trachytes by fractional crystallization, but systematic variations in $^{87}\text{Sr}/^{86}\text{Sr}$ also indicate assimilation of basement rocks, thus suggesting a maximum time span of 40 to 50 kyr (Bohrson and Reid, 1998).

Variations in U-series nuclides reflect different degrees of magma differentiation. The more mafic magmas fractionate at greater depths and the rates of fractional crystallization were higher in the more evolved magmas. This is explained by a cooling model, in which a large volume of primitive magma at deep crustal levels needs longer cooling time than a smaller body of differentiated magma at shallower depths in the crust: Bourdon et al. (1994) in the study on the Laacher See suggests about 100kyr for differentiation of phonolite from parental basanite; at Agua de Pao, Sao Miguel (Azores), need 80kyr to produce trachytic from parental alkali basaltic magmas (Widom et al., 1992); Reagan et al., 1992 inferred a time span of <150ka for the differentiation from basanite to phonolite beneath Mt Erebus in Antarctica. Whole rock isochrones, although rare, show that differentiation can also occur shortly before eruption (Laacher See phonolites Bourdon et al., 1994, Vico ultrapotassic volcanics, Longonot volcano, Kenya trachyte; Evans 1999).

The ages of crystals can be determined based on different methods. However, it is critical to establish the extent of which the compositions of phenocrysts are consistent with crystallization from the host magma, or whether they are xenocrystic in origin. U-Th isotope

studies on zircons from Long Valley indicate pre-eruption residence times of 100ky (Reid et al., 1997). Zircons from Taupo rhyolites have U/Th disequilibria implying pre-eruptive ages of 10ky (Charlier et al., 2000). The Olkaria peralkaline rhyolites of the Kenya Rift Valley point to residence times of 10^3 - 10^5 years (Heumann et al., 1995; Black et al., 1997). The U-Th –mineral-whole-rock isochrones from basaltic andesites erupted from the Soufriere volcano on St. Vincent in the Lesser Antilles arc yield consisted ages of 46-77 ka (Heath et al., 1998b). The scatter of the data around “isochrones” implies that they may represent a mixture of crystals of various ages. However, some of the crystals analyzed would appear to be tens of thousands of years old.

One other way to place constraints on magma storage time is the analysis of minerals present as phenocrysts in volcanic rocks. The principle of the isochrone diagram allows calculation of a meaningful crystallization age and requires that all the minerals have crystallized in a short time interval compared to ^{230}Th half-life, that initial Th equilibration is given and the system remains closed after crystallization. Therefore, U-Th mineral isochrones interpretations can be complicated. Some U-Th isochrones indicate crystallization ages, which are very similar to eruption ages, while in other cases crystallization ages are much older than known eruption ages (10^4 - 10^5 years older). Especially in silicic magma chambers, accessory minerals can be stored for long periods of time ($>10^5$ years, Long Valley, Davies et al., 1994).

1.2 Geological background

The two studied volcanic centers: El Misti volcano ($16^{\circ}17'44''\text{S}$; $71^{\circ}24'30''\text{W}$) and Taapaca Volcanic Complex ($18^{\circ}06'00''\text{S}$; $69^{\circ}30'00''\text{W}$) are located in the Central Volcanic Zone of the Andean Cordillera in South America Fig 1-1. The studied area is located in the southern Peru (El Misti) and northern Chile (Taapaca Volcanic Complex), which correspond to the Central Andes (5° - 33°) in particular to the Western Cordillera of the Central Volcanic Zone. In the following sections, information on the geology and petrology of the studied area is presented along with information on some relevant volcanological principals.

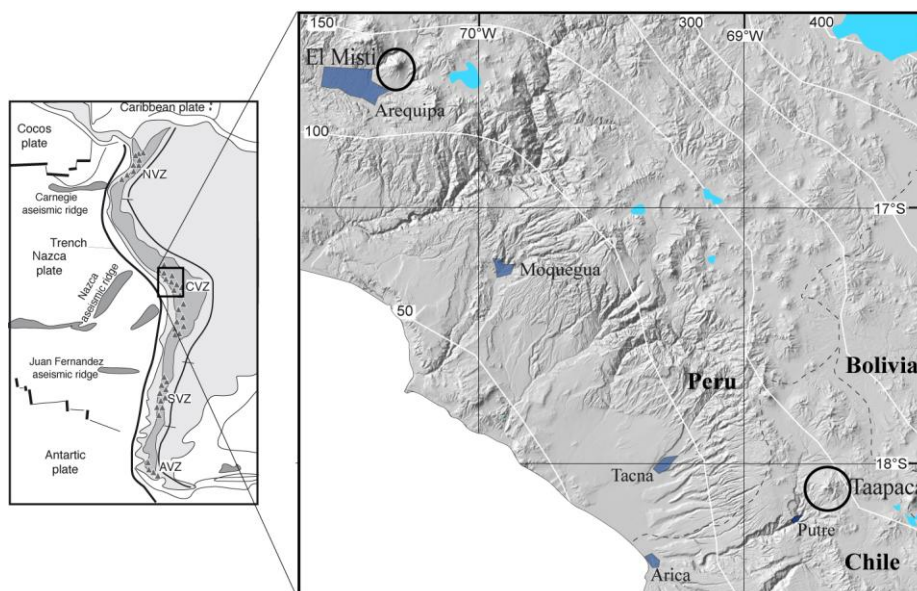


Fig. 1-1 Map of South America and the CVZ with locations of El Misti and Taapaca volcanic centers.

1.2.1 The Andes

The Andes represent a mountain chain, which extends for about 9000 km along the western edge of the South American plate from Colombia to the Chile triple junction around 46°S. This longest and one of the highest mountain ridges in the world (elevations up to 7000m above sea level) represent a non-collisional orogen (Ramos, 1999) located at a convergent plate margin. The most important features that define the Andean orogen are: the subducting Nazca plate with associated sediment free trench, the present active volcanic arc and the fold-and-thrust belt in the foreland. The volcanism occurs here since Paleozoic and Mesozoic to the present. Since Cenozoic times (20-25 Ma) it has a calc-alkaline character and the recently observed volcanism started in the Jurassic due to the eastward subduction of the Farallon-Nazca plate under the continent of South America (Wörner et al., 2000). Since that time, the magmatic arc migrated towards the east.

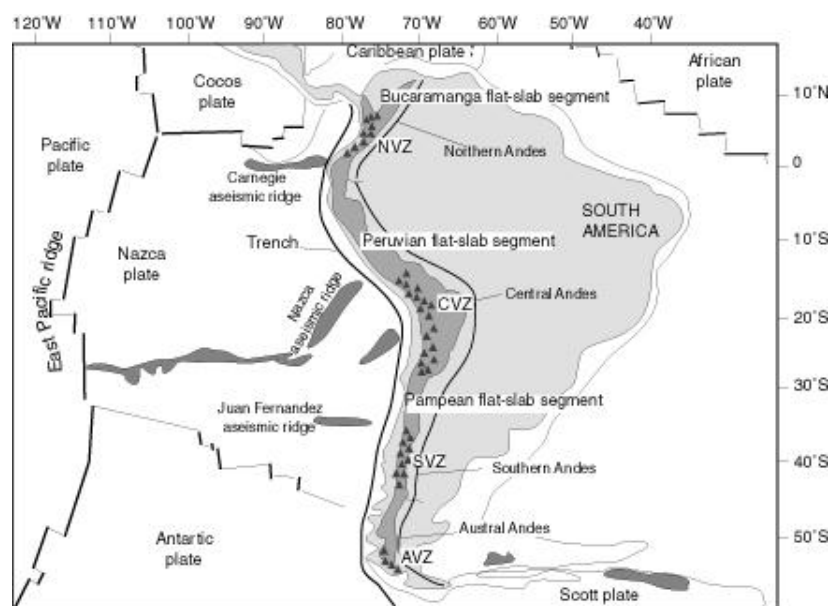


Fig. 1-2 Plate-Tectonic settings of the Andes (based on compilations from Wörner et al., 1988, Stern and Kilian 1996, Ramos 1999, Stern 2004).

Segmentation in the Nazca plate with different convergence direction and dipping angle of the slab caused N-S aligned segmentation of the Andean volcanic chain. These segments with distinct pre-Andean basement ages, Mesozoic and Cenozoic geologic evolution, crustal thickness, structural trends and active tectonics and volcanism form the Andean Cordillera. Therefore, simple division into: Northern, Central, and Southern Andes has been adopted in order to characterize the different regions:

The Northern Andes (10°N-3°S) were formed by Mesozoic and Cenozoic collision of terranes prior to the present Andean-type setting (Bosch and Rodrigues, 1992).

The Central Andes (3°S-33.5°S) are characterized by long history of subduction and volcanic arc activity (Sèbrier and Soler, 1991; Isacks, 1988; Allmendinger et al., 1997). Above the 30° eastward dipping down-going slab (Barazangi and Isacks 1976; Cahill and Isacks 1992), the surface morphology is characterized by active volcanic arc in the Western Cordillera, a broad high plateau (Altiplano in the north and Puna in the south), and active eastward verging foreland belt.

The Southern Andes (33.5°S-46.5°S) show closing of back-arc oceanic basin (Ramos and Kay, 1992; Gorrington et al., 1997). The southern Andes are built on Paleozoic or older ensialic crust and at present are dominated by near orogen-orthogonal shortening (Mpodozis and Ramos 1990, Herve et al., 2000). In the Southern Andes, the Coastal Cordillera is separated by the Central Valley from the Main Andean Cordillera and volcanoes occur in the Main Cordillera.

Austral Andes (49°S-56°S) are distinguished by some authors from the SVZ, they might be seen as separated by a small inactive gap (from 46°-49°S) Stern (2004).

1.2.2 Central Andean evolution

Based on early plate tectonic models (e.g. Mitchell and Reading 1969), the Central Andes have been considered as the type example of an active continental margin and its over-thickened crust and high plateau as typical example for Cordilleran-type orogeny. The volcanic arc and plateau dominates the present form of continental margin. The Andean crust records at least 600 Ma of history as the leading edge of the South American continent. However, relicts from the 2Ga history of the western part of South American craton are present in the basement (Loewy et al., 2004).

The outcrops of Proterozoic to early Paleozoic rocks are exposed along the present-day Andean margin of southern Peru, western Bolivia and northern Chile. The three most important of them are: The Arequipa Massif (southern Peru), the Equistos de Belén (northern Chile) and Co. Uyarani (south-western Bolivia) (Mamani 2006). The isolated exposures of the basement belong to a single basement block (Arequipa-Antofalla Basement) with multiple domains, which were not derived from Amazonia but rather accreted onto it during the 1.0 Ga Sunsás Orogeny (Loewy et al., 2004). Two models are proposed for the development of Arequipa-Antofalla basement:

1. The Arequipa-Antofalla basement as allochthonous block in respect to Amazonia, which was accreted to the pre-Andean margin (Coira et al., 1982; Nur and Ben-Avraham, 1982; Ramos, 1988; Dalziel, 1992, 1993; Balburg and Hevré, 1997).
2. Arequipa-Antofalla basement as par-autochthonous material with respect to Amazonia, emplaced along transcurrent faults (Sadowski and Bettencourt, 1996; Tosdal, 1996).

The Andean chain borders with the Caribbean Plate in the north, Nazca and Antarctic Plate in the west and the Scott Plate in the south. Five distinct segments with shallowly and steeply dipping Benioff zones based on spatial seismological variations have been distinguished (Baranzangi and Isacks, 1976). Four of these segments are associated with recent volcanic activity due to steeply (25-30°) dipping subduction (Thorpe et al., 1982) Fig 1-2:

- a. The Northern Volcanic Zone- NVZ (5°N-2°S)
- b. The Central Volcanic Zone-CVZ (16°S-28°S)
- c. Southern Volcanic Zone-SVZ (33°S-42°S)
- d. The Austral Volcanic Zone-AVZ (47°S-54°S).

The segments with absent volcanic activity are characterized by a shallow dip (5-10°) of the descending plate and correspond to the segments of Bucaramanga (north of 5°N), Peruvian (5-14°S) and Pampean (28°-33°S).

1.2.3 The CVZ

Miocene to recent volcanism in the CVZ occurs in a region of exceptionally thick crust (60-80km; Baranzangi and Isacks 1976, Cahill and Isacks 1992, Beck and Zandt 2002) of mostly Proterozoic to Paleozoic age (Shackleton et al. 1979, Barreiro et al. 1984; Damm et al 1986, 1990). The highest peak of convergence occurred in Late Oligocene, and since that time deceleration of convergence took place. It was also a phase of major continental deformation and initiation of Andean growth; the overthickened crust of the CVZ has probably resulted from extreme tectonic shortening through foreland thrusting and mid-crustal imbrication during the last ca. 15 Ma (Isacks, 1988, Allmendinger 1990).

Today, the plates are moving at convergence rate of 61 ± 3 mm/year and azimuth of $79 \pm 4^\circ$ (estimation based on space geodetic data at southern Peru latitude, Norabuena et al., 1998) and nearly perpendicular in northern Chile (Pilger 1984, Pardo-Casas et al., 1987). Additionally, a < 8 km deep sediment free Peru-Chile trench characterizes the subduction zone of the CVZ (16° - 28°). The modern volcanic arc is located 250-300 km east from the trench (Thornburg et al. 1987) and 120-130 km above the Wadatti-Benioff plane. Geophysical properties suggest partial removal of the mantle lithosphere beneath the active volcanic arc and hot asthenospheric material filling the gap between the crust and subducting plate (Whitman et al 1996; Beck and Zandt 2002). The recent geophysical data suggest that hydration of mantle peridotite may change the petrophysical (elastic) properties to crustal values (Giese et al. 1999). It is also proposed that a thin lithospheric mantle lid is present under the crust of Western Cordillera (Baumont et al. 2001).

The CVZ (16° S to 28° S, Thorpe et al., 1982) includes 44 active volcanic edifices and more than 18 active minor centers or fields and at least 6 potentially active Quaternary large silicic ignimbrite centers or caldera systems (De Silva, 1989; De Silva and Francis, 1991). The volcanic edifices comprise a large variety of volcanic structures (composite cones, cones dominated by pyroclastic deposits or lava flows, dome clusters) and type of activity:

1. Short life (< 0.5 Ma) andesite-dacite stratocones with symmetrical shape and central vent.
2. Long-lived clusters (> 0.5 Ma) dacitic domes with pyroclastic aprons. Lava compositions resulting in low-input, low-output of monotonous compositions are thermally buffered. Magma interaction is recorded in minerals showing complex compositional textures.

Active volcanism in the CVZ is mostly characterized by large composite volcanoes which reach 2-3 km in structural height and lifetime of 0.8-0.6 Ma but sometimes even up to several Ma.

1.2.3.1 Basement under the CVZ

The volcanic arc is built on upper crustal basement, which consists of Mesozoic igneous and marine meta-sedimentary rocks, which overlay Cretaceous continental sediments and Cenozoic volcanic rocks. Lower to mid-crustal metamorphic basement domains occur locally in the Precordillera belt east of the active volcanic front at the Belén (18° S) and the Quebrada Chocha ($21^\circ 5'S$) area (Damm et al. 1986) and around Arequipa (Rio Chili). The isolated upthrust basement blocks comprise a series of mica schists, gneisses, amphibolites, and associated granitoids as well as strongly serpentinised ultramafic lenses. Presumably Proterozoic protoliths (Damm et al., 1986, Damm et al., 1990) were metamorphosed and folded in the Silurian and Ordovician (415-495 Ma). The Belén metamorphic rocks are

correlated with Arequipa massif in southern Peru (Damm et al. 1986, Wörner et al., 1992a, b) as they contain some sedimentary component from the Arequipa massif. The lower crustal section in the CVZ is unknown due to its inaccessibility and the absence of xenoliths. Entenmann (1991) suggests that the composition of Precambrian and early Paleozoic metamorphic rocks from Belén and Quebrada Choja basement blocks may broadly represent the deep crustal basement beneath the Andean arc of northern Chile. For the Arequipa lower crust, probably the Mollendo series on the coast could represent the lower crust composition (Yu-Hsuan Hang 2007).

1.2.3.2 Geochemical composition of the CVZ magma

The erupted magmas of the CVZ belong mainly to the high-K calc-alkaline series with compositions ranging from rare basaltic andesites to rare rhyolites. However, the largest volume is of andesitic and dacitic composition. Some of the volcanic centers have uniform chemistry, others show wide ranges. The rocks studied here are mostly andesites and dacites. Basaltic andesites (53-55 wt% SiO₂) as well as rhyolites (69-74 wt% SiO₂) are present but rare.

The central Andean volcanics are remarkable for their anomalous isotopic ratios and high abundances of large-ion-lithophile (LIL) elements. Sr, Nd and Pb isotopic compositions are characteristic features of the CVZ volcanic processes: higher ⁸⁷Sr/⁸⁶Sr and δ¹⁸O and lower ¹⁴³Nd/¹⁴⁴Nd ratios relative to MORB plus depleted mantle are indicators for contamination by continental crust; most of the CVZ rocks show δ¹⁸O consistently displaced to higher δ¹⁸O values compared to mantle-derived lavas from oceanic regions (+5‰ to +6,5‰; Davidson et al. 1991). The isotopic variation of CVZ volcanics is characterized by: ⁸⁷Sr/⁸⁶Sr=0.7053-0.7083, ²⁰⁶Pb/²⁰⁴Pb=17.89-18.79, ²⁰⁷Pb/²⁰⁴Pb=15.58-15.66, ²⁰⁸Pb/²⁰⁴Pb=38.11-38.78, δ¹⁸O = +6.4 - +9.3‰ (Wörner et al., 1992), which are within the values documented earlier by James, 1982; Harmon et al., 1984; Wörner et al., 1988. On the basis of ²⁰⁶Pb/²⁰⁴Pb and ²⁰⁷Pb/²⁰⁴Pb differing sub-domains have been distinguished by Mamani (2006) in the CVZ region from 17.5 to 22°S.

1.2.3.3 Magma genesis in the CVZ

Principally the magmas originate in the peridotitic mantle wedge, where melting is induced due to addition of LIL-enriched fluids and maybe also melts from the dehydrating subducted plate. Magmas are likely to pond at the base of the crust and undergo fractional crystallization, assimilation and also melting of lower crustal rocks (so called MASH-Melting Assimilation Storage and Homogenisation, Hildreth and Moorbath, 1988). Deep level fractional crystallization processes lead to parental calc-alkaline magmas, and sub-sequent combined processes produce more evolved and enriched compositions.

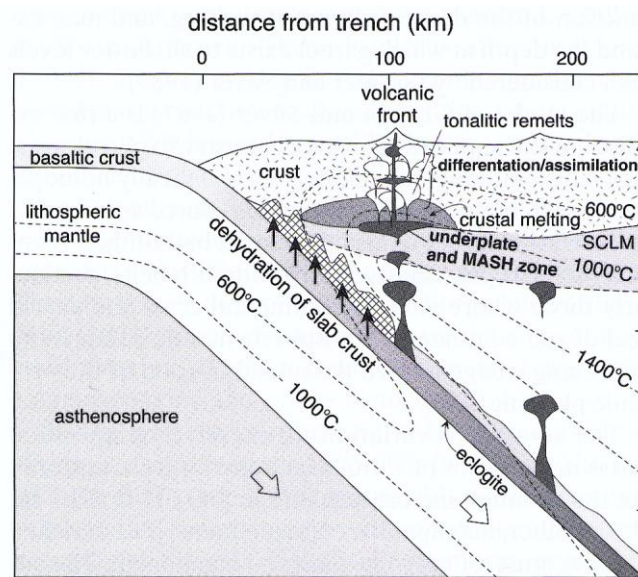


Fig. 1-3 Cross section through a subduction zone (after Winter 2003).

Physically, the volcanic activity in the CVZ can be linked to influx of hot asthenosphere into the mantle wedge thus disturbing prevailing isotherms which in turn leads to above-solidus P-T-conditions (Isack, 1988; Wörner et al., 1994; Kay et al., 1999; James and Sacks, 1999).

In summary, the andesitic to dacitic magmatism is a result of significant crustal involvement and recycling together with intra-crustal differentiation of mantle and hybrid magmas (see also Hildreth and Moorbath, 1988). Arndt and Goldstein (1989) suggested that basaltic magma stagnating at or near the base of the crust will cool, crystallize, and assimilate crustal rocks, resulting in contaminated high density cumulate rocks similar in physical properties to the mantle.

1.3 Principles and methods employed

1.3.1 U-series disequilibrium

Radioactive disequilibria of short-lived U-series nuclides in volcanic rocks are the key geochemical tracers that enable direct dating of magmatic processes for timescales ranging from 10 to 350kyr for ^{238}U - ^{230}Th systematic and 1000 to 8000 yr for ^{230}Th - ^{226}Ra systematic (Ivanovich and Harmon, 1992; Bourdon et al., 2003).

The description of U-series disequilibria is presented in many publications (Bourdon et al., 2003; Ivanovich and Harmon 1992); however, a very short introduction into the method is given below.

The first important application of U-series isotope characteristic for studying magmatic processes, was the successful dating of young (<300ka) volcanic rocks (Kigoshi, 1967; Tadeucci et al., 1967; Allégre 1968). Since these pioneering years, the U-series methods were applied in a much wider range of magmatic processes, largely with the aim to infer the timescales of magma evolution (Oversby and Gast 1968; Allégre and Condomines 1976; Capaldi et al., 1976). The early studies used alpha-spectrometry and physical counting of alpha particles, which were critically limited by the alpha decay rate (Cheng et al., 1992; McDermott et al., 1993), resulted in poor age-resolution when compared to modern analytical methods. The development of U-series nuclides by mass-spectrometry (e.g. Edwards et al., 1986; Cheng et al., 1992) has lead to considerable improvements in precision and sensitivity.

Multi-collector thermal ionization mass spectrometry (MC-TIMS) was the preferred analytical method until the recent development of inductively coupled plasma sources for the same multi-collector mass spectrometers (MC-ICPMS, Goldstein and Stirling 2002).

1.3.2 The radioactivity background

The geochronological principle of U-series dating is based on radioactive disequilibrium between parent-daughter pairs of different elements like U and Th. ^{238}U decays in steps through several intermediate elements to ^{230}Th , which decays to ^{226}Ra and in the end to ^{206}Pb . In a state of radioactive equilibrium the $(^{230}\text{Th}/^{238}\text{U})$ and $(^{226}\text{Ra}/^{230}\text{Th})$ activity ratios are equal to unity because the daughter isotopes decay at the same rate as their (grand)-parents. Any geological process which fractionates U, Th, and Ra from each other causes radioactive disequilibrium in the system. The ^{226}Ra - ^{230}Th - ^{238}U disequilibria is expressed as $(^{230}\text{Th}/^{238}\text{U})$ or $(^{226}\text{Ra}/^{230}\text{Th})$ ratios greater or smaller than unity (parentheses indicate the activity, or decay rate, of each isotope expressed as $\lambda_i N_i$, λ -decay constant, N- number of atoms). The system will then return to radioactive secular equilibrium through either net in-growth or decay of ^{230}Th and/or ^{226}Ra . The return to secular equilibrium is time-dependent and effectively takes place over approximately five times the half-life of the daughter element (for ^{230}Th , c.a. 350 ky, for ^{226}Ra c.a. 8ky). In this short time, the activities of ^{238}U and long-lived ^{232}Th are relatively constant and may be treated as stable isotopes (Allegré 1968). Therefore, it is commonly used to refer measured activities to ^{232}Th by normalization. The ^{238}U decay to ^{230}Th is formulated by decay equation:

$$(^{230}\text{Th}/^{232}\text{Th}) = (^{230}\text{Th}/^{232}\text{Th})_i (1 - e^{-\lambda_{230}\text{Th}t}) + (^{238}\text{U}/^{232}\text{Th}) (1 - e^{-\lambda_{230}\text{Th}t})$$

The graphical presentation of this equation is presented by so called equiline diagram. In the equiline diagram, the line with a slope of 1 (equiline) expresses that $^{230}\text{Th}/^{232}\text{Th}$ and $^{238}\text{U}/^{232}\text{Th}$ activities are equal. If the samples experienced strong chemical fractionation of U from Th they will lie on a horizontal line along the initial $^{230}\text{Th}/^{232}\text{Th}$, which will rotate anticlockwise around an intercept (equipoint) with time into the equiline. The slope of the rotation corresponds to the age of the sample according to the relationship: $m = 1 - e^{-\lambda_{230}\text{Th}t}$.

2 El Misti Volcano, South Peru



2.1 Geologic and eruptive history

Misti (5822 m asl) is one of seven potentially active volcanoes of South Peru. The volcano is located 17 km NE from Arequipa, the second biggest city of Peru (900 000 inhabitants) and about 3500 m above the town. Misti is situated within complex tectonic settings. The Altiplano (NE), the tectonic depression of Arequipa (SW) and two dormant volcanoes (Chachani (NW) and PichuPichu (SE)) surrounds El Misti: The three volcanoes: Chachani, El Misti, Pichu Pichu are aligned on two normal faults: N127 and NWN-SES trending normal fault and N153 (Thouret et al., 2001).

Thouret et al. (2001) presents detailed description of the volcano providing a stratigraphic framework and an overview on age and compositions of erupted materials. Wegner and Ruprecht (2003) gave the stratigraphy of the neighbouring Rio Chili canyon. Starting 112 ka ago, the eruption history of the volcano is divided into 3 stages by Ruprecht (2004) and Ruprecht and Wegner (2003), or 4 stages by Thouret et al., 2001. The age of the base of the volcano is dated at 1.2Ma, however the conical structure itself is younger than 112ka and its deposits have been subdivided stratigraphically into the several units. Misti 1(ca. 833-112ka) is overlapped by two stratocones Misti 2 and Misti 3 (112ka and younger), and Misti summit cone Misti 4 (11ka and younger) according to Thouret et al., (2001). According to Ruprecht and Wegner (2003) Misti 2 and 3 are treated as one phase due to no visible change in the slope (as suggested by Thouret et al., 2001) and petrography of erupted lavas. At 5400 m, an unconformity in elevation can be observed. The volcano shows two craters: a young inner crater and an older one probably due to the last big eruption 2050 a B.P. (Thouret et al., 2001). The most recent eruption took place in between A.D. 1440-1470 (Thouret et al., 2001). The eruption rate over 112ka was estimated to be about 0.63 km³/ka (Thouret et al., 2001). Intensive fumarolic activity and small phreatic events have been observed in the years 1677, 1784, and 1787.

El Misti has been erupting lavas with andesitic and dacitic composition. Eruptions varied between effusive, vulcanian and plinian style resulting in scoria, dense lava and pumice deposits. The most abundant volcanic deposits are andesitic lava flows and dacitic to rhyolitic pyroclastic flows. Also lahars, and block-and-ash flow deposits are present. Magmas from El Misti volcano belong to high-K calc-alkaline andesites (58-63 SiO₂ wt%), dacites (63-68%

SiO₂ wt%) and very rare rhyolites (>68 SiO₂wt%). In the andesitic lava suite Plagioclase dominates the mineral assemblage, however pyroxene is also common.

2.2 Basement under El Misti volcano

The Neogene base, on which El Misti is built, comprises the hydroclastites from Chachani and ignimbrites (Paquereau et al., 2007). The older volcanics overly Jurassic sedimentary rocks and Precambrian rocks of the northernmost domain of Arequipa-Antofalla basement, which elongate in southern Peru from San Juan to Mollendo, and east into the western Bolivia. The Precambrian basement rocks are dated to be ca. 2.0-1.9 Ga (Westeney's et al., 1995; Wörner et al., 2000). The metamorphic age was under debate however, the Rb/Sr and early U/Pb studies (Cobbing et al., 1977 and Shackleton et al., 1979) suggested granulite to amphibolitic facies metamorphism at 1.9 and 1.8 Ga and by Dalmayrac et al., (1977) Paleoproterozoic (1.9 Ga) and Neoproterozoic (0.7) Ga metamorphic events. The data on gneisses at Quilca, Mollendo, and Cerro Uyarani indicate high-grade metamorphism at ca. 1.2-1.0 Ga (Westeney's et al., 1995; Wörner et al., 2000).

In the northern and central domains Paleozoic magmatism and metamorphism have been identified. The Rb/Sr whole rock isochrone ages for intrusions in Peru yield 440 ±7Ma (Shackleton et al., 1979).

The basement rocks of Arequipa region are represented by Charcani gneiss, which is about 2 Ga old (Tilton and Barreiro, 1980), Mollendo gneisses, Ocoña granite. This part of Arequipa Massif extends well into the region of the Arequipa volcanics. Significant similarity exists between Pb isotopic composition of basement and Arequipa volcanic rocks (Wörner et al., 1992).

2.3 Sampling

Data used in this study come partly from the database of the Geochemistry department of Geoscience Center Göttingen. Samples have been collected during the field campaigns in the years: 1999, 2000. Samples collected for this study during fieldwork in 2002 are signed: Wörner&Kiebal2002 (legend on the map Fig. 2-1, data source in the Tab. 2-1). The map with sample location is presented below. The analyses have been provided at the Geochemistry department (GZG Göttingen). The analytical part is presented in the Appendix.

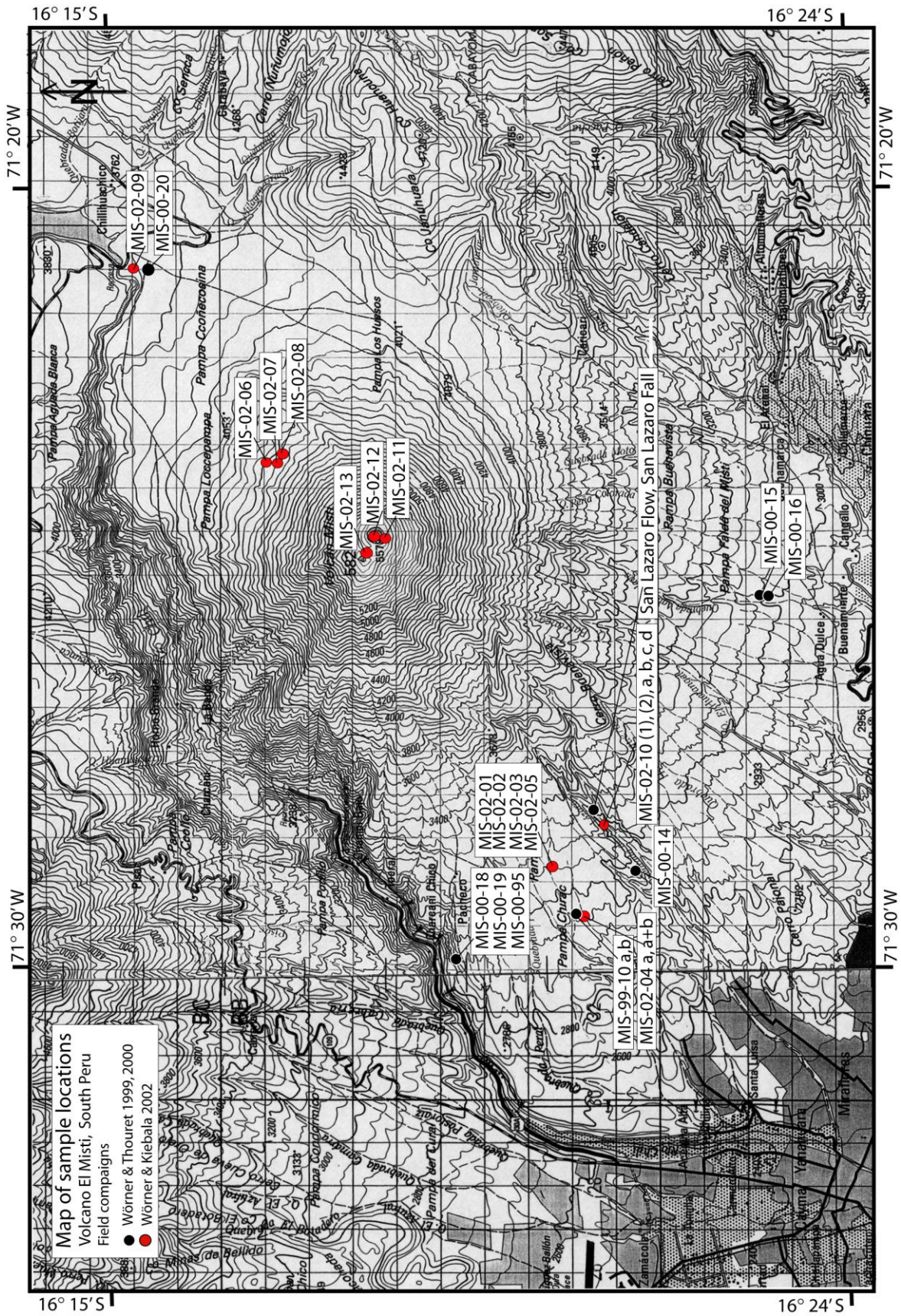


Fig. 2-1 Topographical map of El Misti volcano with sample location (field campaigns 1999, 2000 and 2002).

Tab. 2-1 Major, trace elements and isotopic composition of volcanic rocks from El Misti volcano.

	MIS-00-18	MIS-00-19	MI-00-95	MIS-00-13	MIS-00-14	MIS-02-05 50 ka	MIS-02-08 14 ka< >50 ka
Age (ka)							
rock type	dense andesite	dense andesite	dense grey andesite	andesite from b+a flow	andesite from b+a flow		dense andesitic lava flow
Data source	Wörner&Thouret 1999, 2000	Wörner& Kiebala2002	Wörner& Kiebala2002				
SiO ₂	66,61	66,43	63,10	60,83	61,17	63,05	60,18
TiO ₂	0,51	0,52	0,70	0,77	0,74	0,68	1,01
Al ₂ O ₃	17,26	17,22	17,44	17,29	17,35	17,50	16,87
Fe ₂ O ₃	3,15	3,23	4,56	5,46	5,30	4,54	5,75
MnO	0,07	0,07	0,08	0,10	0,10	0,09	0,09
MgO	0,52	0,64	1,78	3,16	2,91	1,66	3,26
CaO	3,12	3,20	4,66	5,67	5,56	4,34	5,82
Na ₂ O	5,08	5,02	4,34	4,29	4,38	4,26	4,29
K ₂ O	3,46	3,44	3,10	2,18	2,24	3,51	2,39
P ₂ O ₅	0,22	0,23	0,24	0,25	0,25	0,36	0,33
Sum	100,00	100,00	100,00	100,00	100,00	100,00	100,00
Nb	8,0	10,0	8,0	6,0	6,0	8,0	9,0
Zr	282	280	217	149	159	252	184
Y	16,0	14,0	16,0	14,0	12,0	17,0	15,0
Sr	582	587	660	795	777	685	886
Rb	78,0	76,0	82,0	43,0	40,0	63,0	45,0
Ga	19	21	19	21	21	21	21
Zn	62	76	54	68	57	87	87
Cu	1	0	43	70	49	6	71
Ni	1	0	9	30	25	0	38
Co	35,0	4,0	38,0	35,0	50,0	10,0	19,0
Cr	6	8	12	59	48	3	77
V	34	27	104	139	141	69	149
Ba	1310	1291	1043	972	965	1126	1003
Sc	2	7	6	13	14	9	15
Li7							
Mo							
Cs						1,06	0,95
Cd							
La						40,11	32,32
Ce						77	64
Pr						8,91	7,31
Nd						32,68	27,81
Sm						5,65	5,26
Eu						1,73	1,67
Gd						4,89	4,68
Tb						0,62	0,57
Dy						2,59	2,39
Ho						0,51	0,44
Er						1,38	1,16
Tm						0,23	0,19
Yb						1,35	1,05
Lu						0,24	0,19
Hf						6,25	4,66
Ta						0,46	0,51
W						0,31	0,31
Pb						16,53	13,89
Th						3,99	3,13
U						0,61	0,57
⁸⁷ Sr/ ⁸⁶ Sr							
error							
¹⁴³ Nd/ ¹⁴⁴ Nd							
error							
²⁰⁶ Pb/ ²⁰⁴ Pb						17,7926	
error						0,002216	
²⁰⁷ Pb/ ²⁰⁴ Pb						15,5714	
error						0,001972	
²⁰⁸ Pb/ ²⁰⁴ Pb						38,5131	
error						0,005057	

	MIS-02-02	MIS-02-03	MIS-99-10A (mafic)	MIS-99-10B (dacitic)	MIS-02-04a	MIS-02-04 a+b	MIS-02-01
Age (ka)	33.870 ka	33.870 ka	34 ka	34 ka	34 ka	34 ka	24.840 ka
rock type	(rhy)dacitic pumice fall	amphibol andesite	scoria	scoria	mafic scoria flow	mafic scoria felsic pumice flow	dense andesite
Data source	Ruprecht & Wörner2002	Wörner & Kiebala2002	Wörner & Thouret 1999, 2000	Wörner & Thouret 1999, 2000	Wörner & Kiebala2002	Wörner & Kiebala2002	Wörner & Kiebala2002
SiO ₂	63,72	61,43	59,15	60,36	60,99	59,26	59,64
TiO ₂	0,61	0,79	0,91	0,74	0,74	0,92	0,85
Al ₂ O ₃	17,27	17,30	17,54	17,75	17,47	17,46	17,40
Fe ₂ O ₃	4,69	5,42	6,02	5,57	5,64	6,12	5,74
MnO	0,10	0,09	0,10	0,11	0,11	0,10	0,10
MgO	2,23	2,92	3,39	2,98	2,88	3,42	3,38
CaO	4,66	5,53	6,09	5,83	5,53	6,11	6,08
Na ₂ O	4,12	4,00	4,38	4,24	4,00	4,18	4,21
K ₂ O	2,38	2,26	2,12	2,16	2,38	2,14	2,29
P ₂ O ₅	0,22	0,26	0,31	0,26	0,26	0,30	0,31
Sum	100,00	100,00	100,00	100,00	100,00	100,00	100,00
Nb	9,0	8,0	4,0	6,0	8,0	5,0	9,0
Zr	164	162	162	146	157	170	173
Y	13,0	10,0	14,0	13,0	16,0	14,0	13,0
Sr	715	790	862	786	775	868	902
Rb	46,0	40,0	35,0	38,0	41,0	34,0	42,0
Ga	19	19	22	20	19	20	20
Zn	78	84	80	74	79	84	83
Cu	21	36	77	68	41	67	70
Ni	17	25	31	23	20	34	31
Co	12,0	16,0	20,0	18,0	16,0	20,0	21,0
Cr	37	44	57	25	28	67	50
V	94	131	147	125	128	150	145
Ba	921	941	983	935	934	962	1000
Sc	9	12	13	16	11	16	14
Li7			8,8	11,8			
Mo			0,91	0,97			
Cs	1,04	0,91	1,02	1,16	1,00	1,16	0,96
Cd							
La	26,74	29,10	22,45	28,88	29,42	26,80	34,14
Ce	54	54	49	61	57	51	65
Pr	5,53	6,15	5,42	6,88	6,75	5,91	7,44
Nd	20,08	23,44	20,98	25,47	25,78	22,19	28,04
Sm	3,74	4,31	3,58	4,35	5,00	4,23	5,08
Eu	1,33	1,45	1,13	1,25	1,62	1,44	1,61
Gd	3,42	3,81	2,79	3,10	4,44	3,83	4,41
Tb	0,45	0,49	0,42	0,43	0,57	0,51	0,56
Dy	1,92	2,05	2,25	2,34	2,47	2,31	2,41
Ho	0,38	0,39	0,44	0,46	0,48	0,46	0,46
Er	1,02	1,02	1,20	1,24	1,31	1,24	1,18
Tm	0,18	0,17	0,17	0,18	0,22	0,21	0,20
Yb	0,97	0,90	1,15	1,21	1,21	1,20	1,07
Lu	0,17	0,17	0,17	0,19	0,22	0,21	0,19
Hf	2,18	3,55	4,38	5,62	4,26	4,03	4,39
Ta	0,38	0,41	0,32	0,38	0,40	0,41	0,44
W	0,25	0,24	14,13	2,20	0,25	0,25	0,28
Pb	14,91	12,68	13,54	16,67	12,88	14,30	13,52
Th	3,11	2,74	2,22	3,28	2,27	2,51	3,16
U	0,47	0,47	0,35	0,48	0,47	0,49	0,54
⁸⁷ Sr/ ⁸⁶ Sr			0,707567	0,707599			
error			0,000011	0,000011			
¹⁴³ Nd/ ¹⁴⁴ Nd			0,512156	0,512089			
error			0,000004	0,000005			
²⁰⁶ Pb/ ²⁰⁴ Pb			17,8291		17,8065		
error			0,000727		0,000951		
²⁰⁷ Pb/ ²⁰⁴ Pb			15,5273		15,6072		
error			0,000711		0,000900		
²⁰⁸ Pb/ ²⁰⁴ Pb			38,4246		38,6521		
error			0,002155		0,002625		

	MIS-99-04	MIS-99-05	MIS-00-20	MIS-02-09	MIS-02-06	MIS-02-07	El Misti FALL San Lazaro 2000 a
Age (ka)	20.960 ka	20,960 ka		14 <...>11 ka	11 ka	11 ka	
rock type	andesite blocks	pumice	fresh scoria bombs	scoria flow	black ash fall	aphiric andesite	pumice
Data source	Wörner&Thouret19 99, 2000	Wörner&Thouret 1999, 2000	Wörner&Thouret 1999, 2000	Wörner& Kiebala2002	Wörner& Kiebala2002	Wörner& Kiebala2002	Wörner&Thouret 1999,2000
SiO ₂	61,51	60,09	59,11	59,22	60,33	59,23	61,95
TiO ₂	0,70	0,78	0,80	0,81	0,88	0,98	0,76
Al ₂ O ₃	17,49	17,81	17,94	17,88	17,14	16,97	17,35
Fe ₂ O ₃	5,12	5,76	6,00	6,11	5,90	6,25	5,11
MnO	0,10	0,11	0,11	0,11	0,09	0,10	0,09
MgO	2,72	3,14	3,15	3,16	3,49	3,88	2,47
CaO	5,44	5,97	6,24	6,20	5,65	5,94	5,31
Na ₂ O	4,32	4,05	4,30	4,19	4,05	4,05	4,30
K ₂ O	2,34	2,04	2,10	2,08	2,22	2,30	2,41
P ₂ O ₅	0,25	0,25	0,26	0,26	0,25	0,29	0,26
Sum	100,00	100,00	100,00	100,00	100,00	100,00	100,00
Nb	6,0	3,0	7,0	6,0	7,0	8,0	6,0
Zr	156	144	158	163	165	182	153
Y	13,0	13,0	15,0	13,0	14,0	14,0	12,0
Sr	793	783	788	782	778	850	759
Rb	44,0	37,0	44,0	40,0	46,0	44,0	49,0
Ga	17	18	20	22	20	20	23
Zn	74	93	65	83	79	83	76
Cu	78	77	82	70	72	84	64
Ni	22	25	17	19	41	46	15
Co	16,0	19,0	52,0	20,0	18,0	23,0	21,0
Cr	32	25	19	25	85	106	30
V	121	134	144	148	160	172	122
Ba	1009	892	915	911	945	967	929
Sc	12	16	9	8	14	12	5
Li7	15,6	12,2					9,9
Mo	1,18	0,90					1,30
Cs	1,21	0,96		1,16	0,92	0,86	1,12
Cd							
La	26,37	26,58		28,80	29,07	36,24	23,25
Ce	55	55		54	55	67	49
Pr	6,38	6,78		6,42	6,46	7,91	5,64
Nd	23,77	25,72		24,31	24,28	29,33	21,62
Sm	3,90	4,24		4,82	4,58	5,50	3,94
Eu	1,23	1,24		1,57	1,51	1,69	1,14
Gd	3,27	3,41		4,41	4,01	4,78	2,86
Tb	0,40	0,46		0,58	0,54	0,59	0,40
Dy	1,93	2,17		2,60	2,34	2,51	2,00
Ho	0,36	0,41		0,52	0,45	0,49	0,36
Er	1,04	1,19		1,37	1,19	1,26	1,01
Tm	0,14	0,17		0,24	0,20	0,21	0,13
Yb	0,91	1,04		1,31	1,11	1,17	0,90
Lu	0,14	0,16		0,23	0,19	0,21	0,14
Hf	4,36	3,83		4,23	4,14	4,62	4,45
Ta	0,45	0,32		0,39	0,39	0,36	0,54
W	3,26	6,49		0,25	0,21	0,24	18,54
Pb	14,51	12,83		12,79	13,66	13,10	14,86
Th	2,81	3,68		2,85	2,98	3,71	3,03
U	0,44	0,35		0,52	0,45	0,51	0,51
⁸⁷ Sr/ ⁸⁶ Sr	0,707546		0,707459				0,707721
error	0,000010		0,000009				0,000010
¹⁴³ Nd/ ¹⁴⁴ Nd	0,512117		0,512126				0,512139
error	0,000006		0,000004				0,000004
²⁰⁶ Pb/ ²⁰⁴ Pb	17,7684		17,8442		17,7195		17,6815
error	0,00006		0,00007		0,001256		0,00007
²⁰⁷ Pb/ ²⁰⁴ Pb	15,5206		15,6102		15,5847		15,5819
error	0,00006		0,00007		0,001160		0,00007
²⁰⁸ Pb/ ²⁰⁴ Pb	38,4107		38,6550		38,6073		38,5605
error	0,0015		0,0018		0,003082		0,0018

	El Misti FLOW San Lazaro 2000 a	MIS-00-15 2000 a	MIS-00-16 2000 a	MIS-02-10 1 2000 a rhyolitic ignimbrite (floating)	MIS-02-10 2 2000 a rhyolitic ignimbrite (not floating)	MIS-02-10 a 2000 a rhyolitic ignimbrite	MIS-02-10 b 2000 a rhyolitic ignimbrite	MIS-02-10 c 2000 a rhyolitic ignimbrite
Age (ka)								
rock type	pumice	mixed pumice	mixed pumice					
Data source	Wörner&Thoure t 1999, 2000	Wörner&Thoure t 1999, 2000	Wörner&Thoure t 1999, 2000	Wörner& Kiebala2002	Wörner& Kiebala2002	Wörner& Kiebala2002	Wörner& Kiebala2002	Wörner& Kiebala2002
SiO ₂	60,03	63,35	62,93	68,29	66,44	63,48	61,91	60,56
TiO ₂	0,89	0,68	0,72	0,43	0,53	0,68	0,78	0,86
Al ₂ O ₃	17,50	17,02	17,06	15,97	16,33	17,05	17,25	17,49
Fe ₂ O ₃	5,74	4,64	4,79	3,12	3,73	4,68	5,19	5,61
FeO	0,09	0,09	0,09					
MnO	3,04	2,17	2,27	0,07	0,08	0,08	0,09	0,09
MgO	5,91	4,86	5,01	1,30	1,68	2,17	2,57	2,84
CaO	4,38	4,27	4,31	3,39	3,96	4,83	5,35	5,79
Na ₂ O	2,13	2,67	2,58	3,87	3,97	4,14	4,19	4,30
K ₂ O	0,28	0,26	0,26	3,40	3,09	2,64	2,41	2,17
P ₂ O ₅	100,00	100,00	100,00	0,16	0,19	0,25	0,26	0,29
Sum	5,0	8,0	7,0	100,00	100,00	100,00	100,00	100,00
Nb	152	150	152	6,0	9,0	8,0	7,0	7,0
Zr	12,0	13,0	11,0	148	153	158	157	159
Y	802	725	747	12,0	11,0	11,0	14,0	12,0
Sr	39,0	54,0	52,0	560	629	720	768	813
Rb	23	20	21	88,0	74,0	56,0	47,0	41,0
Ga	81	48	58	18	20	20	20	22
Zn	81	66	57	54	61	73	80	82
Cu	25	15	15	28	34	53	62	78
Ni	26,0	72,0	53,0	7	11	13	19	21
Co	53	27	27	9,0	12,0	12,0	16,0	18,0
Cr	146	111	110	14	18	26	38	40
V	881	964	959	63	79	108	123	139
Ba	10	10	10	1030	999	951	925	887
Sc	10,9			8	6	9	10	16
Li7	1,02							
Mo	0,80							
Cs				2,09	1,76	1,51	1,18	0,91
Cd	21,08							
La	46			17,19	21,71	25,88	24,94	23,06
Ce	5,42			40	46	52	49	48
Pr	21,88			3,61	4,51	5,45	5,57	5,46
Nd	3,94			12,82	16,12	20,09	21,34	21,03
Sm	1,18			2,54	3,07	3,94	4,08	4,14
Eu	2,90			1,03	1,16	1,35	1,39	1,42
Gd	0,40			2,30	2,80	3,52	3,60	3,66
Tb	2,01			0,34	0,40	0,46	0,48	0,49
Dy	0,37			1,54	1,74	1,96	2,05	2,07
Ho	1,00			0,33	0,35	0,39	0,40	0,40
Er	0,13			0,89	0,96	1,05	1,04	1,02
Tm	0,86			0,17	0,18	0,18	0,18	0,17
Yb	0,13			0,97	1,00	0,99	1,00	0,94
Lu	4,56			0,18	0,18	0,19	0,19	0,17
Hf	0,50			3,30	3,42	3,89	3,89	4,06
Ta	6,21			0,53	0,45	0,41	0,48	0,45
W	12,20			0,66	0,53	0,42	0,35	0,26
Pb	2,14			22,31	19,53	17,36	15,12	12,79
Th	0,35			4,67	4,42	3,62	2,97	2,17
U	0,707586			0,73	0,69	0,63	0,56	0,47
⁸⁷ Sr/ ⁸⁶ Sr	0,000012							
error	0,512152							
¹⁴³ Nd/ ¹⁴⁴ Nd	0,000004							
error	17,7790							
²⁰⁶ Pb/ ²⁰⁴ Pb	0,0007					17,3965		
error	15,5364					0,006961		
²⁰⁷ Pb/ ²⁰⁴ Pb	0,0007					15,5169		
error	35,6250					0,006324		
²⁰⁸ Pb/ ²⁰⁴ Pb	0,0016					38,3659		
error						0,015740		

	MIS-02-10 d	MIS-02-11 1	MIS-02-12 2	MIS-02-13 3
Age (ka)	2000 a	2000 a	2000 a	2000 a
rock type	rhyolitic ignimbrite	andesite	andesite	andesite
Data source	Wörner& Kiebala2002	Wörner& Kiebala2002	Wörner& Kiebala2002	Wörner& Kiebala2002
SiO ₂	60,44	59,32	60,00	58,75
TiO ₂	0,87	0,98	0,91	1,01
Al ₂ O ₃	17,41	16,93	16,93	17,12
Fe ₂ O ₃	5,69	6,16	6,17	6,23
FeO				
MnO	0,09	0,09	0,10	0,10
MgO	2,97	3,74	3,81	3,88
CaO	5,82	5,97	5,66	6,11
Na ₂ O	4,24	4,08	3,96	4,14
K ₂ O	2,18	2,39	2,21	2,32
P ₂ O ₅	0,28	0,32	0,25	0,34
Sum	100,00	100,00	100,00	100,00
Nb	8,0	6,0	7,0	9,0
Zr	158	189	165	188
Y	15,0	12,0	12,0	16,0
Sr	812	915	763	932
Rb	39,0	46,0	40,0	45,0
Ga	21	21	21	22
Zn	84	85	82	88
Cu	74	69	56	78
Ni	24	44	48	45
Co	14,0	23,0	26,0	25,0
Cr	48	95	110	65
V	143	164	160	164
Ba	882	1043	919	1059
Sc	8	11	13	20
Li7				
Mo				
Cs	0,93	0,79	0,72	0,77
Cd				
La	23,75	37,92	26,76	39,77
Ce	48	71	52	76
Pr	5,60	8,34	5,96	8,72
Nd	21,90	30,82	22,64	32,30
Sm	4,31	5,38	4,33	5,69
Eu	1,42	1,71	1,48	1,77
Gd	3,72	4,74	3,80	4,98
Tb	0,50	0,59	0,52	0,63
Dy	2,14	2,44	2,22	2,59
Ho	0,41	0,46	0,45	0,50
Er	1,07	1,20	1,15	1,26
Tm	0,18	0,20	0,20	0,20
Yb	0,98	1,12	1,09	1,16
Lu	0,18	0,19	0,20	0,20
Hf	3,97	4,80	4,05	4,83
Ta	0,46	0,41	0,38	0,48
W	0,29	0,21	0,20	0,22
Pb	13,00	13,23	8,66	11,66
Th	2,31	3,76	3,12	3,90
U	0,50	0,51	0,42	0,53
⁸⁷ Sr/ ⁸⁶ Sr				
error				
¹⁴³ Nd/ ¹⁴⁴ Nd				
error				
²⁰⁶ Pb/ ²⁰⁴ Pb				
error				
²⁰⁷ Pb/ ²⁰⁴ Pb				
error				
²⁰⁸ Pb/ ²⁰⁴ Pb				
error				

2.4 Geochemistry – major and trace elements

The whole rock analyzes for major, trace elements and isotopes are presented in Tab. 2-1. The classification of samples from El Misti volcano is presented on a diagram (Fig. 2-2, with the nomenclature after Le Maitre 1989). Volcanic rocks from the El Misti Volcano are plotted together with compiled data of the CVZ rocks (data from Mamani 2006). Samples of El Misti span compositional range from andesites to rhyodacites with silica content from 58.75 to 68.29 SiO₂wt%. The volcanics belong to medium to high K series with K₂O content between 2.03-3.49 (Fig. 2-2). Harker plots show the typical positive and negative correlations due to the processes of fractional crystallization and mixing (Fig. 2-3).

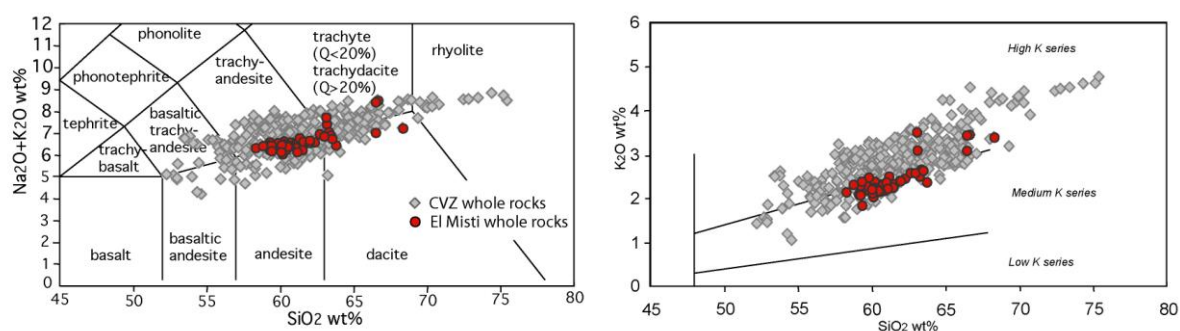


Fig. 2-2 Classification of calk-alkaline series after Le Maitre (1989) used for El Misti volcanics. The oxide contents are recalculated to 100% on a volatile-free basis and with all Fe as FeO.

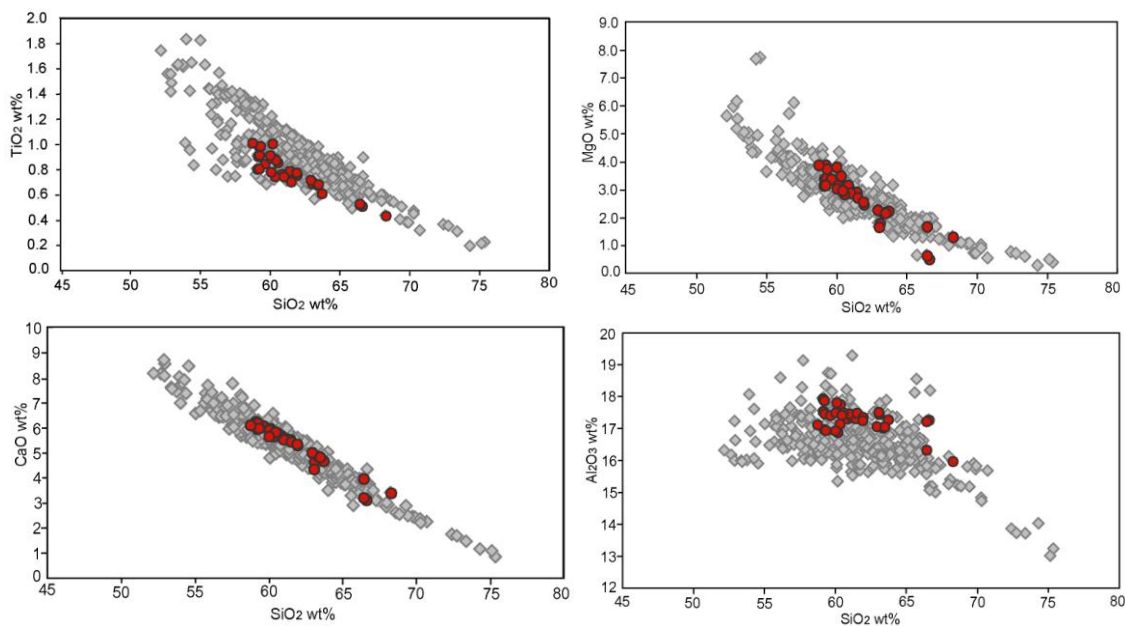


Fig. 2-3 Harker type diagrams for major elements and SiO₂ wt% of the El Misti magmas. The symbols are as at Fig. 2-2.

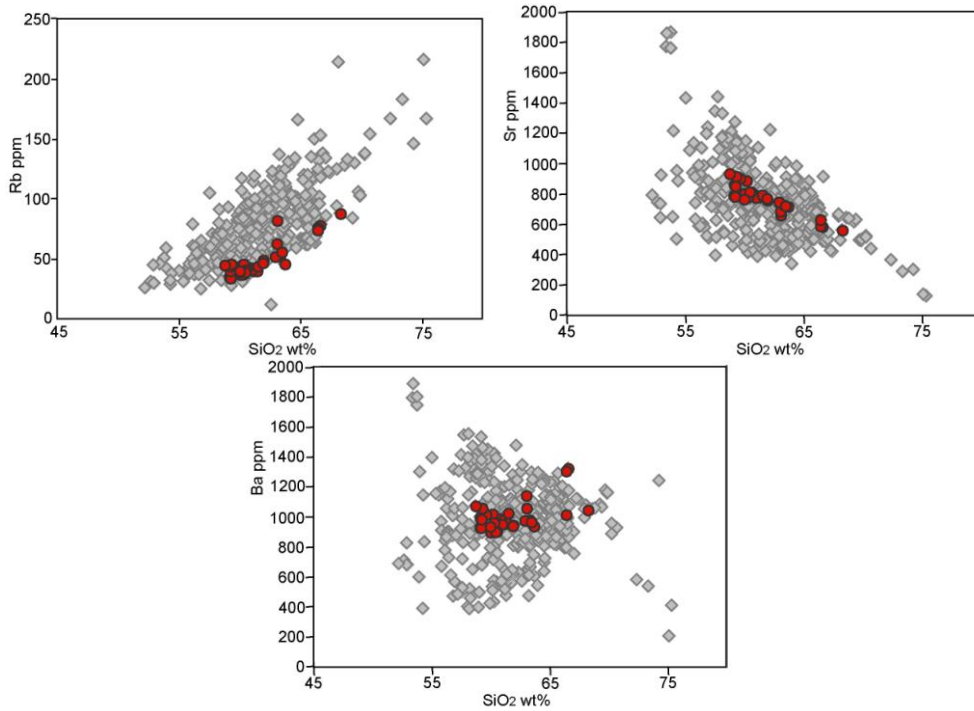


Fig. 2-4 Trace element (ppm) diagrams plotted versus silica content (SiO₂ wt%) for rocks from El Misti Volcano. Symbols are the same as at Fig. 2-2.

2.4.1 Spider diagram

Mantle normalized (Sun and McDonough, 1989) multi element diagram is presented at Fig. 2-5. The volcanic rocks from El Misti volcano (red lines) are plotted together with CVZ data (colored lines).

The trace element composition of analyzed samples from El Misti follow a general pattern of CVZ magmas. The diagram show a typical island-arc basalt characteristic with selective enrichment of elements with low ionic potential (Sr, K, Rb, Ba, ±Th) and low abundances of high ionic potential elements (Ta, Nb, Ce, P, Zr, Hf, Sm, Ti, Y, Yb) compared to MORB. Peaks at K, Sr are typical for subduction-related magmas, due to subduction-zone fluids enriched in LILE (Sr, K, Rb, Ba, U) in their petrogenesis. HFSE (Nb, Ta, Hf, Zr, Ti) depletion is also characteristic for this tectonic environment.

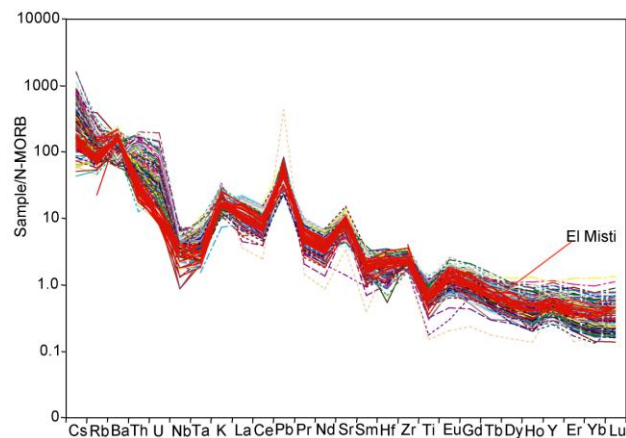


Fig. 2-5 Multi element diagram for El Misti samples normalized to N-MORB (Sun and McDonough 1989) showing typical pattern for lavas related to subduction zones.

2.4.2 Rare earth elements

A good tool to characterise the composition of volcanic rocks is a REE plot. The chondrite normalized (Boyton, 1984) REE diagram of El Misti volcanic rocks together with CVZ data is presented on Fig. 2-6. The shape of REE pattern shows enrichment of LREE relative to HREE. Decrease in HREE, has been suggested to be connected with the garnet residue in the melting zone (Malburg Kay and Mpodozis, 2002; Mamani et al., 2004; Wörner et al., 2004 and Thouret et al., 2005).

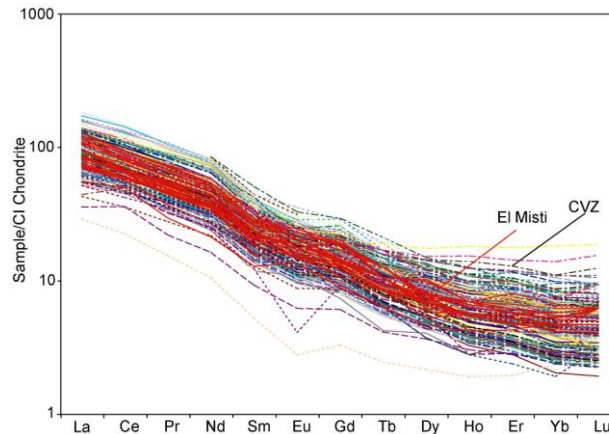


Fig. 2-6 REE-pattern of El Misti lavas normalized to chondrite C1 (Boyton 1984).

2.4.3 Sr, Nd, Pb isotopes

The Sr, Nd and Pb isotopic composition of the CVZ volcanic rocks is dominated by the crustal contribution to the magmas (Davidson et al., 1991). Diagrams presenting the Sr, Nd and Pb isotopic composition of magmas from El Misti volcano plotted together with CVZ and crustal basement rocks around El Misti are presented on the Fig. 2-7. The erupted volcanics from CVZ are enriched in ^{87}Sr relative to the mantle-derived magmas. Measured values of $^{87}\text{Sr}/^{86}\text{Sr}$ for El Misti whole rock samples are uniform ranging between 0.7075-0.7077. The Nd isotopic composition of analysed El Misti samples show lower $^{143}\text{Nd}/^{144}\text{Nd}$ values ($\epsilon\text{Nd} - 9.3$ to -10.7) in comparison to mantle values.

A distinctive way to characterise the studied rocks especially in this tectonic settings comprise Pb isotopes. Around El Misti (Quebrada San Lazaro and Quebrada Aquada Blanca) very low values of $^{207}\text{Pb}/^{204}\text{Pb}$ isotopes ranging between 17.68 and 17.84 have been measured (much lower values than in other locations of Arequipa domain).

The $^{208}\text{Pb}/^{204}\text{Pb}$ values are similar to all other samples from CVZ ranging from 38.41 to 38.65 for El Misti and 38.4 – 38.8 for the CVZ.

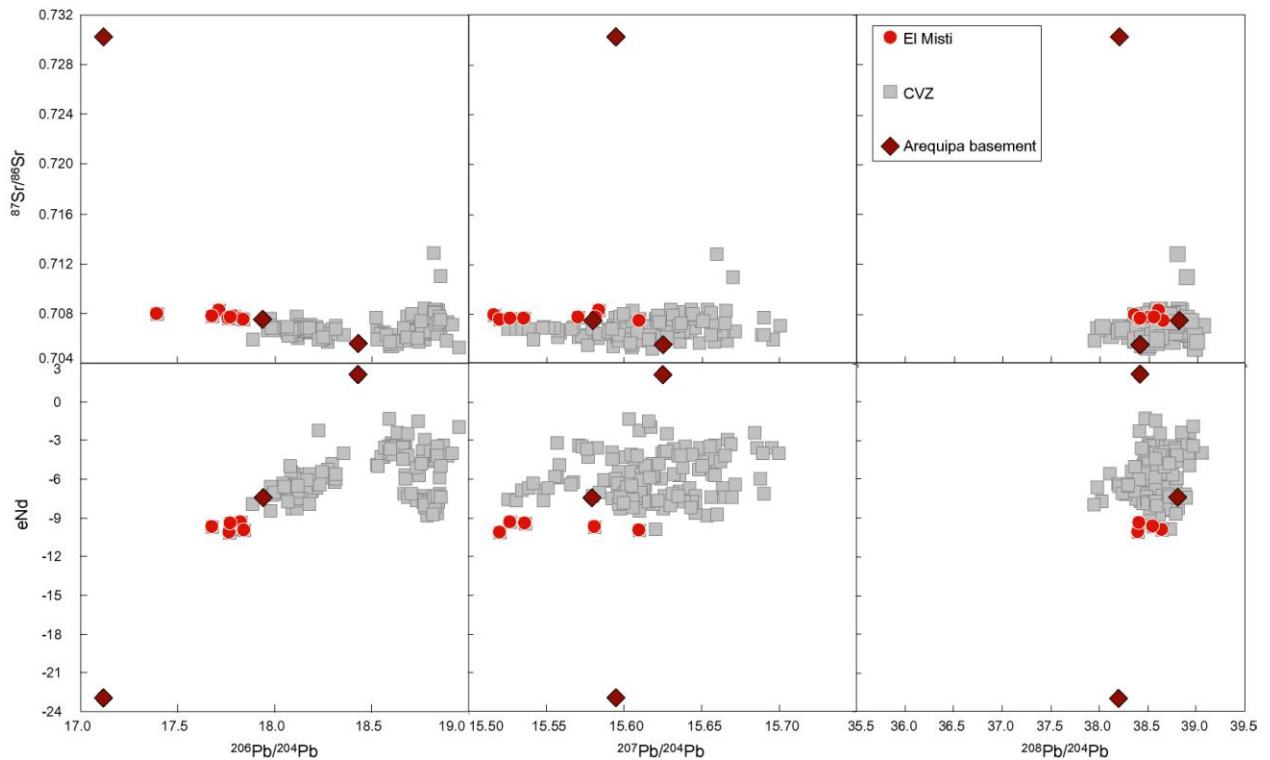


Fig. 2-7 Nd, Sr and Pb isotopic composition of El Misti volcanics presented with CVZ data.

2.5 U-Th isotopes

The concentration and isotopic composition of U and Th elements for samples from El Misti volcano are presented in Tab. 2-2 and on Fig. 2-8. The explanation of measuring method is given in the Appendix.

Results

The concentrations of U and Th in the whole rock samples from El Misti volcano are relatively low in compare to rocks from other volcanic centres of the CVZ. Th concentration (ICP MS) at El Misti ranges from 2.2 to 4.7 ppm. The U concentration is much lower, scooping from 0.35 to 0.7 ppm. Th/U ratio of 7.3 is almost constant over the whole composition range of El Misti samples (7.05-7.44).

The U-Th isotopic composition of samples from El Misti volcano is characterized by ^{238}U enrichment. The whole rock ($^{230}\text{Th}/^{238}\text{U}$) activity ratios range between 0.609 and 0.828 showing ^{238}U excess. The samples show eruption age corrected ($^{230}\text{Th}/^{232}\text{Th}$) activity ratios between 0.325 and 0.498. These data represent the lowest ever measured ($^{230}\text{Th}/^{232}\text{Th}$) values for volcanic rocks. The ($^{234}\text{U}/^{238}\text{U}$) activity ratios range from 0.986 to 1.033 suggesting that the U systematic have not been disturbed by interaction with ground or meteoric water.

Tab. 2-2 Whole rock U-Th isotopic data for El Misti volcanic rocks.

Sample	[Th] μg/g	[U] μg/g	$(^{238}\text{U}/^{232}\text{Th})$	$(^{230}\text{Th}/^{232}\text{Th})$	$(^{230}\text{Th}/^{238}\text{U})$	$(^{234}\text{U}/^{238}\text{U})$
MIS-02-01	3,16	0,60	0,578±6	0,470±8	0,766±10	0,998±8
MIS-02-04a	2,64	0,53	0,610±2	0,498±6	0,748±10	1,000±10
MIS-02-06	2,97	0,43	0,444±3	0,365±20	0,804±4	0,996±7
MIS-02-08	3,19	0,62	0,586±2	0,448±6	0,732±10	1,005±12
MIS-02-09	2,71	0,49	0,551±2	0,421±6	0,733±10	0,986±10
MIS-02-10 1	6,61	1,38	0,635±3	0,391±4	0,609±7	1,009±8
MIS-02-10 2	5,35	1,05	0,596±2	0,395±3	0,657±5	1,033±10
MIS-02-12 2	3,06	0,39	0,391±9	0,325±3	0,828±7	1,009±12

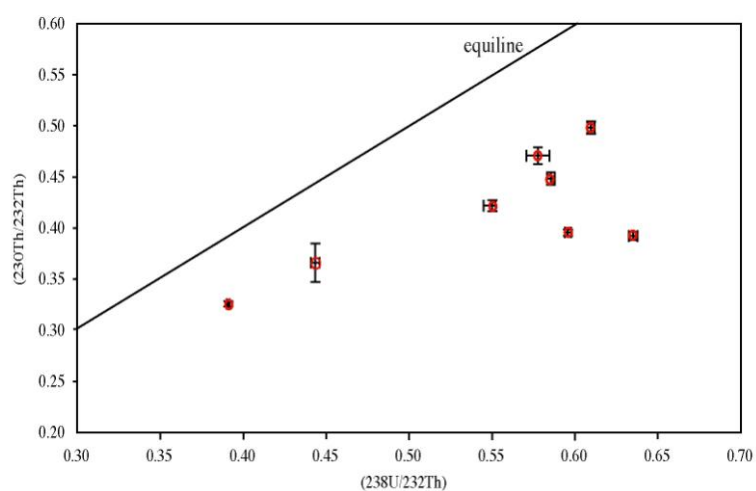


Fig. 2-8 Equiline diagram for $(^{238}\text{U}/^{230}\text{Th})$ results for El Misti volcanic rocks (whole rock data).

3 Taapaca Volcanic Complex, North Chile



3.1 Geological settings

Taapaca Volcanic Complex is a mainly dacitic stratocone rising to an altitude of 5824 m asl. This 2000 m high volcanic structure is composed almost entirely of a cluster of dacitic domes and associated block-and-ash flows. They partly filled surrounding valleys and plains and form terraces on which the town of Putre has been constructed (ca 2000 inhabitants). The published ages range from 1.27 ± 0.004 Ma to 38.0 ± 0.0026 ka and 0.086 ± 0.04 (Wörner et al., 2000; Wörner et al., 2004; Clavero et al., 2004). Even younger deposits have been identified based on morphology (Diplomkartierung Kohlbach and Lohnert, 1999 and Diplomarbeit, Lohnert 1999 Univ. Göttingen, Clavero et al., 2004).

The Taapaca Volcanic Complex evolved from an early shield-type volcano composed by andesitic lava flows at its first stage (60-61% SiO₂). Three stages of evolution of the Taapaca Volcanic Complex have been recognized (Kohlbach and Lohnert, 1999). These are: the oldest stage I of shield like cone, the second stage II of steep-sided stratovolcano formed of lava flows and lava domes and its associated block and ash flow and the youngest stage III built by steep-sided small volume flows and dome complexes which now form the summit. Between stage II and III a transitic stage was recognized. The main focus of eruptive activity migrated 4-5 km toward the south-southwest during the three-stage evolution of the Taapaca Volcanic Complex. Andesites and dacites erupted during the history of the Taapaca volcano are monotonously porphyritic and all contain abundant large plagioclase phenocrysts, which comprise about 25-30 vol% (based on examined thin sections). The phenocrysts show a mineral mode of plagioclase, sanidine, pyroxene, amphibole, biotite, quartz, ore minerals, sphene, and accessory apatite and/or zircon. The mineral assemblage is dominated by plagioclase phenocrysts throughout all three volcanic stages. The groundmass consists mainly of plagioclase, amphibole as well as ore minerals. A characteristic feature of lavas from the second stage II and of the transitional II-III volcanics is the occurrence of large (up to 8cm in size) euhedral sanidine megacrysts (Kohlbach and Lohnert, 1999).

3.2 Basement under Taapaca Volcanic Complex

The basement rocks, which underlie the Taapaca Volcanic Complex, belong to the central domain of Arequipa-Antofalla Basement. The central domain extends from the Peru-Chile border to Quebrada Choja in northernmost Chile.

Crystallization ages on zircons from migmatite and orthogneisses suggest 1254 \pm 97/-9 Ma and 1213 \pm 28/-25 Ma (Damm et al., 1990). Metavolcanic rocks from Belén show imprecise Sm/Nd isochrone age of 1469 \pm 448 Ma (Damm et al., 1990).

The metamorphic basement rocks at Belén (18°30'S, 69°30'W) are exposed in a NNW-SSE oriented elongate belt (ca. 2x10km) and are situated within the western Altiplano escarpment of Central Volcanic Zone in Northern Chile. The outcrop of Precambrian rocks consists of intercalated amphibolite, amphibole-gneiss, gneiss, schist, minor quartzite, ultramafic rocks, and dioritic intrusion. The main foliation strikes NNW-SSE and dips 45-70°E. Alteration of quartz-rich gneisses and mafic amphibolites on a sub-meter scale and gradational contacts between different lithologies suggest that some of the structures reflect pre-metamorphic contacts and stratigraphic layering, and sedimentary mixing of the precursor rocks (Wörner et al., 2000). Tosdal (1996) suggests that the Belén protoliths show a strong sedimentary contribution from the Arequipa Massif.

Detailed description of Belén basement rocks, are to be found in Wörner et al. 2000.

The unit is unconformably overlain by >2000m of folded and faulted Mesozoic-Cenozoic strata (García et al. 1996; Lezaun et al., 1997). The basement rocks are fault-bounded. The unradiogenic Pb in whole-rock basement samples from the Central Andes has been interpreted as resulting from depletion of U relative to Th early in their history, possibly through granulite-facies metamorphism (Tilton and Barreiro, 1980; Mukasa and Henry, 1990; Tosdal, 1996).

3.3 Sampling

The samples from Taapaca Volcanic Complex used for this study come from the collection and database at the Geochemistry Department at Geoscience Center Göttingen. Wide range of samples and some analyses (for major, trace elements and partly isotopes) of the Taapaca volcanics already existed and therefore, only few of them have been re-sampled during the fieldwork 2002. These samples are signed Wörner&Kiebal2002 (look map with sample location Fig. 3-1, and Tab. 3-1). All results of U-Th isotopes for Taapaca volcanic rocks come from this study.

Tab. 3-1 Major, trace elements and isotopes of whole rock samples from Taapaca Volcano.

Sample	TAP-97-41	TAP-97-40	TAP 97-43	TAP 97-02	TAP-97-10	TAP-97-13	TAP-97-17
Age (Ma) ± error (ka)	3.72± 110	2.13± 109					0.958± 76
rock type	dacite	dacite	andesite	andesite	andesite	dacite	dacitic andesite
Comments	flow						
Source data	Kohlbach&Lohnert1997						
SiO ₂	63,39	70,76	62,38	62,69	65,75	65,49	64,45
TiO ₂	0,85	0,31	0,96	0,69	0,71	0,69	0,82
Al ₂ O ₃	17,28	15,67	16,71	17,00	18,53	16,35	16,42
Fe ₂ O ₃	4,96	2,00	5,39	5,24	4,52	3,89	4,44
FeO	0,20	0,00	0,00	0,00	0,00	0,00	0,00
MnO	0,07	0,04	0,09	0,09	0,03	0,06	0,06
MgO	1,24	0,54	2,46	2,45	0,64	1,49	1,60
CaO	4,12	2,23	4,73	5,07	2,88	3,73	3,94
Na ₂ O	4,72	4,44	4,44	3,75	3,65	4,78	4,64
K ₂ O	2,83	3,90	2,55	2,83	3,08	3,24	3,25
P ₂ O ₅	0,34	0,10	0,30	0,20	0,21	0,28	0,36
Summe	100,00	100,00	100,00	100,00	100,00	100,00	100,00
FeO (tot)	4,67	1,80	4,85	4,71	4,07	3,50	3,99
Nb	6,0	8,5	9,0	7,0	9,0	6,0	7,0
Zr	157	138	155	146	153	171	194
Y	8,0	6,5	10,0	11,5	17,0	9,0	10,0
Sr	911	438	688	564	592	880	980
Rb	79,0	158,5	68,0	87,5	96,0	93,0	86,0
Ga	24	21	22	20	19	21	23
Zn	79	60	83	77	93	68	78
Cu							
Ni	22	2	18	13	8	11	14
Co	16,0	3,0	14,0	17,0	15,0	8,0	9,0
Cr	42	5	32	22	17	11	14
V	81	35	97	126	93	90	126
Ba	1056	912	781	839	982	1138	1252
Sc	6	7	13	12	10	6	13
Li7	16,6	32,0		11,0	6,8	20,6	19,4
Mo		1,72			1,35	1,18	0,79
Cs		10,30		7,20	4,42	6,76	5,21
Cd		0,15			0,15	0,18	0,20
La	34,30	17,70		28,90	18,20	32,00	34,10
Ce	70	39		59	41	63	69
Pr	8,60	3,87		6,30	4,34	7,45	8,65
Nd	32,70	12,20		23,00	15,40	28,90	33,30
Sm	5,50	2,05		3,90	3,35	4,73	5,11
Eu	1,00	0,51		0,80	0,94	1,28	1,48
Gd	4,10	1,62		5,40	3,01	4,07	4,56
Tb	0,40	0,19		0,40	0,46	0,42	0,45
Dy	1,90	0,69		2,00	2,24	1,74	1,95
Ho	0,30	0,15		0,40	0,46	0,31	0,32
Er	0,90	0,40		1,10	1,35	0,76	0,85
Tm	0,10	0,05		0,10	0,17	0,10	0,10
Yb	0,70	0,36		0,90	1,26	0,60	0,63
Lu	0,10	0,06		0,10	0,19	0,11	0,10
Hf	0,80	2,64		1,30	3,28	3,14	4,11
Ta	1,80	0,48		3,30	0,39	0,41	0,40
W	0,80	1,30		3,00	1,78	1,19	1,34
Pb	13,50	22,70		17,50	16,50	19,30	17,90
Th	5,60	10,80		13,20	10,00	6,64	7,06
U	1,30	3,00		3,50	1,83	2,69	2,60
⁸⁷ Sr/ ⁸⁶ Sr		0,706757					0,706740
error		0,000011					0,000014
¹⁴³ Nd/ ¹⁴⁴ Nd		0,512277					0,512280
error		0,000005					0,000005
²⁰⁶ Pb/ ²⁰⁴ Pb							
error							
²⁰⁷ Pb/ ²⁰⁴ Pb							
error							
²⁰⁸ Pb/ ²⁰⁴ Pb							
error							

Sample	TAP-97-22	TAP-97-18	TAP-97-11	TAP-97-06	TAP-97-37	TAP-97-37-1	TAP 97-39
Age (Ma) ±error (ka)	0.910± 69	0.819± 165	0.388± 21				
rock type	andesite	dacite	dacite	andesite	andesite	basaltic andesite	dacite
Comments	flow	flow	flow	flow	flow	inclusion	flow
Data source	Kohlbach& Lohnert1997						
SiO ₂	62,88	64,62	64,94	61,88	63,72	53,96	65,98
TiO ₂	0,91	0,77	0,84	1,07	0,62	1,01	0,63
Al ₂ O ₃	16,22	16,13	16,44	16,21	17,43	18,06	16,57
Fe ₂ O ₃	5,17	4,30	4,42	2,90	5,23	9,01	4,03
FeO	0,00	0,00	0,00	2,99	0,00	0,00	0,00
MnO	0,07	0,07	0,06	0,08	0,09	0,15	0,06
MgO	2,51	1,97	1,61	2,64	1,93	4,51	1,57
CaO	4,67	4,18	3,77	4,92	4,11	8,01	3,54
Na ₂ O	4,42	4,54	4,70	4,37	4,05	3,27	4,51
K ₂ O	2,84	3,13	2,94	2,61	2,66	1,76	2,93
P ₂ O ₅	0,31	0,30	0,28	0,33	0,17	0,26	0,18
Summe	100,00	100,00	100,00	100,00	100,00	100,00	100,00
FeO (tot)	4,65	3,87	3,97	5,60	4,71	8,10	3,63
Nb	9,0	6,0	6,0	7,5	7,0	6,0	8,0
Zr	155	156	167	160	128	126	136
Y	10,0	8,0	8,0	10,0	12,0	22,0	10,0
Sr	768	878	652	719	559	647	581
Rb	79,0	89,0	90,0	74,0	95,0	59,0	105,0
Ga	21	22	23	21	21	21	21
Zn	79	70	81	85	63	103	68
Cu							
Ni	28	16	14	24	4	9	26
Co	14,0	15,0	17,0	18,0	13,0	21,0	14,0
Cr	58	28	12	41	22	35	39
V	124	90	86	140	98	139	73
Ba	949	1124	810	862	729	581	818
Sc	6	8	10	13	15	24	8
Li7	18,9	23,9	25,3	20,4	15,3	21,4	
Mo	0,88	0,59	0,93	1,27	0,42	0,20	
Cs	3,56	5,78	6,07	5,04	5,94	3,46	
Cd	0,19	0,18	0,19	0,18	0,17	0,22	
La	25,80	32,60	23,80	23,10	12,80	16,90	
Ce	54	65	49	50	30	40	
Pr	6,92	7,41	5,64	6,58	3,12	5,24	
Nd	27,30	27,80	21,90	25,40	12,30	20,20	
Sm	4,52	4,87	4,04	4,42	2,42	4,06	
Eu	1,32	1,30	1,06	1,35	0,67	1,28	
Gd	4,26	4,01	3,31	3,96	2,36	4,23	
Tb	0,45	0,44	0,36	0,46	0,31	0,62	
Dy	2,12	1,80	1,38	2,08	1,80	3,75	
Ho	0,35	0,34	0,26	0,33	0,35	0,69	
Er	0,92	0,82	0,59	0,88	1,01	2,23	
Tm	0,11	0,10	0,07	0,09	0,14	0,28	
Yb	0,68	0,64	0,44	0,64	0,95	2,04	
Lu	0,11	0,11	0,08	0,09	0,15	0,28	
Hf	3,40	3,34	3,61	3,57	2,49	3,23	
Ta	0,40	0,34	0,30	0,36	0,46	0,30	
W	0,89	1,03	1,32	1,00	1,06	1,15	
Pb	16,20	18,60	19,10	14,70	16,70	13,20	
Th	5,64	5,86	5,42	5,84	5,77	4,07	
U	2,21	1,82	2,40	2,44	1,96	0,40	
⁸⁷ Sr/ ⁸⁶ Sr		0,706613		0,706655	0,706310	0,705884	
error		0,000011		0,000011	0,000012	0,000012	
¹⁴³ Nd/ ¹⁴⁴ Nd		0,512283		0,512313	0,512330	0,512356	
error		0,000005		0,000005	0,000005	0,000005	
²⁰⁶ Pb/ ²⁰⁴ Pb							
error							
²⁰⁷ Pb/ ²⁰⁴ Pb							
error							
²⁰⁸ Pb/ ²⁰⁴ Pb							
error							

Sample	TAP-97-34	TAP-97-28	TAP-02-02-a	TAP-02-02-b	TAP-97-29	TAP 97-29/1	TAP-02-03
Age (Ma) ± error (ka)	0.034± 38	0.033	0.033	0.33	0.01	0.01	0.01
rock type	dacite	dacite	dacite	basaltic andesite	dacite	basaltic andesite	andesite
Comments	flow Kohlbach& Lohnert1997	flow Kohlbach& Lohnert1997	Baf Wörner& Kiebala2002	inclusion Wörner& Kiebala2002	flow Kohlbach& Lohnert1997	inclusion Kohlbach& Lohnert1997	Block flow Wörner& Kiebala2002
Source data							
SiO ₂	66,58	65,80	65,13	57,77	64,74	56,39	64,15
TiO ₂	0,69	0,71	0,80	1,37	0,85	1,56	0,88
Al ₂ O ₃	16,06	16,05	16,13	16,17	16,16	16,97	16,37
Fe ₂ O ₃	3,75	3,55	4,32	7,19	2,39	7,86	4,67
FeO	0,00	0,38	0,00	0,00	2,09	0,00	0,00
MnO	0,06	0,06	0,06	0,09	0,06	0,09	0,06
MgO	1,48	1,68	1,75	3,57	1,84	3,67	1,85
CaO	3,52	3,70	3,98	5,95	4,07	6,48	4,29
Na ₂ O	4,47	4,57	4,48	4,05	4,46	4,13	4,54
K ₂ O	3,16	3,24	3,07	3,23	3,06	2,31	2,89
P ₂ O ₅	0,23	0,27	0,27	0,60	0,28	0,54	0,30
Summe	100,00	100,00	100,00	100,00	100,00	100,00	100,00
FeO (tot)	3,37	3,57	3,88	6,47	4,24	7,08	4,20
Nb	6,0	7,0	9,0	11,0	6,0	7,0	9,0
Zr	166	150	180	245	170	211	176
Y	5,0	10,0	12,0	15,0	9,0	13,0	12,0
Sr	662	775	845	1439	742	1101	790
Rb	96,0	95,0	96,0	71,0	85,5	45,0	81,0
Ga	22	23	22	24	22	22	20
Zn	67	65	72	104	85	111	78
Cu			44	70			40
Ni	9	10	10	24	14	31	15
Co	10,0	11,0	6,0	25,0	11,5	23,0	13,0
Cr	12	11	11	24	23	46	25
V	87	85	98	165	108	195	108
Ba	936	1072	1116	1534	1051	1104	970
Sc	8	8	9	19	10	15	6
Li7	28,8	24,1	20,4	35,6	26,3		24,8
Mo	1,46	1,21	1,33	1,45	1,42		1,33
Cs	6,27	6,26	4,87	2,06	5,99		5,22
Cd	0,17	0,17	0,18	0,28	0,19		0,18
La	25,00	25,30	26,20	53,90	27,90		29,00
Ce	51	54	55	125	56		59
Pr	5,65	6,45	6,73	14,20	6,61		7,02
Nd	19,90	22,10	23,50	56,00	26,00		28,10
Sm	3,51	3,72	3,98	9,11	4,53		4,82
Eu	0,95	1,08	1,20	2,43	1,22		1,33
Gd	2,81	3,04	3,36	7,95	3,93		4,24
Tb	0,32	0,36	0,38	0,82	0,42		0,44
Dy	1,21	1,47	1,60	3,53	1,78		1,87
Ho	0,24	0,27	0,27	0,62	0,31		0,32
Er	0,59	0,75	0,75	1,67	0,75		0,78
Tm	0,07	0,08	0,08	0,20	0,09		0,09
Yb	0,47	0,59	0,55	1,23	0,57		0,57
Lu	0,08	0,09	0,08	0,19	0,09		0,09
Hf	3,35	3,32	3,41	5,92	3,71		3,39
Ta	0,29	0,30	0,33	0,34	0,37		0,32
W	1,26	1,12	1,09	0,68	1,31		1,14
Pb	18,90	16,30	16,80	15,30	19,00		18,70
Th	6,06	6,63	6,50	5,12	6,02		5,32
U	2,05	2,12	2,24	0,91	2,43		2,23
⁸⁷ Sr/ ⁸⁶ Sr	0,706725	0,706471		0,706703		0,706546	
Error	0,000011	0,000011		0,000011		0,000017	
¹⁴³ Nd/ ¹⁴⁴ Nd	0,512290	0,512305		0,512299		0,512293	
Error	0,000005	0,000005		0,000004		0,000005	
²⁰⁶ Pb/ ²⁰⁴ Pb						18,1657	
Error						0,0016	
²⁰⁷ Pb/ ²⁰⁴ Pb						15,6643	
Error						0,0015	
²⁰⁸ Pb/ ²⁰⁴ Pb						38,5853	
Error						0,0038	

Sample	TAP-87-002	TAP-97-01	TAP-97-45	TAP-97-48	TAP-001	TAP-002	TAP-003
Age (Ma) ±error (ka)	0.009± 6	0.01	0.044± 16		0.009± 4		
rock type	dacite	dacite	dacite	dacite	dacite	basaltic andesite	basaltic andesite
Comments	BAf	BAf	BAf	BAf	BAf		
Source data	Fieldwork1987	Kohlbach&Lohnert1997	Kohlbach&Lohnert1997	Kohlbach&Lohnert1997			
SiO ₂	65,17	66,21	65,14	65,64	64,62	55,06	54,04
TiO ₂	0,78	0,70	0,77	0,75	0,85	1,82	1,83
Al ₂ O ₃	16,19	16,22	15,98	15,98	16,25	17,13	16,90
Fe ₂ O ₃	4,27	3,72	4,21	4,14	4,46	8,25	8,52
FeO	0,00	0,00	0,00	0,00	0,00	0,00	0,00
MnO	0,06	0,05	0,06	0,06	0,06	0,09	0,09
MgO	1,69	1,48	1,86	1,73	1,85	3,64	4,32
CaO	3,95	3,60	3,92	3,77	4,06	6,56	6,96
Na ₂ O	4,50	4,63	4,59	4,40	4,35	4,33	4,28
K ₂ O	3,13	3,14	3,18	3,24	3,22	2,39	2,29
P ₂ O ₅	0,27	0,24	0,28	0,29	0,28	0,75	0,76
Summe	100,00	100,00	100,00	100,00	100,00	100,00	100,00
FeO (tot)	3,84	3,35	3,79	3,73	4,01	7,42	7,67
Nb	6,0	7,0	8,0	7,0	8,0	17,0	14,0
Zr	167	164	165	162	173	266	243
Y	7,0	9,0	9,0	8,0	8,0	17,0	17,0
Sr	737	686	805	803	752	1430	1213
Rb	87,0	88,0	94,0	95,0	85,0	40,0	42,0
Ga	22	22	19	22			
Zn	71	74	97	70	69	113	111
Cu					31	57	45
Ni	13	9	10	10	12	28	45
Co	11,0	9,0	13,0	10,0	23,0	27,0	33,0
Cr	17	11	13	17	16	45	77
V	99	87	103	97	92	170	186
Ba	1034	959	1040	1039	1231	1380	1286
Sc	6	10	7	8			
Li7	20,8	26,6	22,8	23,7			
Mo	0,81	1,36	1,09	1,51			
Cs	3,82	5,90	5,37	6,60			
Cd	0,18	0,19	0,18	0,16			
La	23,80	23,10	26,90	27,80			
Ce	50	48	57	59			
Pr	6,11	5,16	6,39	7,34			
Nd	21,80	19,60	22,20	26,80			
Sm	3,71	3,51	3,94	4,12			
Eu	1,11	0,92	1,12	1,21			
Gd	3,06	2,82	3,14	3,55			
Tb	0,36	0,31	0,38	0,39			
Dy	1,51	1,15	1,46	1,74			
Ho	0,26	0,23	0,28	0,29			
Er	0,69	0,51	0,72	0,81			
Tm	0,07	0,06	0,08	0,09			
Yb	0,53	0,41	0,57	0,62			
Lu	0,08	0,07	0,09	0,10			
Hf	3,40	3,24	3,50	3,52			
Ta	0,25	0,29	0,29	0,33			
W	0,96	1,21	1,04	1,19			
Pb	17,10	18,80	17,50	12,50			
Th	6,58	4,55	6,55	6,74			
U	2,24	1,74	2,13	2,49			
⁸⁷ Sr/ ⁸⁶ Sr	0,706711				0,706680	0,706500	
error	0,000013						
¹⁴³ Nd/ ¹⁴⁴ Nd	0,512296					0,512344	
error	0,000006						
²⁰⁶ Pb/ ²⁰⁴ Pb						18,0990	
error							
²⁰⁷ Pb/ ²⁰⁴ Pb						15,6190	
error							
²⁰⁸ Pb/ ²⁰⁴ Pb						38,3990	
error							

Sample	TAP-004	TAP-005	TAP-006	TAP-007
Age (Ma) ±error (ka)				
rock type	andesite	dacite	andesite	andesite
Comments				
SiO ₂	62,91	65,16	62,75	62,46
TiO ₂	0,98	0,72	0,72	0,75
Al ₂ O ₃	16,18	16,60	17,51	16,99
Fe ₂ O ₃	5,21	4,08	4,92	5,29
FeO	0,00	0,00	0,00	0,00
MnO	0,07	0,05	0,07	0,08
MgO	2,52	1,62	2,23	2,42
CaO	4,55	3,87	5,02	4,95
Na ₂ O	4,28	4,40	3,02	3,35
K ₂ O	2,96	3,27	3,54	3,51
P ₂ O ₅	0,34	0,23	0,21	0,20
Summe	100,00	100,00	100,00	100,00
FeO (tot)	4,69	3,68	4,43	4,76
Nb	8,0	7,0	7,0	6,0
Zr	162	158	157	150
Y	10,0	7,0	12,0	12,0
Sr	763	786	593	536
Rb	84,0	89,0	119,0	101,0
Ga				
Zn	72	66	79	75
Cu	20	41	38	44
Ni	24	9	7	9
Co	29,0	24,0	26,0	27,0
Cr	65	23	11	11
V	111	79	102	113
Ba	1002	1099	1016	913
Sc				
Li7				
Mo				
Cs				
Cd				
La				
Ce				
Pr				
Nd				
Sm				
Eu				
Gd				
Tb				
Dy				
Ho				
Er				
Tm				
Yb				
Lu				
Hf				
Ta				
W				
Pb				
Th				
U				
⁸⁷ Sr/ ⁸⁶ Sr				
Error				
¹⁴³ Nd/ ¹⁴⁴ Nd				
Error				
²⁰⁶ Pb/ ²⁰⁴ Pb				
Error				
²⁰⁷ Pb/ ²⁰⁴ Pb				
Error				
²⁰⁸ Pb/ ²⁰⁴ Pb				
Error				

3.4 Geochemistry

The analyses for major, trace elements, and isotopes were carried out on selected samples from Taapaca volcano and results are presented in Tab. 3-1. The analytical part is explained in the Appendix.

3.4.1 Major and trace elements

The volcanic rocks from Taapaca volcano belong to the high-K calc alkaline series (Fig. 3-2). The volcanic rocks have a narrow range of 60 to 68wt% of SiO₂ (Fig. 3-2) and 5 to 8wt% total alkalis. They represent dacitic composition with only few andesites. Few samples are mafic inclusions (basaltic andesites) with SiO₂wt% of 53.96 to 56.39wt%. The K₂O content ranges between 2.55-3.78 for Taapaca dacites and 1.76-3.23 for the mafic inclusions. Differentiation trend is observed on the base of Harker type diagrams showing the typical positive and negative correlations due to processes of fractional crystallization and/or mixing (Fig. 3-3).

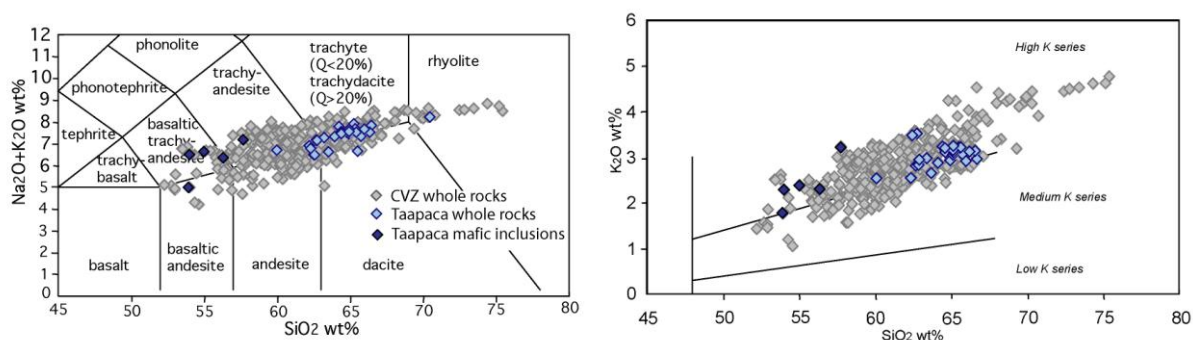


Fig. 3-2 Classification of calc-alkaline series after Le Maitre (1989) for Taapaca volcanics. The oxides contents are recalculated to 100% on volatile-free basis and with all Fe as FeO.

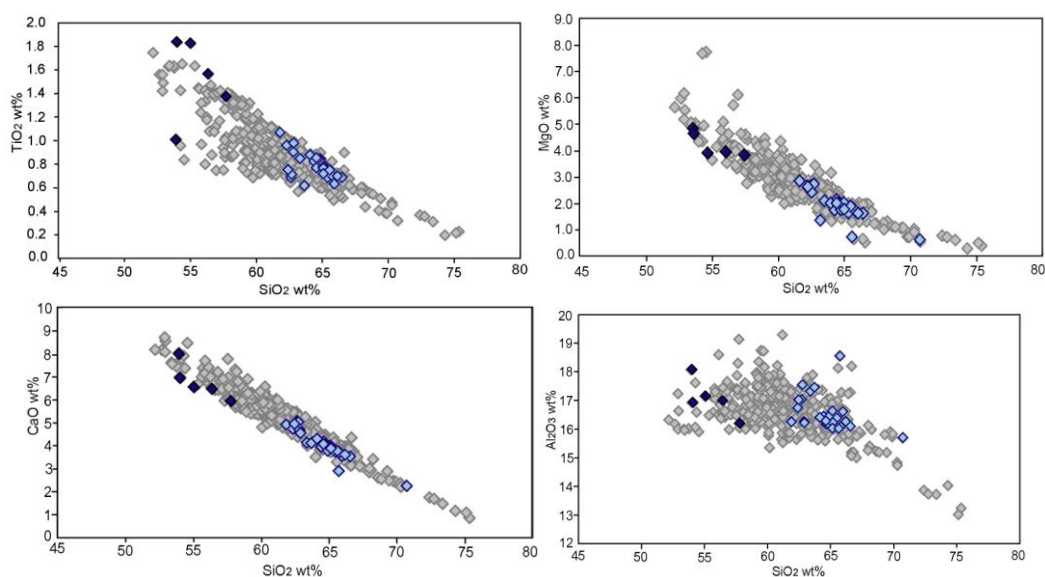


Fig. 3-3 Major element diagrams plotted versus SiO₂ wt % for Taapaca volcanic rocks. Symbols are the same as presented at Fig. 3-2.

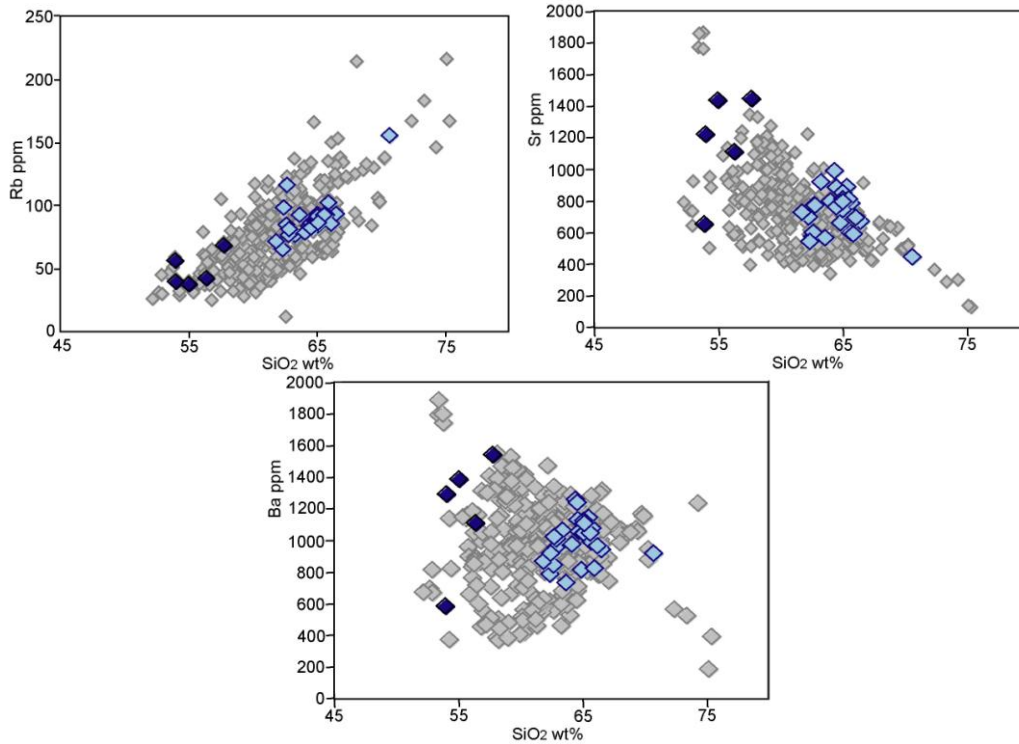


Fig. 3-4 Trace element (ppm) diagrams plotted versus silica content (SiO₂ wt%) for volcanic rocks from Taapaca.

3.4.2 Spider

N-MORB normalized (Sun and McDonough 1989) multi element diagram for Taapaca volcanic rocks is presented on Fig. 3-5. The CVZ data (coloured lines) are plotted on the same diagram as reference. Taapaca rocks shows a typical island-arc basalt characteristic with enrichment in LILE and peaks at K, Sr, Ba but low abundances of high ionic potential elements (Ta, Nb, Ce, P, Zr, Hf, Sm, Ti, Y, Yb) compared to MORB. The enrichment of K, Sr, Rb, Ba U presented on the diagram is due to subduction-zone fluids enriched in LILE. Relative depletion in Nb, Ta is also a characteristic pattern for subduction zone magmas.

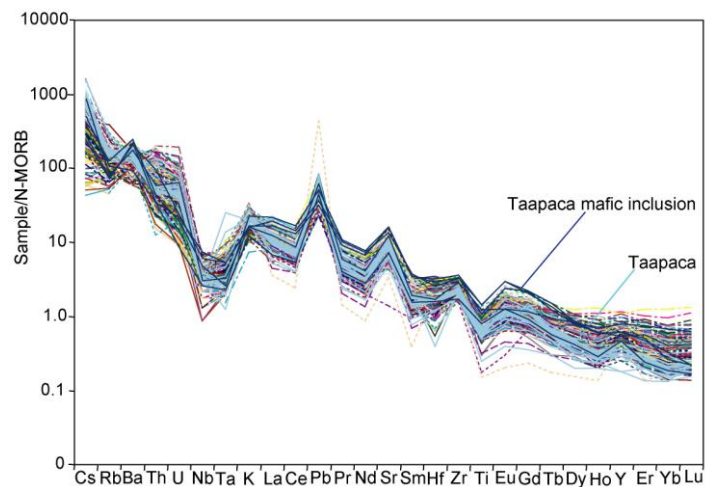


Fig. 3-5 Spider diagram for Taapaca volcanic rocks (light blue lines) and the CVZ volcanic rocks (coloured lines). Normalization after Sun and McDonough 1989.

3.4.3 Rare earth elements

Rare earth element characteristic is presented by the chondrite-normalized plot (Fig. 3-6). Data from the CVZ are plotted as reference. The diagram shows general enrichment of LREE in compare to HREE. Additionally diagram shows strong depletion in HREE (stronger at Taapaca than at El Misti) pointing to the role of garnet in the system at the melting region at Taapaca.

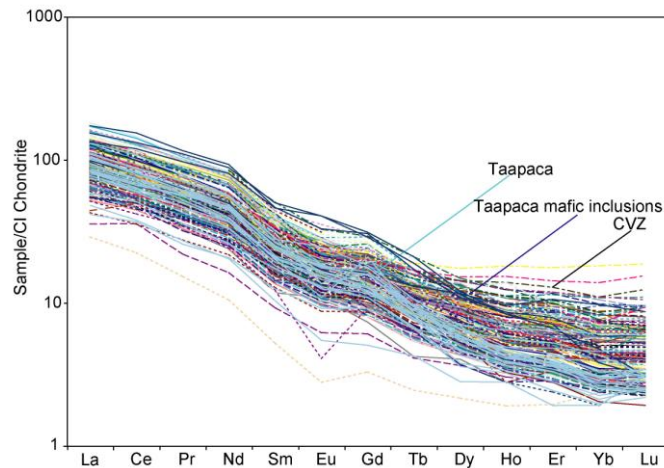


Fig. 3-6 REE-pattern of Taapaca volcanic rocks normalized to C1 (Boyton 1984).

3.4.4 The isotopes (Nd, Sr, Pb)

The isotopic composition of volcanic rocks from the whole CVZ region as explained before is dominated by the crustal contribution to the magmas. The isotopic compositions of Taapaca volcanic rocks are presented at Figs 3-7 together with data from CVZ and basement rocks. The whole rock analyses from Taapaca show enrichment in $^{87}\text{Sr}/^{86}\text{Sr}$ of 0.7065 and 0.7067 (Tap-97-29/1, Tap-002) compared to MORB values. However the Taapaca samples have lower $^{87}\text{Sr}/^{86}\text{Sr}$ isotopic ratios than previously presented rocks from El Misti volcano. The Nd isotopes show ϵNd composition of -5.7 and -6.7 (Tap002, Tap-97-29/1). Higher $^{206}\text{Pb}/^{204}\text{Pb}$ of 18.1 have been measured for the mafic inclusion (Tap-97-29/1) and (Tap-002) at the Taapaca Volcanic Complex.

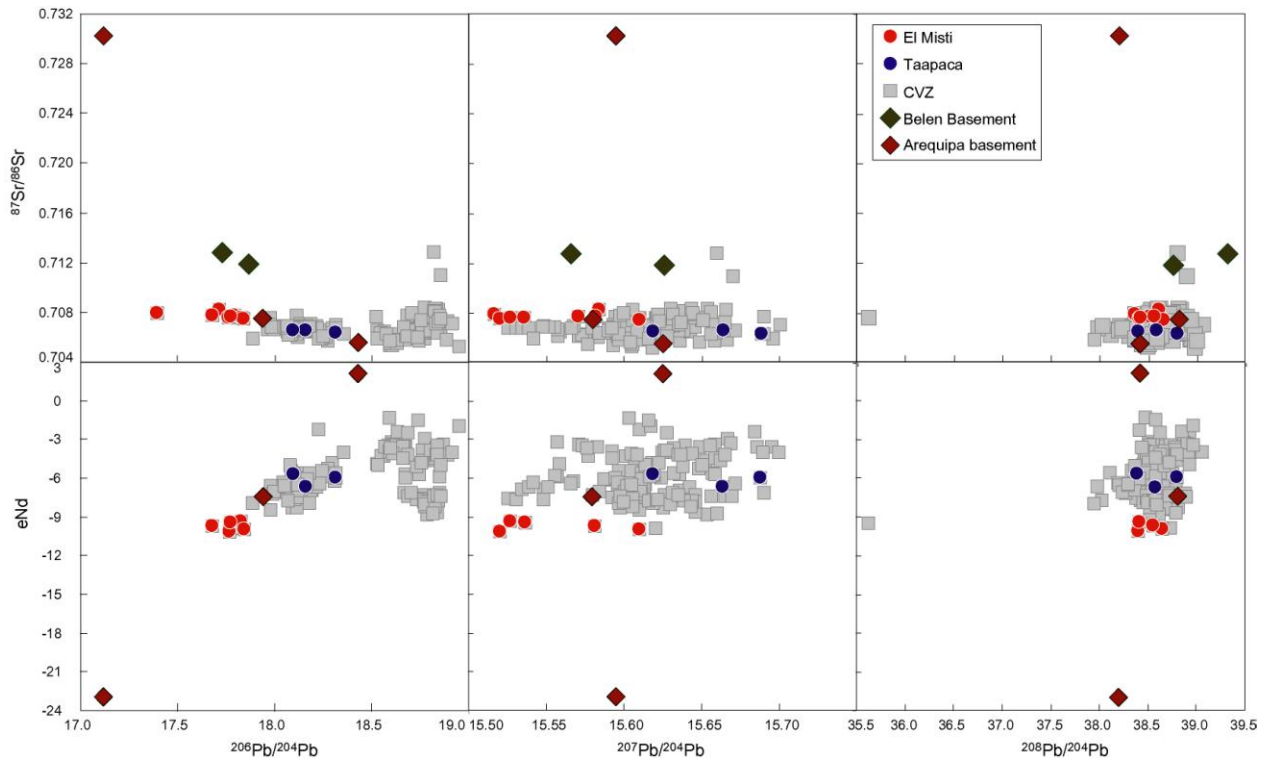


Fig. 3-7 Plot of $\text{Nd}/^{144}\text{Nd}$ versus $^{87}\text{Sr}/^{86}\text{Sr}$ of Taapaca volcanic rocks with isotopic range of CVZ data. El Misti data and Arequipa Basement are plotted for comparison.

3.5 Ar-Ar data

The Ar-Ar method allows small quantities of samples of young volcanic rocks to be dated with a high precision in order to estimate the eruption age (Gansecki et al., 1996; Singer et al., 1996; Singer et al., 1998; Singer and Pringle, 1996).

14 separates of sanidine crystals from samples representing different eruption stages of Taapaca Volcanic Center have been hand-picked, cleaned and prepared for Ar-Ar dating. Samples have been dated (total fusion experiments) in the laboratory of B. Singer at the Department of Geology & Geophysics at University of Wisconsin (USA). The results are listed below in Table 3-2. Results show very big range of eruption ages with oldest samples of 2.1 Ma (TAP-97-40) in the northern part of the edifice and youngest samples of 9.4 ka for the most southern located sample (TAP-87-002).

Additional age information from unpublished Diplomarbeit (Lohnert 1999) has been presented for collecting all possible age information. Analyses include four pieces gained by microsampling from the sanidine megacryst from core to rim and one analyses of plagioclase separates from the host, the dacite lava flow TAP-97-28. Several different zones of the sanidine megacryst (four pieces from core to the rim) were prepared and dated in order to estimate the eruption age and to test for an age “gradient” from core to rim. This is based on the idea that size of the megacryst may allow an at least partial retention of ^{40}Ar in the core. Ar-Ar ages range between 33.0 ± 4.8 ka and 38.6 ± 5.2 ka (2σ errors). The core of sanidine shows an age of 38.6 ± 5.2 ka. An eruption age of 33.2 ± 3.6 ka (MSWD 00.14) is derived from the weighted mean of sanidine sample from the rim and from the plagioclase of the host. The 2σ errors of all samples between core and rim overlap, there is no significant temporal trend.

Tab. 3-2 $^{40}\text{Ar}/^{39}\text{Ar}$ data from total fusion experiments on individual crystals from Taapca lavas and tephtras.

Sample site Experiment no.	material	K/Ca (total)	Steps Used (i.e. not xenocrysts)					Isochron Analysis				
			All Fusions Age (ka)	Laser Pow %	^{39}Ar (%)	Age \pm 2 (ka)	MSWD	N	MSWD	$^{40}\text{Ar}/^{36}\text{Ar}$ \pm 2 intercept	Age \pm 2 (ka)	
TAP-97-41												
UW41E38	sanidine	30,91	3920,0 \pm 110,0	40	87,4	3690,0 \pm 100,0	0,68	5 of 6	0,49	288,3 \pm 12,9	3720,0 \pm 110,0	
TAP-97-40												
UW41E37	sanidine	28,49	2133,3 \pm 53,4	40	87,0	2124,4 \pm 55,2	0,21	4 of 5	0,29	275,9 \pm 189,2	2134,0 \pm 109,0	
TAP-97-17												
UW41D33	sanidine	27,72	953,0 \pm 30,9	40	100,0	954,1 \pm 29,5	0,34	5 of 5	0,45	293,1 \pm 39,7	958,3 \pm 75,8	
TAP-97-18												
UW41E34	sanidine	54,11	931,8 \pm 25,6	40	100,0	937,2 \pm 28,3	1,69	4 of 4	0,35	514,4 \pm 320,2	819,4 \pm 165,0	
TAP-97-22												
UW41E35	sanidine	19,68	916,7 \pm 27,0	40	100,0	921,6 \pm 29,8	1,53	4 of 4	2,11	303,0 \pm 38,5	909,9 \pm 68,6	
TAP-97-11												
UW41D32	sanidine	53,13	405,9 \pm 16,9	40	100,0	401,7 \pm 18,3	1,39	6 of 6	0,68	305,6 \pm 10,2	388,4 \pm 21,1	
TAP-97-01												
UW41D31	sanidine	67,64	67,5 \pm 51,3	40	100,0	61,3 \pm 49,7	0,77	5 of 5	0,05	440,9 \pm 253,1	-19,1 \pm 84,8	
TAP-02-02A												
UW46B37	sanidine	53,89	48,8 \pm 27,1	40	100,0	46,0 \pm 11,0	0,14	7 of 7	0,17	295,7 \pm 4,1	45,9 \pm 12,4	
TAP-97-45												
UW41E39	sanidine	59,96	45,0 \pm 16,2	40	100,0	43,8 \pm 13,8	0,77	5 of 5	1,01	296,6 \pm 28,2	43,7 \pm 16,0	
TAP-97-34												
UW41E36	sanidine	45,85	28,7 \pm 14,6	40	88,8	33,3 \pm 15,9	0,25	5 of 6	0,33	293,2 \pm 141,4	34,3 \pm 38,3	
TAP-97-06												
UW46B35	sanidine	43,49	36,3 \pm 38,6	40	100,0	31,0 \pm 20,0	0,18	7 of 7	0,22	295,4 \pm 3,8	31,7 \pm 24,5	
TAP-97-29												
UW46B36	sanidine	41,61	27,1 \pm 9,1	40	88,4	16,5 \pm 5,9	0,72	7 of 8	0,71	301,8 \pm 14,5	12,8 \pm 8,1	
TAP-87-002												
UW46B34	sanidine	81,33	15,5 \pm 8,6	40	100,0	11,4 \pm 6,4	1,08	8 of 8	1,09	298,0 \pm 5,1	9,4 \pm 5,5	

^aAges calculated relative to 1.194 Ma Alder Creek Rhyolite sanidine standard.

3.6 U-Th isotopes

3.6.1 Whole rock data

Th concentration for Taapaca whole rocks samples ranges from 4.07 ppm to 16.5 ppm (ICP-MS, Tab. 3-1). The U concentration ranges from 1.3 to 4.7 ppm for Taapaca dacitic samples and of 0.40 ppm for the mafic inclusions (basaltic andesites). The Th/U ratios range between 2.21 to 5.46 for samples from Taapaca with extremely high value of 10.27 for the mafic inclusion.

The results of the U-Th isotope measurements on the whole-rock samples from Taapaca volcano are given in Tab. 3-3 and by the aquiline diagram ($^{238}\text{U}/^{232}\text{Th}$ versus $^{230}\text{Th}/^{232}\text{Th}$, Fig. 3-8). The Taapaca samples show mostly equilibrium values for some whole rock analyses. The whole rock ($^{230}\text{Th}/^{238}\text{U}$) activity ratios range between 0.94 and 1.024, and the value of 1.067 for the mafic inclusion. Group of younger samples show low ^{238}U enrichment and ($^{230}\text{Th}/^{238}\text{U}$) activity ratio of 0.94-0.99. Furthermore the samples show eruption age corrected ($^{230}\text{Th}/^{232}\text{Th}$) activity ratios between 1.02 and 1.033, but much lower value of 0.66 for the mafic inclusion. The ($^{230}\text{Th}/^{238}\text{U}$) activity ratios for most of the samples of Taapaca Volcano cluster around the value of 1. However the very high ($^{230}\text{Th}/^{232}\text{Th}$) activity ratios are at the

same time the highest measured values for the whole CVZ being the upper bordering ($^{230}\text{Th}/^{238}\text{U}$) signature.

The ($^{234}\text{U}/^{238}\text{U}$) activity ratios are in equilibrium giving proof that the U systematic has not been disturbed by interaction with ground or meteoric water.

Tab. 3-3 U and Th concentrations and ($^{238}\text{U}/^{230}\text{Th}$) activity ratios for Taapaca volcanic rocks. ($^{230}\text{Th}/^{232}\text{Th}$) activity ratio is given as eruption age corrected.

Sample	[Th] $\mu\text{g/g}$	[U] $\mu\text{g/g}$	($^{238}\text{U}/^{232}\text{Th}$)	($^{230}\text{Th}/^{232}\text{Th}$)	($^{230}\text{Th}/^{238}\text{U}$)	($^{234}\text{U}/^{238}\text{U}$)
TAP-87-002	6,62	2,79	1,280 \pm 6	1,296 \pm 20	1,013 \pm 10	0,983 \pm 13
TAP-97-06	4,10	1,92	1,419 \pm 5	1,355 \pm 10	0,940 \pm 8	0,974 \pm 10
TAP-97-17	6,24	2,53	1,230 \pm 8	1,230 \pm 11	0,962 \pm 11	0,986 \pm 16
TAP-97-18	6,31	2,09	1,002 \pm 8	1,023 \pm 19	1,023 \pm 21	1,014 \pm 16
TAP-97-28	6,60	2,83	1,303 \pm 5	1,309 \pm 13	1,007 \pm 10	1,007 \pm 10
TAP-97-37	6,14	2,17	1,073 \pm 5	1,072 \pm 8	0,981 \pm 9	0,998 \pm 11
TAP-97-37/1	4,09	0,89	0,657 \pm 4	0,658 \pm 20	1,067 \pm 32	1,040 \pm 11
TAP-97-40	12,60	4,79	1,153 \pm 12	1,153 \pm 36	1,014 \pm 33	0,992 \pm 10
TAP-97-48	6,70	3,03	1,374 \pm 4	1,346 \pm 5	0,969 \pm 5	0,995 \pm 11
TAP-97-34	6,84	2,94	1,305 \pm 6	1,298 \pm 12	0,993 \pm 10	0,992 \pm 12

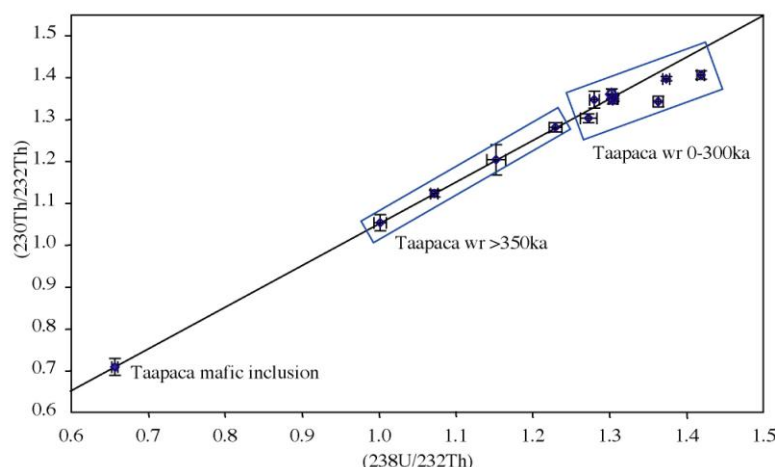


Fig 3-8 U-Th equiline diagram for whole rocks from the Taapaca volcano.

3.6.2 Mineral separates

Isotopic composition of U and Th was measured on the mineral separates of magnetite, amphibole, biotite, sphene, and apatite. Unfortunately not all prepared mineral separates could be measured. Difficulties at the preparation stage (dissolution) and during the measuring procedure (look Appendix for analytical explanations) disabled the use of all samples as reliable results. Mineral separates on sample TAP-02-01 were measured only for two phases (sphene and biotite + whole rock) from which the biotite has extremely big error. Mineral separates from sample TAP-02-02 have unreliable results due to significant remnants and not complete dissolutions of amphibole, biotite, and magnetite. Some of the samples could not be measured with enough precision or failed during measurement (1-3 blocks measured). All available results for mineral separates are listed in Tab. 3-4 and presented on the Fig 3-9.

The Th concentration in mineral separates ranges from 0.69ppm in biotite (Tap-02-02 bt,) to 102.94ppm in sphene (Tap-02-01sph). U concentration is between 0.32 ppm in biotite (Tap-02-02bt) to 30.81ppm in sphene (Tap-02-01 sph).

Reliable data of U-Th isotopic composition from minerals come only from separates from sample Tap-02-03 and therefore only these results are taken into account in the discussion. The mineral separate ($^{230}\text{Th}/^{238}\text{U}$) signature for amphibole, magnetite, and apatite (Tap-02-03) is characterized by ^{238}U enrichment with ($^{230}\text{Th}/^{238}\text{U}$) activity ratios between 0.978 for magnetite to 1.88 in sphene. Measured values for sphene characterize ^{230}Th enrichment of 9% (Fig. 3-10).

The mineral internal isochrone on sample Tap-02-03 (dacite) give an age of 171ka \pm 26ka, which is significantly older than eruption age of the whole rock (12+-8.1 ka).

Tab. 3-4 U-Th isotopic composition for whole rocks and mineral separates from Taapaca dacites. Abbreviations: wr-whole rock, mt-magnetite, amph-amphibole, sph-sphene, ap-apatite.

Sample (lab code)	[Th] $\mu\text{g/g}$	[U] $\mu\text{g/g}$	($^{238}\text{U}/^{232}\text{Th}$)	($^{230}\text{Th}/^{232}\text{Th}$)	($^{230}\text{Th}/^{238}\text{U}$)	($^{234}\text{U}/^{238}\text{U}$)
Tap-02-01 wr (451)	7.66	3.21	1.27 \pm 11	1.252 \pm 10	0.982 \pm 10	0.995 \pm 19
Tap-02-01 mt (456)	2.57	1.12	1.32 \pm 6	1.267 \pm 9	0.958 \pm 9	0.989 \pm 10
Tap-02-01 amph (455)	2.06	1.04	1.52 \pm 8	1.192 \pm 11	0.763 \pm 8	0.993 \pm 15
Tap-02-01 sph (458)	102.94	30.81	0.91 \pm 7	1.013 \pm 5	1.126 \pm 10	0.992 \pm 12
Tap-02-01 ap (457)	6.92	3.40	1.49 \pm 11	1.528 \pm 29	1.026 \pm 21	0.974 \pm 17
Tap-02-01 bt (459)	0.83	0.44	1.62 \pm 40	1.429 \pm 14	0.869 \pm 23	-
Tap-02-02 wr (449)	6.28	2.70	1.31 \pm 6	1.299 \pm 7	0.994 \pm 7	0.995
Tap-02-02 mt (400)	2.74	-	-	-	-	-
Tap-02-02 mt (451)	3.20	-	-	-	-	-
Tap-02-02 amph (450)	-	1.02	-	-	-	-
Tap-02-02 sph (453)	22.98	7.22	0.95 \pm 14	1.024 \pm 21	1.099 \pm	0.974
Tap-02-02 ap (452)		7.43	-	-	-	0.992
Tap-02-02 bt (411)	0.69	0.32	1.36 \pm 15	1.383 \pm 121	1.024 \pm 90	1.006
Tap-02-02 bt (461)	0.76	-	-	-	-	-
Tap-02-03 wr (564)	4.77	2.14	1.36 \pm 6	1.291 \pm 13	0.94 \pm 11	1.011 \pm 5
Tap-02-03 mt (565)	1.59	0.71	1.35 \pm 8	1.321 \pm 12	0.978 \pm 11	0.988 \pm 17
Tap-02-03 amph (566)	2.06	0.71	1.05 \pm 7	1.127 \pm 10	1.086 \pm 12	0.999 \pm 12
Tap-02-03 sph (568)	1.79	0.55	0.93 \pm 3	0.999 \pm 12	1.088 \pm 10	1.002 \pm 18
Tap-02-03 ap (569)	2.79	1.44	1.56 \pm 5	1.542 \pm 14	0.984 \pm 10	0.990 \pm 35

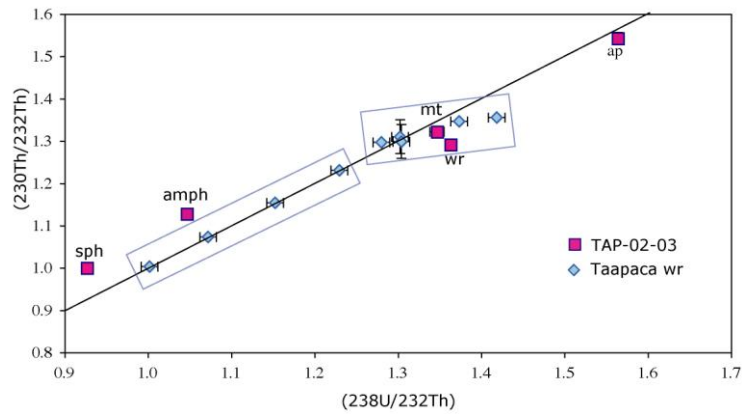
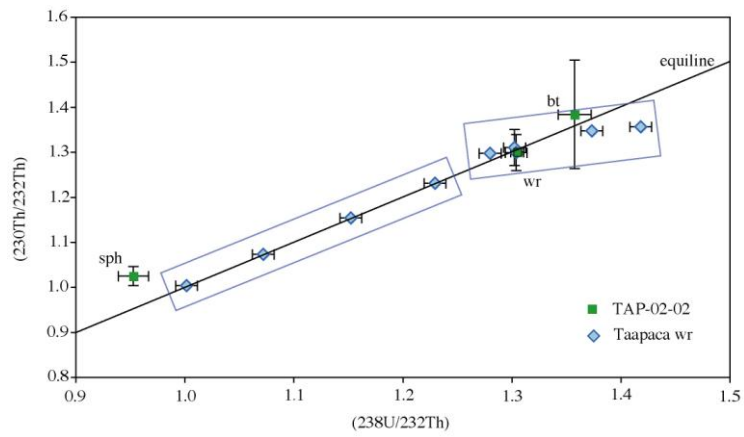
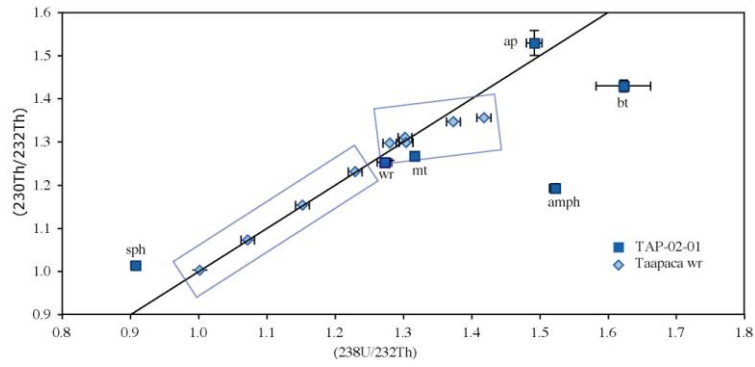


Fig 3-9 Equiline diagram for Tap-02-01, Tap-02-02, Tap-02-03 dacite samples from Taapaca volcano, for separate minerals of magnetite-mt, amphibole-amph, sphene-sph, apatite-sp and whole rock-wr.

4 Discussion

Subduction zones represent the areas with very complex tectonic and petrologic settings. Several components are involved in magma genesis in these environments: peridotitic mantle wedge, subducted altered oceanic crust plus sediment, fluids expelled from the down going slab, and a thick continental crust (Bourdon et al., 2000, Bourdon et al., 2003). Since melt generation and segregation as well as magma evolution involve all these lithologic varieties, the chemical and isotopic complexity of erupted lavas is wide. In this study, combined major and trace element as well as isotope data are used to constrain the petrogenesis of lavas of two volcanic centers El Misti and Taapaca.

In order to have closer look to the processes involved in the El Misti and Taapaca volcanic rocks, qualitative and quantitative modelling is employed below. Geochemical modelling of these systems is hampered by the fact that there is no primitive mantle derived magma present in the Central Volcanic Zone. All erupted volcanics are already affected by assimilation and fractionation on their way through 70km thick crust.

4.1 Whole rock U-Th signatures of El Misti, Taapaca and other CVZ volcanics.

Fig. 4-1 presents the equiline diagram with U-Th data of rocks from the CVZ (Mercier unpublished data, grey circles) with samples from two studied volcanoes El Misti (red circles, this study) and Taapaca Volcanic Center (blue diamonds, this study). Data from Marianas (black squares, Elliot et al., 1997) and MORB (dark red crosses, Goldstein et al., 1989) are plotted for reference.

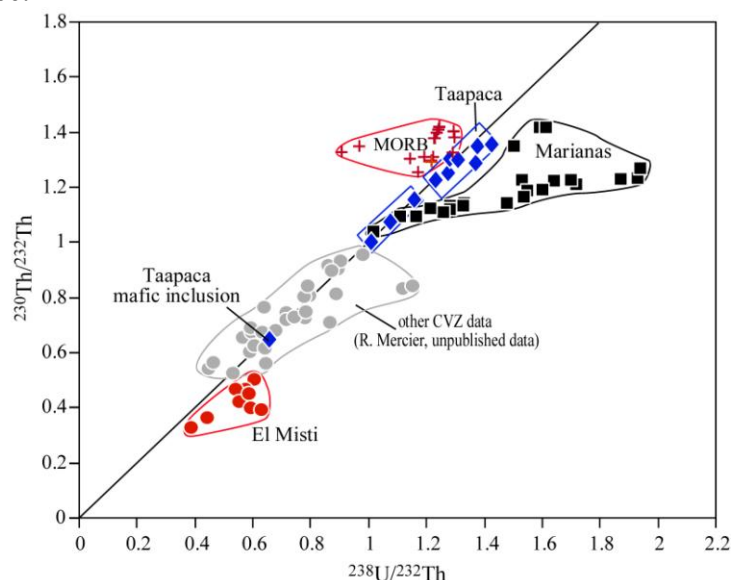


Fig. 4-1 Equiline diagram for whole rocks from the Central Volcanic Zone. Red circles represent El Misti whole rock data, blue diamonds are for Taapaca samples. The data of Mariana arc (Elliot et al., 1997) and MORB (Goldstein et al., 1989) are plotted as reference.

The ($^{230}\text{Th}/^{232}\text{Th}$) values of volcanic rocks from the CVZ show in Fig. 4-1 cover a wide range of activity ratios from 0.325 to 1.346. The majority of samples from the CVZ are lower in ($^{230}\text{Th}/^{232}\text{Th}$) than MORBs and also lower than Mariana island arc volcanics. Only the

Taapaca Volcanic Complex is characterised by high Th activity ratios similar to that of MORB and Marianas. The Taapaca values are also the highest in the whole CVZ. In contrast, the El Misti volcanic rocks have the lowest ($^{230}\text{Th}/^{232}\text{Th}$) activity ratios ($(^{230}\text{Th}/^{232}\text{Th})=0.325$) among the CVZ data. The Taapaca with the highest and El Misti with the lowest values could be treated therefore as “end member U-Th signatures” of the Central Volcanic Zone.

The majority of the volcanic rocks from the CVZ plot along the equiline with ($^{230}\text{Th}/^{238}\text{U}$) within or close to equilibrium. However, some volcanic centers (Licancabur, Lascar, Mercier unpublished data) are characterised by significant ^{238}U enrichment. In contrast, samples from e.g. San Pablo San Pedro, Andagua, and Ubinas (Mercier unpublished data) show ^{230}Th excesses and, in addition, data from e.g. Parinacota show both ^{230}Th and ^{238}U enrichment for different volcanic stages (Bourdon et al., 2000).

The ^{238}U excesses in subduction zone settings are typically explained by the addition of fluids from the subducted oceanic lithosphere to the mantle wedge (Gill and Williams 1990; Turner et al., 2003; Turner and Hawkesworth 1997; Elliot et al., 1997; Turner et al., 1997, 2000; Hawkesworth et al., 1997; Allegre and Condomines 1976). The mechanism to produce ^{230}Th excesses is more complex. In the petrogenetic model of Cotopaxi Volcano in Southern Volcanic Zone (Garrison et al., 2006), low to moderate degrees (up to 20%) of melting of eclogite or meta-pelitic schists in the lower crust was suggested to generate magmas that have ^{230}Th excesses (Garrison et al., 2006).

4.2 The U-Th fractionation in subduction zones as recent event

It has been suggested that global U-Pb-U-Th and Th-Sr isotope systematics require a recent U-Th fractionation in subduction zone lavas (e.g. Bourdon et al., 2003).

In a $^{208}\text{Pb}^*/^{206}\text{Pb}^*$ versus Th/U diagram (Fig. 4-2), the mantle array defined by OIB and MORB is presented (Allégre et al., 1986; Gill and Williams, 1990; McDermott and Hawkesworth, 1991). From this figure, it can be seen that subduction zone lavas do not fall on this mantle array and that recent addition of U is required. The El Misti and Taapaca lavas together with other CVZ magmas plot on an array that is rather oblique to the mantle array. The explanation for this could be that recent addition of U rich fluids reduced the Th/U ratio of the erupted lavas, or assimilated meta-sediments contributed some Th.

In Parinacota lavas, the Pb isotope ratios are markedly unradiogenic in $^{206}\text{Pb}/^{204}\text{Pb}$ (Bourdon et al., 2000) but have relatively high $^{208}\text{Pb}^*/^{206}\text{Pb}^*$. The basement under Belèn is also characterized by unradiogenic $^{206}\text{Pb}/^{204}\text{Pb}$ and high Th/U. The isotopic composition of Pb at Taapaca is similar to that of Parinacota. The fact that El Misti also has significantly higher $^{208}\text{Pb}^*/^{206}\text{Pb}^*$ could point to crustal contribution and, thus, suggests recent U-Th fractionation.

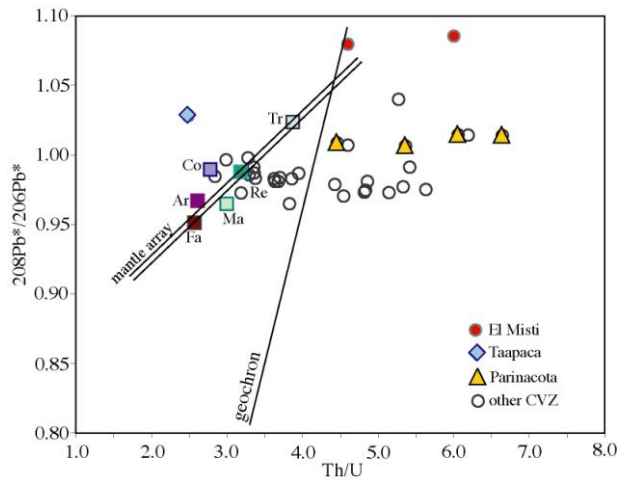


Fig. 4-2 $^{208}\text{Pb}^*/^{206}\text{Pb}^*$ versus Th/U for El Misti and Taapaca volcanics. The mantle array (Allegre et al., 1986) and Parinacota (Bourdon et al., 2000) are plotted as references. Abbreviations: Ar- Ardoukoba, Atlantic Ridge; Fa- Fayal Azores, Atlantic Ocean; Ma- Marion, Indian Ocean; Co- Karthala, Comores, Indian Ocean; Re- Reunion, Indian Ocean; Tr- Tristan de Cunha, Atlantic Ocean come from Allegre et al., (1986).

4.3 Crustal involvement

The very thick continental crust already has been suggested to be involved in the petrogenesis of volcanics erupted along the arc in the Andes (Hildreth and Moorbath 1988). The main evidence for crustal contamination comes from Pb and Sr isotopes. It has been shown that Pb isotope composition of erupted lavas correlate along the CVZ with the composition of crustal rocks of the basement (Wörner et al., 1992, Aitchison et al., 1995). However, the nature and the location of the interaction between mantle-wedge melts and crustal rocks are still not known exactly.

A further characteristic feature for erupted volcanics at the CVZ is their restricted Pb and Sr isotopic composition. In Fig. 4-3 ($^{87}\text{Sr}/^{86}\text{Sr}$ versus $^{206}\text{Pb}/^{204}\text{Pb}$), samples from El Misti and Taapaca plot similar to Parinacota lavas suggesting similar crustal involvement when compared to fields of MORBs and OIBs.

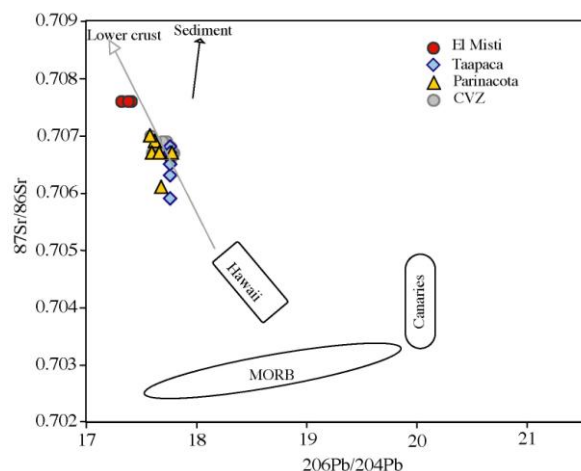


Fig. 4-3 $^{87}\text{Sr}/^{86}\text{Sr}$ versus $^{206}\text{Pb}/^{204}\text{Pb}$ show the island basalts and MORB magmas according to Sr and Pb characteristic. The Parinacota data (Bourdon et al., 2000) is plotted as reference. MORB and OIB data are from Allegre et al., 1986.

4.4 Fluid addition

El Misti and Taapaca volcanics show several of typical signatures related with subduction magmatism (e. g. LILE enrichment relative to HFSE, partly ^{238}U excesses). A distinguishing feature that could bring information about an extend, to which U-enriched expelled fluids are involved, is the correlation of ^{238}U excesses with Ba/Hf ratios. Fig. 4-4 presents the correlation between the U-Th isotopes and trace element ratios for El Misti and Taapaca volcanics. A correlation exists for El Misti magmas roughly pointing in the direction of slab-derived fluids. No such strong correlation exists for the Taapaca volcanics.

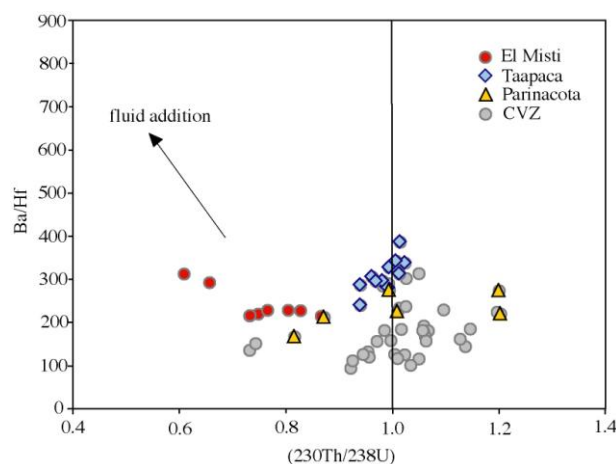


Fig. 4-4 Ba/Hf versus ($^{230}\text{Th}/^{238}\text{U}$) for El Misti and Taapaca magmas pointing to fluid component at El Misti lavas.

4.5 Components involved in magma genesis at the CVZ.

Many recent studies have argued that at least 3 components are involved in magma genesis in the most arc lavas: depleted peridotite, fluids derived from altered upper oceanic crust and from the subducted sediment layer (Kay 1980; Miller et al., 1994; Turner et al., 1996, 1997; Elliot et al., 1997; Hawkesworth et al., 1997a). This study considers 4 input parameters using additionally crustal component in the source of magma to explain magma composition at El Misti and at Taapaca volcanoes.

Crustal component as a source contaminant

The involvement of crustal rocks at magma petrogenesis at the CVZ volcanoes is unquestionable (Davidson et al., 1990, Wörner et al., 1992). However, the unusual idea of this study is to put few % of crust into the mantle wedge.

The argument to use crustal component as one of the contaminant in the source of magma in the mantle wedge beneath El Misti and Taapaca volcanic centers, is based on two aspects: 1) a simple assimilation processes in the crust (AFC) is not able to explain low ($^{230}\text{Th}/^{232}\text{Th}$) of El Misti lavas unless the assimilation $>50\%$, what is unreasonable; 2) Oxygen isotope data of El Misti and Taapaca volcanics suggest source contamination by the crust of up to 7% (Yu-Hsuan Hang 2007).

The precise pointing of contaminating rocks is still not so straightforward. The database of Arequipa Basement compositions is presented in the Appendix (Arequipa Basement Table 6-3). The Oxygen isotope data (Yu Hsuan Hang 2007) suggest the Mollendo basement rocks as

major crustal source contaminant. However, to be able to explain the Th isotopic composition at El Misti, sample with the lowest ($^{230}\text{Th}/^{230}\text{Th}$) activity ratio (0.2) of all available data from Arequipa Basement (the Charcani Gneisses) has been used in the modelling for U-Th isotopes (Tab. 6-3 Appendix). For the modelling of major and trace elements the average of available basement rocks was introduced.

At Fig. 4-5, a simple relation of U-Th signatures between DMM (depleted MORB mantle) mixed with Arequipa Basement (Charcani gneisses) is presented. About 1% of crust mixed with Depleted MORB Mantle extremely pulls the ($^{230}\text{Th}/^{232}\text{Th}$) to the values below 0.4 (enough to explain the low El Misti Th isotopes). An order of magnitude higher concentration of crustal rocks in compare to the content in the mantle allows for overprinting the DMM signature. The way to introduce the crustal material into the source of magma could be explained e.g. by subducted erosional material (e. g. Stern 1991, von Huene et al., 1999).

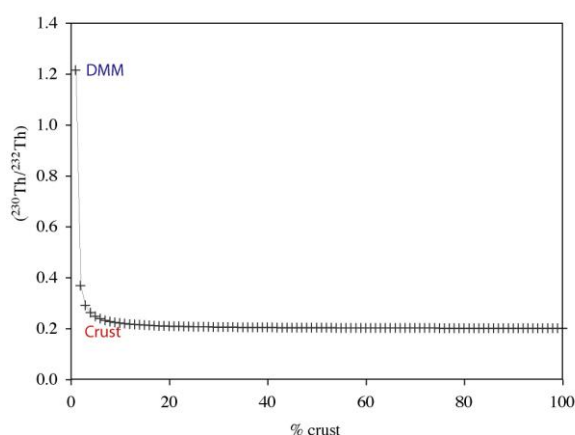
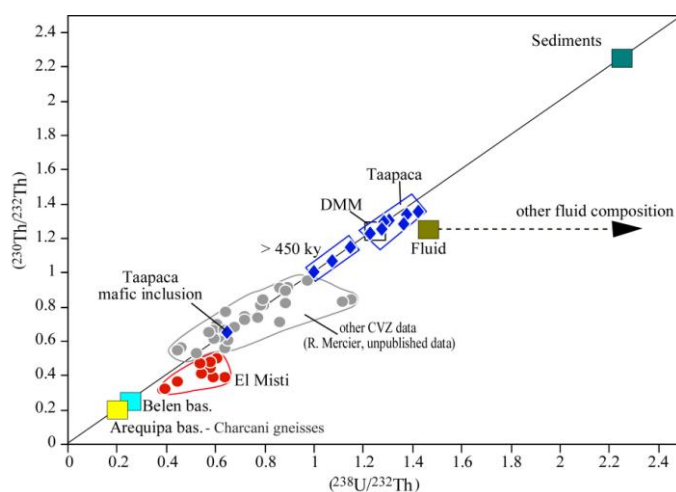


Fig. 4-5 Diagram presenting mixing of Depleted MORB mantle (DMM, data from Workmann et al., 2005) with crust.

Fig. 4-6 presents the 4 input parameters plotted at the equiline diagram together with whole rock data from El Misti and Taapaca Volcanic centers according to their U-Th isotope signatures.



- **Fig. 4-6 Equiline diagram showing the composition of whole rock data from El Misti and Taapaca along with input data for the 4 components involved. See text for source of data and Appendix Tab. 6-3 for the Arequipa Basement (Charcani gneisses).**

Depleted mantle corresponds to an average Depleted MORB Mantle (DMM), with composition taken from Workman et al 2005.

Fluid composition generated by the breakdown of hydrous phases in the basaltic portion of the subducted slab was assumed to be identical to subducted oceanic crust in sense of isotopic composition (MORB + altered oceanic crust, 9:1, estimations similar to McCulloch and Gamble 1990). Pb isotopes of fluid are identical to MORB composition. Major elements were taken from Manning 2004 (MORB-based model eclogite). Trace element concentrations of the fluid phase were determined by applying simple batch equilibrium melting, given by

$$C^{\text{fluid}}=C_o/(F+(1-F)*D)$$

where C_{fluid} is the concentration in the slab-derived fluid, C_o is the initial concentration in the bulk reactants, F is the mass fraction of fluid, and D is the solid/fluid partition coefficient. The solid phase from which the fluid was expelled was assumed to be eclogitic composition consisting of 40% of garnet and 60% of clinopyroxene.

Mineral-fluid partition coefficients for garnet and clinopyroxene were compiled from the literature (Brenan et al., 1995, Stalder et al., 1998, Ayers et al., 1997 and Keppler 1996).

Sediment composition subducted beneath the CVZ was calculated by taking 1:1 mixture of clay and carbonate ooze. The data used for modelling was compiled from literature (major elements: Plank and Langmuir 1993, trace elements: Hole et al., 1984; Böstrom et al., 1976, rare earth elements: Otman et al., 1986, isotopic composition of Pb and Nd: Otman et al., 1986, Sr isotopes: Unruh et al., 1976 mixed with data for modern-ocean seawater).

Crust composition involved in magma genesis in the CVZ was estimated separately for El Misti and Taapaca due to the different basement domains (Mamani 2006) under both studied volcanic centers.

- a. For El Misti volcano the crust composition was taken as equivalent to the average of amphibolites and gneisses around Arequipa and Mollendo on the coast. However for U-Th isotopes the sample with lowest Th activity ratio (Charcani gneisses) needed to be used in order to explain the low Th isotopes at erupted volcanic rocks.
- b. The composition of crustal component under Taapaca volcano was calculated by taking estimated amount of 10%amphibolite+40%gneiss+50%ampibolite and gneiss (Wörner personal communication) with major and trace element and isotopic compositions based on data from Mamani 2006, Wörner et al., 2000 and Loewy et al., 2004 for the Bélen basement.

The results of this compilation are presented in Tab. 4-1 for the major elements and in Tab. 4-2 are given for the trace elements and isotopes. Additionall data for Arequipa Basement rocks is presented in the Appendix (Tab 6-3).

Tab. 4-1 The composition of major elements for input parameters used in modelling.

Element	Depleted MORB Mantle	Fluid	Sediment Peru trench	Avg- Arequipa basement	Belén basement
SiO ₂	45,08	40,01	45,08	66,19	59,33
TiO ₂	0,13		0,42	0,44	0,88
Al ₂ O ₃	4,01	0,15	8,85	16,67	16,84
Fe ₂ O ₃				4,28	2,96
FeO	8,25		6,50	0,00	5,10
MnO	0,13		0,58	0,097	0,16
MgO	39,05	0,000075	2,43	1,91	3,75
CaO	3,20	0,84	32,89	4,45	6,41
Na ₂ O	0,13	59,00	1,72	3,64	2,75
K ₂ O	0,01		1,29	2,17	1,68
P ₂ O ₅	0,02		0,25	0,14	0,13
Total	100,00	100,00	100,00	100,00	100,00

Tab. 4-2 The composition of trace elements and isotopes for input parameters used in modelling.

Element	Depleted MORB Mantle	Fluid	Sediment Peru trench	Avg- Arequipa basement	Belén basement
Rb	0,05	4,72	12,5	61,25	44,89
Sr	7,66	326	893	304	329
Ba	0,56	712	6381	588	546
La	0,19	4,629	34,81	25,33	16,78
Ce	0,55	12,22	58,48	47,45	30,91
Nd	0,58	6,16	36,71	21,59	13,70
Sm	0,24	1,42	7,95	3,03	2,88
Eu	0,096	0,22	1,84	0,96	0,77
Gd	0,36	0,484	7,65	2,33	2,34
Dy	0,51	0,234	7,06	2,15	2,49
Er	0,35	0,085	4,04	1,12	1,41
Yb	0,36	0,048	3,70	1,20	1,43
Lu	0,06	0,006	0,58	0,19	0,22
Nb	0,15	4,865	3,25	7,67	12,08
Zr	5,08	7,263	76,5	117,00	140,78
Hf	0,16	0,213	2	1,37	0,64
Pb	0,02	14,097	37,68	13,05	5,08
Th	0,0079	0,569	5,30	3,56	3,67
U	0,0032	0,275	1,37	0,53	0,17
⁸⁷ Sr/ ⁸⁶ Sr	0,70263	0,70283	0,70985	0,72588	0,71234
¹⁴³ Nd/ ¹⁴⁴ Nd	0,51313	0,51313	0,51234	0,51199	0,51188
²⁰⁶ Pb/ ²⁰⁴ Pb	18,27	18,3	18,48	17,83	17,71
²⁰⁷ Pb/ ²⁰⁴ Pb	15,49	15,49	15,52	15,60	15,60
²⁰⁸ Pb/ ²⁰⁴ Pb	37,89	37,89	38,13	38,47	39,13
(²³⁸ U/ ²³² Th)	1,214	1,46	2,25	0,45	0,25
(²³⁰ Th/ ²³² Th)	1,214	1,25	2,25	0,45	0,25
(²³⁰ Th/ ²³⁸ U)	1,00	0,853	1,00	1,00	1,00

El Misti and Taapaca whole rock analyses are presented in Fig. 4-7 and Fig. 4-8 in the form of equiline diagrams along with the 4 components considered to be involved in the CVZ magma generation and evolution.

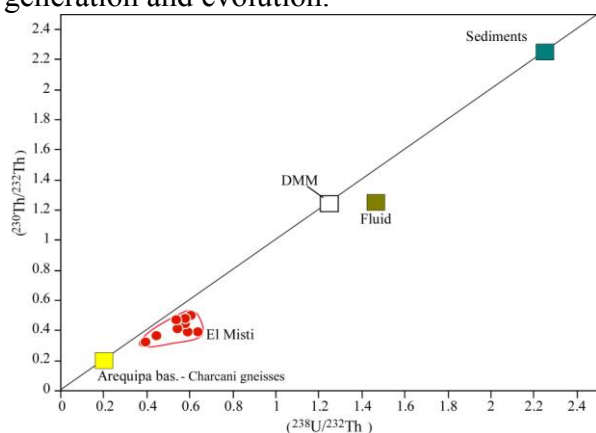


Figure 4-7 Equiline diagram for El Misti whole rock analyses and 4 input parameters: depleted MORB mantle -DMM, Fluids, Arequipa Basement – Arequipa bas-Charcani gneisses (Tab. 6-3 Appendix), and Sediments included in modelling, look in text for derivation of the parameters (look text for data source).

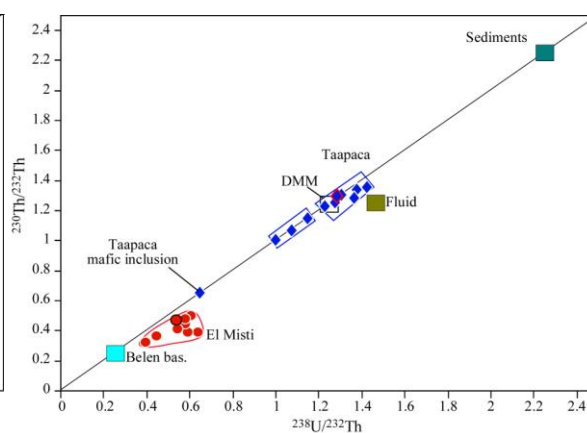


Fig. 4-8 Equiline diagram for Taapaca volcanic rocks and parameters involved in magma genesis (look text for derivation of the parameters and data source).

A remarkable feature of the U-Th signatures of El Misti volcanic rocks is their having very low ($^{230}\text{Th}/^{232}\text{Th}$) activity ratios. In addition, El Misti samples are characterized by ($^{230}\text{Th}/^{238}\text{U}$) disequilibria with ^{238}U excesses of up to 40%. These two observations seem to be characteristic for the El Misti volcanics investigated here. The observed low ($^{230}\text{Th}/^{232}\text{Th}$) activity ratios at El Misti rocks are probably due to the incorporation of a component with adequately low ($^{230}\text{Th}/^{232}\text{Th}$) activity ratios. A likely candidate is the Arequipa crustal basement with its ($^{230}\text{Th}/^{232}\text{Th}$) = 0.2). It is quite convincing this type of basement plays a significant role in the evolution of El Misti magmas. An additional argument for involvement of such crust comes from Pb, Sr (Davidson et al., 1990, Wörner et al., 1992) and Oxygen isotopes, which strongly point to significant crustal involvement on magmas from this region (Yu-Hsuang Hang 2007).

Second deciding component at El Misti lavas is the one that brings U addition into the system.

The samples from Taapaca plot close to equilibrium line. Two different groups can be distinguished: i) a group of older rocks (300-900ka) with lower ($^{230}\text{Th}/^{232}\text{Th}$) and ($^{230}\text{Th}/^{238}\text{U}$) within equilibrium and ii) a group of younger samples having higher ($^{230}\text{Th}/^{232}\text{Th}$) and partly ^{238}U enrichment. The rocks from the first group are old enough so that U-Th disequilibrium already decayed back to secular equilibrium. The relatively high ($^{230}\text{Th}/^{232}\text{Th}$) activity ratios of both groups must be controlled at Taapaca by the end-member with a high Th activity ratio. The relevant component with $^{230}\text{Th}/^{232}\text{Th} > 1.4$ relates to sediment. Therefore, for Taapaca samples significant contributions of pelagic sedimentary material are suggested to be involved in magma evolution.

4.5.1 Mass balance calculation

The quantitative modelling has been done on two samples. For El Misti the El Misti Flow was chosen, for Taapaca it is sample TAP-87-002. The respective chemical and isotope data have already been compiled in Tab. 4-1 and Tab. 4-2 and Tab. 6-3 in the Appendix.

The modelling for U-Th isotopic system was done in two steps.

- 1) Melt generation in enriched mantle wedge produces the “initial magma”. The relative contributions of the components DMM, fluids, sediment and crustal material will be assessed.
- 2) Magma evolution after segregation of the initial magma from its source with early fractionation of olivine plus orthopyroxene on its way to the base of the crust is calculated followed by an attempt to quantitatively modelling fractionation and contamination within the crust.

4.5.1.1 Process of mantle wedge enrichment-contribution from the mantle wedge, slab fluids, sediment and crust

A plot presenting mixing of Depleted MORB Mantle with crust, fluid, and sediment and calculated composition of initial magma is presented for El Misti and for Taapaca in Fig. 4-8, Fig. 4-9.

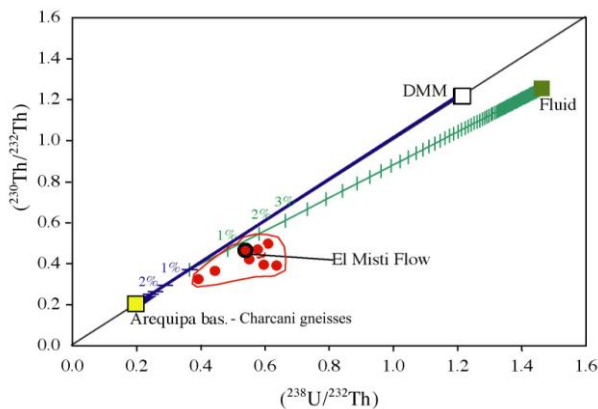


Fig. 4-8 Mixing of DMM with basement rocks (Arequipa basement), Fluids and Sediment. The tics of symbols mean % of each component. Look text for data source

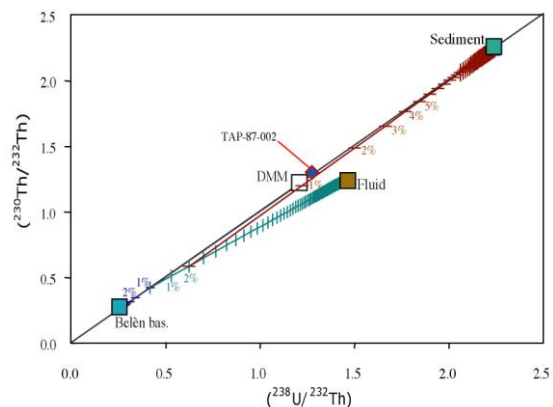


Fig. 4-9 Mixing of DMM with basement rocks (Belén basement), Fluids and Sediment. The tics of symbols mean % of each component. Look text for data source

According to the calculation presented in Fig. 4-8, 97% DMM, 1% of Arequipa basement Charcani gneisses and 2% of slab-derived fluids are found to mirror for the composition of magma in the source at El Misti (DMM*). No sediments (oceanic material at the top of subducted plate) should be involved in magma genesis at El Misti.

At Taapaca (Fig. 4-9), the first stage modelling suggests about 95% depleted MORB mantle, 1% of Belén basement, 2% of slab derived fluids, and 2% of sediments, that are involved in the magma source.

Fluid component

The relatively low concentration of U in the expelled fluid comes from calculation based on compilation of partition coefficients, which is of a significant importance for this subject. In fact the literature data give compositions of fluids that are much more enriched in U (Elliot et al., 1997). However, it must be kept in mind that the composition of fluids may be very much different depending on tectonic settings. It is very probable that fluids from the oceanic island arcs are richer in U. In addition, the depth at which the fluid is expelled from the slab could be important. Several experimental studies give data on partitioning of trace elements between mineral and fluids (Brenan et al., 1995, Stalder et al., 1998, Ayers et al., 1997 and Keppler 1996).

Results of additional calculations for the involvement of U-rich fluid are presented on Fig. 4-10, Fig. 4-11. The alternative fluid composition is based on calculation with partition coefficients from Kessel et al. (2005). Significantly different (higher) contents of this component can be derived.

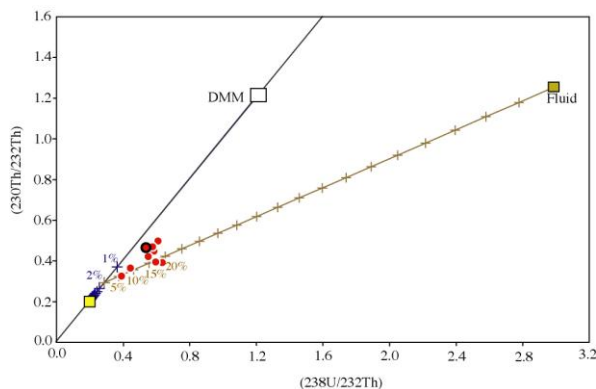


Fig. 4-10 Mixing of DMM with Arequipa basement, fluid and sediment. See text for source of data.

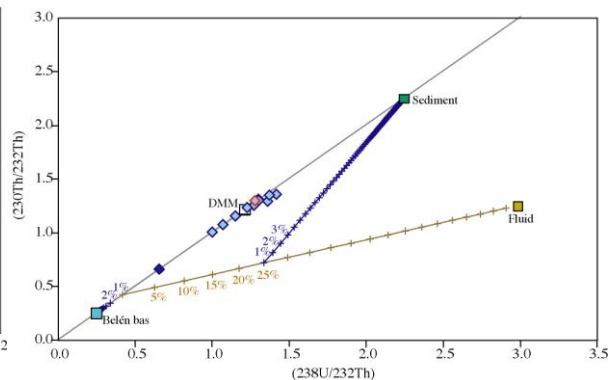


Fig. 4-11 Mixing of DMM with Belén basement, fluid and sediment. See text for source of data.

Sediments component

The floors of the oceans are covered by sediments from slow accumulation of calcareous and siliceous biogenic oozes capped by fine clays carried in suspension to the middle of the oceans. Near the continents there may be greater accumulation of clastic sediments brought in by deltas and turbidity currents and redistributed by bottom water currents. In northern Chile and Peru the sediment supply is very limited because of the arid climate (Davies and Blanckenburg 1995; von Huene & Scholl 1993). Also major faults parallel to the coast tend to obstruct the rivers. However few percent of sedimentary input was suggested for the CVZ environments (Bourdon et al., 2000).

The modelling of magma composition in the mantle wedge of Taapaca suggests involvement of little % sediment in the magmas source. This is based on a simple batch-mixing calculation. However models that explain melt input from the down going slab suggest that melt stems from the whole subducted pile of the subducted crust also from sediments. Some laboratory melting experiments allow also to derive melting of pelagic red clays at pressures

up to 40kbar, equivalent to depth of 120km (Nichols et al., 2002). Melting of sediment and gabbro dehydration can occur at the same temperature but this requires at the same time rather specific thermal structure in subduction zone (Nichols et al., 2002).

Summing this discussion, it is suggested that the characteristic geometry of the trench of South America, where pelagic sediments are probable to be collected up to few percent at Arica elbow, could explain the unusual presence of sedimentary signatures at Taapaca Volcanic Complex.

4.5.1.2 Assimilation processes in the crust

Primary arc lavas rarely have primary compositions implying that significant fractional crystallization and assimilation took place during ascent and storage. Processes of fractional crystallization are discussed later. Processes of crustal contamination are well documented for arc lavas especially erupted through such thick (70km) crust.

Quantitative estimation of crustal assimilation is done in the second stage of modelling. The simple two component mixing of calculated contaminated source (DMM*) with crust suggest between 10-15 % assimilation of the Arequipa basement to explain El Misti Flow2 and 8-10% of Belén basement for Taapaca (TAP-87-002), see Fig. 4-12 and Fig. 4-13.

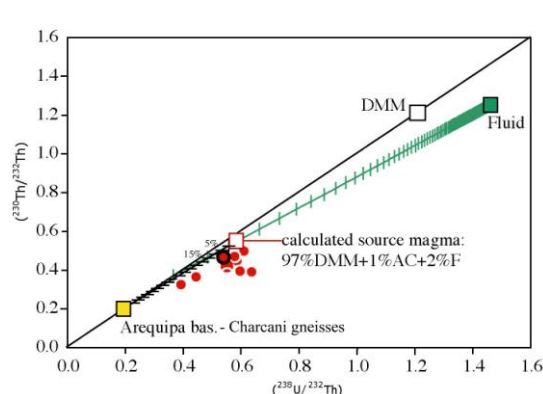


Fig. 4-12 Calculated DMM* mixed with basement rocks (the abbreviation “AC” mean Arequipa Crust relates to Arequipa basement). Tics are equal to % of component involved.

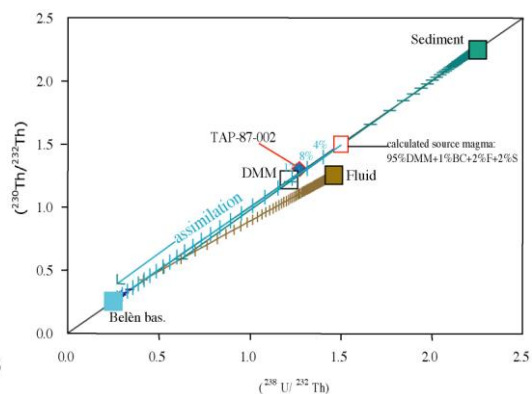


Fig. 4-13 Calculated DMM* mixed with basement rocks (Belén basement). Tics are equal to % of component involved.

Assimilation of crust or crustal melts

The calculation presented above is based on a simple two component mixing. However, if the crustal material were introduced into the system rather by melting than bulk mixing, the consequences on the U-Th isotopic system would be more complex. Bulk addition is not expected to produce disequilibria since $(^{238}\text{U}/^{230}\text{Th})=1$ in the crust >350ka old. ^{230}Th - ^{238}U disequilibrium would be created only if the assimilant is a ^{230}Th or ^{238}U enriched partial melt. Lithologies with refractory phases that retain U over Th refer to garnet, Al-rich clinopyroxene or accessory phases like zircon or allanite (Garrison et al., 2006). Presence of these minerals by anatexis processes would lead to formation of a ^{230}Th enriched partial melts. Arequipa and Belén basements are characterised by gneisses and amphibolite lithologies. Many numerical

models have shown that ^{230}Th excesses can be generated in mafic magmas by melting of garnet-bearing lithologies (Dufek and Cooper 2003; McKenzie 1985). Models of lower crustal melts suggest high melt fractions (10-40%), which do not generate significant ^{230}Th excesses (Berlo et al., 2004). Only by degrees of partial melts <10%, ^{230}Th enrichment increases significantly. Taapaca does not show ^{230}Th enrichment in the erupted lavas. However, if melting of lower crustal rocks did occur in the past, the probable ^{230}Th excess had to decay over the last 350ka so that it is no longer seen today.

Study on the Cotopaxi volcano show that the highest ^{230}Th excess is produced by melting of eclogite up to 13% at 3% melt and melting of pelitic schist produces ^{230}Th excesses of up to 5%. The ^{230}Th excesses may partially overprint initial fluid-derived ^{238}U excesses. Melting of garnet amphibolite and amphibolite on the other hand produces ^{238}U excesses of up to 20%. This points surprisingly, that some degree of ^{238}U enrichment can come from the melting of lower crustal lithologies and not from addition of U-rich fluids to the mantle wedge.

4.5.1.3 Shallow level fractional crystallization processes

A strong argument for fractional crystallisation at Taapaca is derived from petrographic observations on the erupted lavas. Dacites from Taapaca Volcanic Complex show several mineral phases crystallized: magnetite, rare clinopyroxene, significant amphiboles, biotite, plagioclase, and characteristic up to 6cm in diameter sanidines. There are also apatite and zircon as accessory phases. The apatite occurs in the matrix (250-500 μm) as well as inclusions in amphibole and biotite (<250 μm). Rare zircons have been found as inclusions in biotites (<125 μm).

Major mineral phases do not influence the U-Th signature by low to moderate degree of crystallization, as they do not strongly fractionate U and Th. In contrast, accessory minerals like zircon, apatite or sphene have $K_{\text{ds}} \gg 1$ and, thus, are able to significantly fractionate U from Th by small amount of crystallization (Ewart et al., 1994, Foley et al., 2000, Irving et al., 1978).

4.5.2 Magma petrogenesis - major elements

The direct reconstruction of the major and trace element evolution of ElMisti and Taapaca is not easily derived from the data of volcanic rocks samples at the surface because in the CVZ no primary unfractionated and uncontaminated melt compositions have been found yet. However, the information of both major and the trace element composition are important for understanding the magmatic systems. In this study, the reconstructing of the major element evolution is done separately from the calculation of the trace element evolution because different approaches have been chosen.

Therefore, for the reconstruction of primary melts composition the most mafic rocks occurring in the CVZ are taken, namely the andesite composition from Nicolson. Because of its low Mg-# of 56.9 and its low Ni content of 69 ppm, the Nicolson magma cannot be primitive but must have experienced mafic minerals. Mafic minerals, which crystallise from primary subduction-related magmas (high-Al-basalt) are olivine and orthopyroxene and may be some clinopyroxenes (Tatsumi et al., 1983). Thus, the major element composition of the parental melt can be calculated by mixing olivine and orthopyroxene back into the evolved composition (Nicolson andesite) so that the conditions of a primitive melt is reached.

The following assumptions are made for this calculation:

- 1) Primary melts in equilibrium with mantle olivine (Mg-#89-93) have Mg-# of 68 to 72.
 - 2) For calculation the Mg-# a value of 85% of total Fe is taken as FeO, this also applies if data for ferric Fe exist.
 - 3) The composition of fractionating olivine and orthopyroxene minerals remains fixed.
- For the crystallisation/fractionation process it is further assumed that
- 4) Olivine and orthopyroxene crystallise and fractionate at equal proportions (1olivine + 1orthopyroxene), or at the proportion of 3ol+1opx.

For the calculation of primary melts the SiO₂, Al₂O₃, FeO, MgO and MnO values are used; the remaining major elements are incompatible for both olivine and orthopyroxene. In Tab. 4-2 the results are shown graphically for the recalculation of a primary melt that fulfils the above conditions in terms of Mg-#: olivine and orthopyroxene data as 1ol+1opx or as 3ol+1opx are added to the Nicolson composition until the Mg-#68, 70 and 72 are achieved. The results of Fig. 4-14 for Mg-# are for Fe=0.85Fe^{tot} and for Fe=Fe^{tot}; Fig. 4-6 shows only differences result in the recalculated Si, Mg, Fe and Al for the different ferrous/ferric iron ratios.

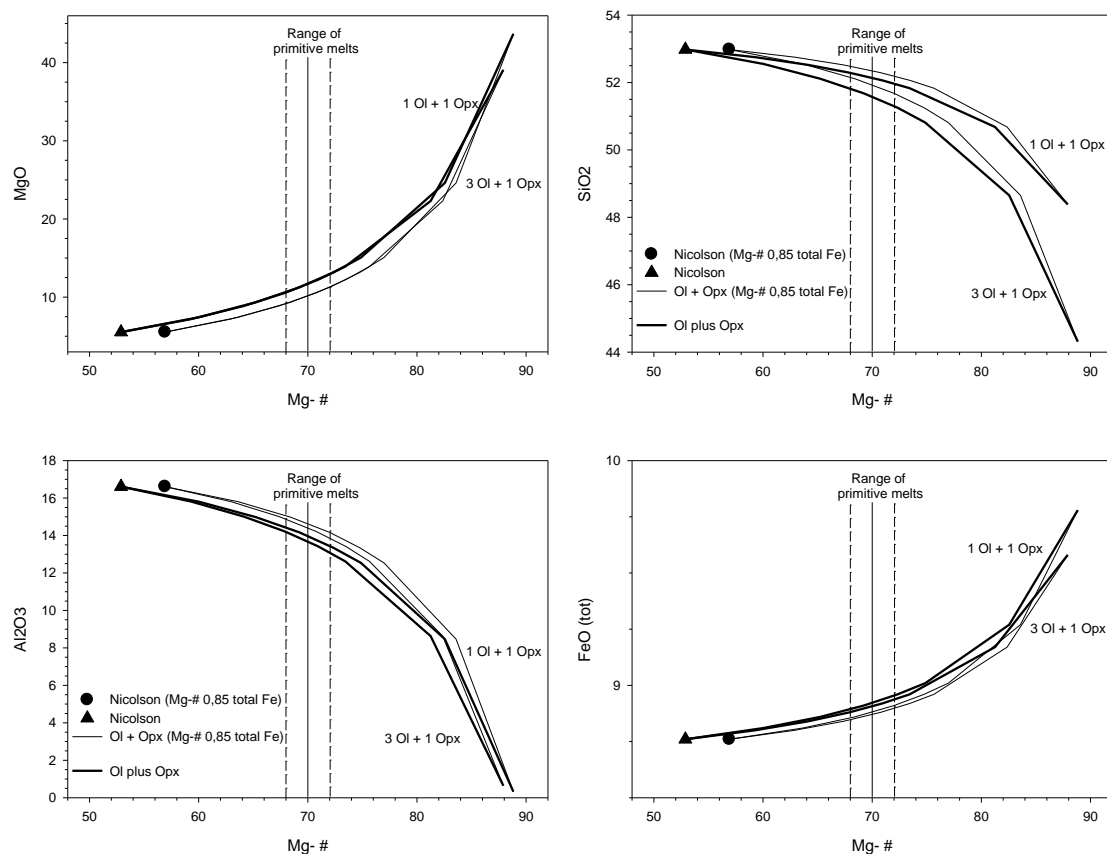


Fig. 4-14 Effects of addition of olivine and orthopyroxene of constant composition to Nicolson andesite. Thick line: addition of 1ol+1opx; thin line: addition of 3ol+1opx. Triangles represent data for Nicolson andesite at Mg-# with all Fe^{tot}=Fe²⁺; dots are for Nicolson andesite at Mg-# with Fe²⁺=0.85 of total Fe. The vertical lines bracket the range of SiO₂, Al₂O₃, FeO and MgO at Mg-# 68 to 72.

The results of this “inverse fractionation” are presented in Tab. 4-2 for Mg-#68 of the primary melt and 1ol+1opx fractionation as well as 3ol+1opx. Because there is no independent information for the olivine composition in the source peridotite, the data at Mg-#68 represent minimum MgO and maximum SiO₂ values. The effect of slightly higher Mg-# is mainly that MgO will increase and SiO₂ decrease in the melt as can be seen in Tab. 6- in the appendix, which shows all calculations for Mg-#68 to 72 and 1ol+1opx as well as 3ol+1opx, respectively. All other major elements are simply the Nicolson andesite values corrected for 10.8% and for 9.5% fractionation 1ol+1opx and 3ol+1opx respectively.

Tab. 4-2 Calculated composition of primary melts from olivine plus orthopyroxene fractionation models (see text for farther explanation). Olivine and orthopyroxene data are from Tatsumi and Ishizaka (1981): Primary melts 1 and 2 have Mg-#68 and are in equilibrium with mantle minerals; amounts of olivine plus orthopyroxene that are needed to arrive from Nicolson andesite to primary melt 1 and primary melt 2 is listed in the lowermost lines. All Mg-# are for the Fe=0.85 total Fe; Fe₂O₃*calculated from the difference of FeO to FeO^{tot}.

	Nicolson Andesite	Olivine	Opx	Primary Melt 1	Primary Melt 2
SiO ₂	52,98	40,25	56,5	52,48	52,16
TiO ₂	1,49			1,32	1,34
Al ₂ O ₃	16,61	0,00	1,28	14,89	15,06
Fe ₂ O ₃ *	1,46*			1,30*	1,32*
FeO	7,45	9,98	9,17	7,68	7,67
MnO	0,14	0,15	0,26	0,15	0,15
MgO	5,52	48,3	29,85	9,14	9,15
CaO	8,54			7,62	7,73
Na ₂ O	3,76			3,35	3,40
K ₂ O	1,85			1,65	1,68
P ₂ O ₅	0,35			0,31	0,32
Sum	100,15	98,68	97,06	99,90	99,97
FeO ^{tot}	8,76	9,98	9,17	8,85	8,86
Mg-#	56,9	89,7	85,3	68,0	68,0
Wt.-% Ol				5,4	7,1
Wt.-% Opx				5,4	2,4

The calculated melt compositions of Primary Melt1 and Primary Melt2 of Tab. 4-2 are very similar to each other. In fact, there are no significant differences between these data. The amount of fractionated olivine plus orthopyroxene from primary melts to Nicolson andesite composition is 10.8% for equal amount of fractionated olivine and orthopyroxene and is 9.5% for a fractionated assemblage having three times more olivine than orthopyroxene. The difference between 10.8% and 9.5% has no practical consequences for the enrichment in compatible elements caused by the separation of the two mafic minerals. As a consequence, the calculated trace element concentrations derived by partial melting as described below must be 10% higher in the melt that results from this first stage evolution. This holds for almost all trace elements with distribution coefficients below 0.1. A few elements that are compatible to olivine and orthopyroxene, e.g. Ni, Co, Cu, are not included in this set of trace element data.

The first stage of fractionation takes place during ascent of the melt through the mantle wedge; thus, no crustal contamination is taken into account. In the next step, the fractionation is calculated from this ‘stage 1 magma’ - which lost some 10% of olivine and orthopyroxene -

to compositions named ElMisti-15 and Taapaca-10, respectively. El Misti-15 means the ElMisti composition reduced by 15 % of avg Arequipa Basement, likewise, Taapaca -10 means the Taapaca composition reduced by 10% of Belén basement. The value 15% and 10% reduction of the respective crustal contaminant have been derived from the above (chapter 4.5.1.2) U-Th isotopic modelling.

There are no independent information about the nature and the composition of fractionated minerals of the ‘stage 1 magmas to the surface. However, following Davidson et al. (1990), their mineral compositions are used to calculate the amount of minerals fractionated by least squares fittings. The results of these least squares fittings are summarized in Tab. 4-3 and Tab. 4-4.

Tab. 4-3 Least squares fit for fractionation of the ‘stage 1’ magma (represented by Nicholson andesite) to ElMisti-15; major element data of minerals according to Davidson et al. (1990); ElMisti major elements reduced by 15 % of average Arequipa Basement.

Mineral	Plag	Ol	Cpx	Hbl	Mt	EM-15	Nicholson
SiO ₂	55,87	38,82	50,57	41,58	0,67	58,47	52,98
TiO ₂	0,00	0,00	0,96	4,30	14,4	0,966	1,49
Al ₂ O ₃	26,97	0,00	3,20	12,36	2,3	17,89	16,61
FeO	0,90	19,76	7,27	10,74	75,02	6,19	8,76
MgO	0,00	40,99	14,98	14,56	3	3,3	5,52
CaO	9,96	0,16	21,99	11,36	0	6,37	8,54
K ₂ O	0,54	0,00	0,00	0,74	0	1,96	1,85
Na ₂ O	5,59	0,00	0,00	2,60	0	4,57	3,76
P ₂ O ₅	0,00	0,00	0,00	0,00	0	0,317	0,35
Sum	99,8	117,9	99,0	98,2	95,4	100,1	100,0
Wt.-%	15,0	1,2	8,6	11,4	3,8	59,9	

Tab. 4-4 Least squares fit for fractionation of the ‘stage 1’ magma (represented by Nicholson andesite) to Taapaca-10; major element data of minerals according to Davidson et al. (1990); Taapaca major elements reduced by 10% of average Belén Basement.

Mineral	Plag	Ol	Cpx	Hbl	Mt	TAP-10	Nicholson
SiO ₂	55,87	38,82	50,57	41,58	0,67	66,11	52,98
TiO ₂	0,00	0,00	0,96	4,30	14,4	0,77	1,49
Al ₂ O ₃	26,97	0,00	3,20	12,36	2,3	16,19	16,61
FeO	0,90	19,76	7,27	10,74	75,02	3,42	8,76
MgO	0,00	40,99	14,98	14,56	3	0,05	5,52
CaO	9,96	0,16	21,99	11,36	0	1,47	8,54
Na ₂ O	5,59	0,00	0,00	2,60	0	4,72	3,76
K ₂ O	0,54	0,00	0,00	0,74	0	3,69	1,85
P ₂ O ₅	0,00	0,00	0,00	0,00	0	3,30	0,35
Sum	99,8	117,9	99,0	98,2	95,4	0,28	100,0
Wt.-%	27,6	0,0	8,8	22,3	5,4	64,05	

The results for the least squares fits show that there is very little additional olivine is fractionated. Many trials of minerals associations in the bulk of the fractionated phases (cumulate) revealed that orthopyroxene and garnet have not been fractionated. The main components of the bulk cumulate fractionated from Nicholson andesite to arrive at ElMisti-15 are plagioclase, hornblende and clinopyroxenes followed by magnetite.

A similar result is achieved for the least squares fits for the fractionation from Nicholson andesite composition to Taapaca-10. The main mineral phases involve: plagioclase, hornblende, clinopyroxene and magnetite. However no olivine should be fractionated at Taapaca based on the least squares fit. Additionally the degree of fractionation >50% is surprisingly high.

4.5.3 Magma genesis - trace elements

The trace elements in the mantle wedge as the source of the primary melts are calculated by consequent mixing (according to U-Th modelling) of 95%-97% depleted mantle (DMM) with 1%-2% of Arequipa/Belén basement, 2% of fluids and 2% of pelagic sediments. The results of the mixing are listed in Tab 4-6. This enriched mantle, further called DMM* is taken as the source for the melting.

In order to calculate the trace elements concentrations in the primary melt derive from this source, batch melting has been chosen according to

$$C_1/C_0 = 1/F + D - F * D$$

where C_1 is the concentration of element in the liquid, C_0 is the concentration in the solid, F is the degree of melting, and D is the distribution coefficient based on partition coefficient of existing minerals.

Values for partition coefficients used in this calculation are given in the appendix (Tab, 6-3). The modal mineralogy of the mantle source was calculated by least squares fits from the major element data of DMM and of olivine, orthopyroxene, clinopyroxene and garnet data from the literature (mineral data from Deer et al, 1982, 1987). The results of the least squares fit for the mantle mineralogy is given in Tab, 4-5.

Amphibole which principally might occur because of the addition of water to the peridotite by the fluid is not stable at pressure above 25kbars at 1000°C. Also, spinel is not stable in such conditions (see Wilson 1989). The water that was present by addition of the fluid component is assumed to have entered the melt directly without producing a hydrous residual mineral like amphibole.

Tab. 4-5 Results of least squares calculations for the mineralogy of DMM.

Mineral	Ol	Opx	Cpx	Gar	DMM
SiO ₂	40,78	53,26	53,04	41,33	45,31
TiO ₂	0,00	0,17	0,45	0,28	0,13
Al ₂ O ₃	0,03	6,59	6,22	21,83	4,13
FeO ^{tot}	8,19	6,61	1,72	10,30	7,78
MnO	0,18	0,12	0,05	0,44	0,13
MgO	50,19	31,29	14,56	19,60	38,67
CaO	0,05	2,14	18,90	4,40	3,21
Na ₂ O	0,00	0,07	2,29	0,00	0,16
K ₂ O	0,00	0,00	0,07	0,00	0,04
P ₂ O ₅	0,00	0,00	0,01	0,00	0,02
Sum	99,7	100,3	97,3	98,2	99,8
Wt,-%	55,2	24,4	11,5	9,0	

This modal mineralogy was taken to calculate the D-values for the batch melting process. The results for incompatible trace elements in this primary mantle derived by 5 % melting of the enriched mantle source DMM* are presented in Tab, 4-6.

Tab. 4-6 Composition of the mantle source (DMM*= DMM enriched in avgArequipa/Belén Basement, fluid expelled from the slab and sediment) and results incompatible trace elements derived by for batch melting of DMM*.

	El Misti		Taapaca	
	DMM*	Result for 5% melting of DMM*	DMM*	Result for 5% melting of DMM*
	97%DMM+ 1%avgAreqBas+2%F	55,2 ol + 24,4opx+11,5 cpx + 9,0 gar	95%DMM+1%BelénBas +2%Fluid+2%Sediment	55,2 ol + 24,4opx+ 11,5cpx + 9,0 gar
ppm				
Rb	0,84	11,6	3,09	27,96
Sr	16,6	275	26,68	441
Ba	20,8	391	25,16	474
La	0,55	9,62	0,98	16,87
Ce	1,30	18,8	2,08	26,39
Nd	0,92	10,5	1,23	13,27
Sm	0,30	2,80	0,33	3,14
Eu	0,11	0,81	0,12	0,91
Gd	0,39	2,88	0,43	2,96
Dy	0,53	1,44	0,55	1,47
Er	0,36	0,82	0,36	0,80
Yb	0,37	0,76	0,38	0,71
Lu	0,06	0,10	0,06	0,11
Nb	0,33	3,40	0,36	3,44
Zr	6,53	42,0	8,83	41,53
Hf	0,17	1,42	0,23	1,41
Pb	0,44	8,49	0,57	11,05
Th	0,06	1,16	0,11	2,21
U	0,01	0,27	0,02	0,36

The concentrations of trace elements have been than corrected due to fractionation of 10,4 olivine+orthopyroxene in the mantle simply by multiplying the primary melt composition by 1,1.

For the subsequent fractionation of plagioclase, amphibole, olivine, clinopyroxene, magnetite at crust depths was calculated by simple fractional crystallisation as already described above (chapter 4.5.2). The value for D in the exponent of the respective equation is derived from individual mineral partition coefficients multiplied by their amounts in the cumulate as given in the bottom lines of Tab. 4-6 for ElMisti and Taapaca, respectively. The results of these calculations are given in Tab. 4-7 for ElMisti-15 and in Tab. 4-8 for Taapaca-10.

Tab. 4-7 Calculated trace element concentrations of a fractionated melt after 10,1 % olivine+orthopyroxene and 40,1 % plagioclase, amphibole, clinopyroxene, magnetite, olivine fractionation for El Misti-15.

	Source melting F 5 %	mantle fractionation (C ₀) ol+opx	crustal fractionation (C _i)	El Misti-15	C _i /ElMisti-15
ppm					
Rb	11,6	12,76	20,32	33,64	1,66
Sr	275	302,50	315	896	2,85
Ba	392	431,20	623	931	1,50
La	9,62	10,58	16,45	21,2	1,29
Ce	18,8	20,68	31,57	48,1	1,52
Nd	10,5	11,55	17,18	21,4	1,25
Sm	2,80	3,08	4,37	4,08	0,93
Eu	0,81	0,89	1,22	1,11	0,91
Gd	2,88	3,17	4,46	3,49	0,78
Dy	1,44	1,58	2,25	2,17	0,97
Er	0,82	0,90	1,29	0,98	0,76
Yb	0,76	0,84	1,21	0,84	0,70
Lu	0,10	0,11	0,16	0,13	0,79
Nb	3,40	3,74	5,81	4,38	0,75
Zr	42	46,20	67,88	153	2,25
Hf	1,42	1,56	2,43	4,56	1,88
Pb	8,49	9,34	13,83	15,0	1,08

Tab. 4-8 Calculated trace element concentrations of a fractionated melt after 10,1 % olivine+orthopyroxene and after 64,05 % plagioclase, amphibole, clinopyroxene, magnetite fractionation for Taapaca-10.

	Source melting F 5 %	mantle fractionation (C ₀) ol+opx	crustal fractionation (C _i)	Taapaca-10	C _i /Taapaca-10
ppm					
Rb	27,96	30,76	77,33	89,46	1,16
Sr	441	485	458	798	1,74
Ba	474	521	1086	1117	1,03
La	16,87	18,56	43,21	24,58	0,57
Ce	26,39	29,03	63,24	52,34	0,83
Nd	13,27	14,60	28,25	22,70	0,80
Sm	3,14	3,45	4,86	3,80	0,78
Eu	0,91	1,00	1,38	1,15	0,83
Gd	2,96	3,26	4,19	3,14	0,75
Dy	1,47	1,62	1,42	1,40	0,99
Er	0,80	0,88	0,84	0,61	0,73
Yb	0,71	0,78	0,78	0,43	0,55
Lu	0,11	0,12	0,11	0,06	0,61
Nb	3,44	3,78	11,24	7,55	0,67
Zr	41	45	68,74	184	2,68
Hf	1,41	1,55	3,18	3,71	1,16
Pb	11,05	12,16	26,05	18,44	0,708

In a perfect modelling approach that successfully describes the natural process of melt generation and evolution by fractionation the calculated data of CI should be very close to the measured values.

Whereas for the trace elements Rb, Sr, Zr, and Th there are marked differences, the rest of the calculated trace element data are in reasonable accordance with the measured data. Problems of non-convergence are probably due to the dilemma that the calculations are done on an Arequipa Basement database, which is not representative as assimilant for trace elements and Sr Nd, and Pb isotopes (see below). More Arequipa Basement samples are necessary to arrive at a representative data set.

Presumably, this is also the reason why the classical AFC calculations did not work. The Assimilation Fractional Crystallisation calculation has no internally consistent solution due to insufficient data of the contaminant for El Misti samples. Obviously, a large variety of components are involved in magma genesis at El Misti and Taapaca. The unknown contaminating crustal component is one example explained already. It was also mentioned earlier, that fluid composition depends strongly from depth and mineralogy (composition) of subducted slab from which it is expelled, as well as the from partition coefficient, which are varying up to an order of magnitude. All these variables must be taken and used with caution.

4.5.4 Magma genesis – isotopes

For the isotopes of Sr, Nd and Pb the two-step modelling was done following the calculations used for U-Th isotopes. The depleted mantle was mixed with 2% of Arequipa/Belén Basement, and 2% of fluid and 2% of sediments. This relates to DMM*. As suggested by U-Th isotopes, the mantle-derived magma was affected by 15% of assimilation by the Arequipa Basement at El Misti and 10% of Belén basement at Taapaca. Therefore, the samples on which the model was done (El Misti Flow, Tap-87-002) were reduced by 15% and 10% of crustal composition (EM-15, TAP-10), respectively, to achieve the depleted mantle composition (DMM*). However, as can be seen from Tab. 4-9, Tab. 4-10 the calculated DMM* isotopic composition is not equivalent to calculated EM-15 and TAAP-10. Further detailed modelling which includes representative assimilant lithologies is necessary to explain the magma petrogenesis for each of Sr, Nd, Pb isotopic systems.

Tab. 4-9 Table presenting a try of modeling the isotopic composition at ElMisti volcanic rocks.

	El Misti FLOW 2	Reduction of crust (15%) EM-15	DMM+1%crust+2%fluid DMM*
ppm $^{87}\text{Sr}/^{86}\text{Sr}$	802 0,7077	890 0,706604	17 0,706856
ppm $^{143}\text{Nd}/^{144}\text{Nd}$	21,58 0,512139	21,58 0,512165	0,90 0,512857
ppm $^{206}\text{Pb}/^{204}\text{Pb}$	14,79 17,68	15,10 17,66	0,43 18,14

Tab. 4-10 Table presenting a try of modeling the isotopic composition at Taapaca volcanics.

	TAP-87-002	Reduction of crust (10%) TAAPACA-10	DMM+1%crust +2%fluid+2%sediment DMM*
ppm $^{87}\text{Sr}/^{86}\text{Sr}$	751 0,7067	798 0,70644	34,94 0,70727
ppm $^{143}\text{Nd}/^{144}\text{Nd}$	21,80 0,512296	23,00 0,512324	1,55 0,512646
ppm $^{206}\text{Pb}/^{204}\text{Pb}$	17,10 18,17	18,43 18,18	1,10 18,39

4.6 Timescales of magmatic processes at Taapaca

The timescales of magmatic processes can be estimated on U-Th isotopic composition measured on the minerals, ^{230}Th - ^{238}U internal isochrone for minerals from Tap-02-03 is presented at Fig. 4-16. The corresponding isochrone age for this sample is $171\text{ka} \pm 26\text{ka}$. Isochrone calculation was done following York (1969). Mineral data from Taapaca suggest that old crystals are in young (12ka eruption age, $^{40}\text{Ar}/^{39}\text{Ar}$ dating) magma. In contrast to this conclusion, Sr-diffusion studies (Wegner 2003) suggest much younger times ranging from 100 to few years. However, the Sr-diffusion studies give relative ages indicating how long a mineral has been at a particular temperature. Therefore, much younger ages from Sr diffusion profiles reflect shorter periods of time than those obtained by U-Th isotopes.

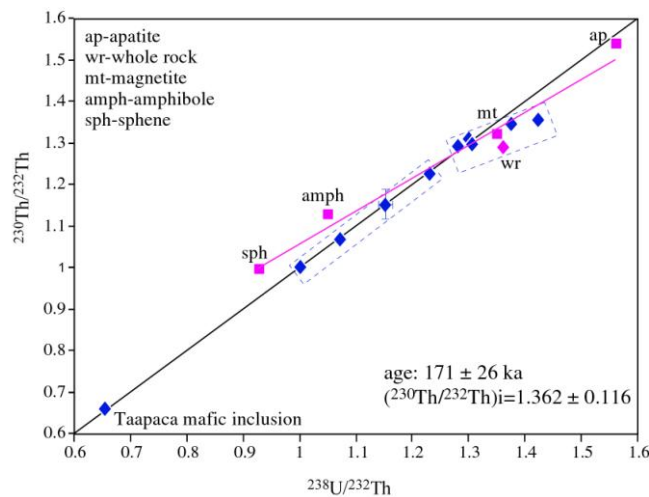


Fig. 4-16 Internal U-Th isochrone diagram for Taapaca dacite TAP-02-03.

4.7 Constrains on timescales of magmatic processes at El Misti

The measured U-Th disequilibria on whole rock samples from El Misti volcano suggest short time since magma generation in the mantle. The system must be young enough (<350ka) to still keep U-Th disequilibrium. It is generally believed that Th is not mobilised into subduction zone fluids and therefore, the U-Th array reflects the time since U addition. However, in the studied area magma genesis involves mixing of several components. This unables the use of whole rock isochrone as a dating tool. The only time information that can be derived from whole rock data at El Misti is the U-Th disequilibria suggesting that the system must be younger than 350ka.

Unfortunately, no mineral separates have been measured for U-Th isotopes (see analytic appendix for explanations). Therefore, a more detailed evaluation on timescales of magmatic processes involved in magma genesis at El Misti is not possible. Further data on mineral separates are needed to fulfil this issue.

4.8 Different magmatic systems

El Misti and Taapaca represent two contrasting magmatic regimes. El Misti is a young (<0,5Ma) stratocone volcano with symmetrical shape and central vent, where magma composition ranges from andesitic-dacitic to rhyolitic. In contrast, Taapaca represents a long-lived cluster (>0,5Ma) with dacitic domes and pyroclastic aprons where lava results in low-input, low-output of monotonous compositions.

The two volcanic examples differ in their time and way of evolution. The estimated eruption rate at El Misti of 0,63km³/ka (Thouret et al., 2001) contrasts with much slower eruption rate at Taapaca of 0,01 km³/ka (calculation based on estimated erupted volume of 88 km³; Kohlbach 1999 and age 1,27Ma; Wörner et al., 2004). This argument points to huge differences in the activity and time of evolution at the two volcanic edifices. El Misti represents rather fast and frequently erupting center, while Taapaca obviously is a low input and low output, slow and old system.

The depth of magma evolution at the El Misti and Taapaca is not known exactly. Estimations have been done based on garnet signature and amphibole composition (Wörner et al., 2004, Banaszak 2006). The presence of strong HREE fractionation suggests garnet present in the system, which at the same time causes ²³⁰Th enrichment. No such signature is to be observed at lavas erupted at Taapaca volcano. However the ²³⁰Th enrichment could have decayed back since the Taapaca is such an old system (1,27 Ma, Wörner et al., 2004).

There is no such strong HREE fractionation at El Misti volcanics suggesting different regime of magma evolution. Higher eruption rates and signs of magma mixing suggest that El Misti is an active and fast regime volcano. Additionally the U-Th disequilibrium and ²³⁸U enrichment in erupted volcanics support the implication that El Misti is a fast system at which the evolution since magma production (melting in the mantle wedge) to its eruption took <350ka.

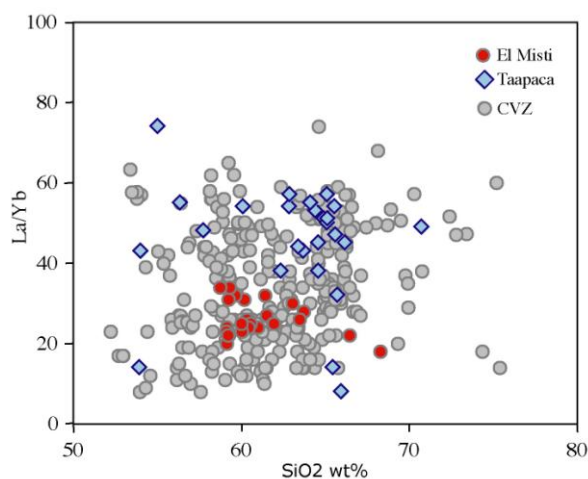


Fig. 4-17 La/Yb versus SiO₂ wt% for rocks from El Misti, Taapaca and CVZ showing stronger fractionation of HREE at Taapaca.

Available data on Taapaca amphibole composition suggest two magma chambers (Lohnert 1999) and the geobarometer based on analyzed amphibole minerals from Taapaca dacite (TAP-97-28) argument magma chamber deeper in the crust at 17-20 km and at shallower level at 9-12km (Lohnert 1999). In contrary, Banaszak 2006 gives a model for Taapaca Volcanic Complex with one magma chamber at shallow depths of 7-8km.

Significant REE fractionation at Taapaca suggests presence of garnet and the depth of magma evolution in the garnet stability field (1,5GPa). Garnet signature at Taapaca may come either from melting in the mantle wedge (within garnet stability field 1,5GPa) or from melting of crustal rocks with residual garnet. However, melting of surrounding rocks requires rather strong thermal contrast between the ascending magma and the crust, which is unknown at Taapaca. The system must be thermally controlled and heated to keep activity for over 1Ma but whether the contrast between the magma and surrounding rocks is enough to melt crustal rocks or it rather keeps the system slowly working is still a question.

5 Conclusions

Magma genesis at the subduction zone of the CVZ is very complex due to many processes, which affect the magma during its evolution from partial melting in the mantle wedge to eruption at the surface. According to the data and discussion presented here, it is suggested that the CVZ magmas are controlled by source processes as well as assimilation and fractional crystallisation in the crust.

Although both volcanic centers are located in similar general geological settings (the CVZ) they show very distinct magmatic evolution.

El Misti is a rather young (112ka) single stratocone erupting magmas with wide range of silica content (58-68wt% SiO₂). By contrast Taapaca is a long-lived dome cluster (1,27Ma to Holocen), with majority of samples falling into the narrow range (63-67wt% SiO₂).

The two volcanoes differ also in their radiogenic isotope systematics. The radiogenic Sr-isotopic compositions are slightly higher for El Misti (0.7075-0.7078) than for Taapaca (0.7063-0.7067). Pb isotopes differ as well reflecting most probably the composition of assimilated continental crust ($^{206}\text{Pb}/^{204}\text{Pb}$ =17.68-17.84 for El Misti, and 18.10 for Taapaca).

The studied volcanic systems are very different in their U-Th disequilibria measured by Thermal Ionisation Mass Spectrometer. Surprisingly the Th/U isotopic compositions define end-members of the whole of CVZ. Misti volcanic rocks have very low ($^{230}\text{Th}/^{232}\text{Th}$) activity ratios (0.33-0.5) possibly the lowest measured in volcanic rocks. ($^{230}\text{Th}/^{232}\text{Th}$) at Taapaca is 1.02-1.36 for dacites and at the upper bound of the CVZ. Misti rocks are enriched in ^{238}U with surprisingly high ($^{238}\text{U}/^{230}\text{Th}$) of up to 1,4. Samples from Taapaca fall close to equilibrium values ($^{238}\text{U}/^{230}\text{Th}$)=0.93-1.06.

El Misti volcano is mostly influenced by Arequipa Basement (Charcani gneisses) with its very low (0,2) U-Th isotopic composition. As a second characteristic component is the fluid from subducting oceanic crust bringing the ^{238}U enrichment to El Misti volcanics, which was added to the system less than 350ka ago. El Misti represents a rather fast system due to the U-Th disequilibria, which is still to be seen. The processes of magma genesis and evolution, which include the contaminated source melting and magma segregation, magma ascent, assimilation/fractional crystallization, must have occurred within short timescale <350ka.

The Taapaca Volcanic Center represents a contrasting system. The magma source is controlled by different basement (Belén Basement) and is strongly influenced by sediments due to the high ($^{230}\text{Th}/^{232}\text{Th}$) activity ratios of erupted volcanics. The samples from Taapaca are within or close to U-Th equilibrium, which means that the system is rather old. Addition of fluid to the mantle wedge probably occurred, but its ^{238}U enrichment signature has already decayed to the state of secular equilibrium. Old mineral ages (171±26ka) support this statement.

The major elements of erupted rocks at El Misti and Taapaca volcanic centers point to mineral fractionation (10,08 %) of olivine and orthopyroxene deep in the mantle followed by assimilation and fractionation processes in the crust. The fractionation processes in the crust involve mineral assemblage of: plagioclase, amphibole, clinopyroxene, magnetite, which are similar at El Misti and Taapaca magmas however olivine is present only at El Misti. According to the last square fitting calculations magma experienced different degree of fractionation at each volcanic center (40,1% for El Misti, 64,05% for Taapaca). Trace elements of erupted volcanics were re-constrained by calculating the composition of initial

magma (mantle wedge contamination by the crust, fluids and sediments) and farther correction by fractionation processes. The trace elements, which do not fit with the composition of erupted volcanic rocks at El Misti and Taapaca could be explained by the uncertainties in composition of contaminating crust or fluids. The isotope systems of Sr, Nd and Pb need farther explanations and a more detailed studies, which take into account complexity and specific character of each system.

The differences in composition (major, trace elements and radiogenic isotopes) and by this the rates and styles of magma evolution between the two Andean volcanic centers can be caused by several processes like different magma production rates in the mantle, different depth of magma evolution, different composition of the crust and different structure of the basement. The last one may cause an easy and rapid magma ascent resulting in frequent magma mixing events and large range of erupted compositions (like at El Misti) or make conditions at which magma is stored and evolves at depth in relatively undisturbed reservoirs for longer time (Taapaca).

Simplified schematic models of magmatic system at El Misti and Taapaca are presented below on Fig. 4-18 and Fig. 4-19.

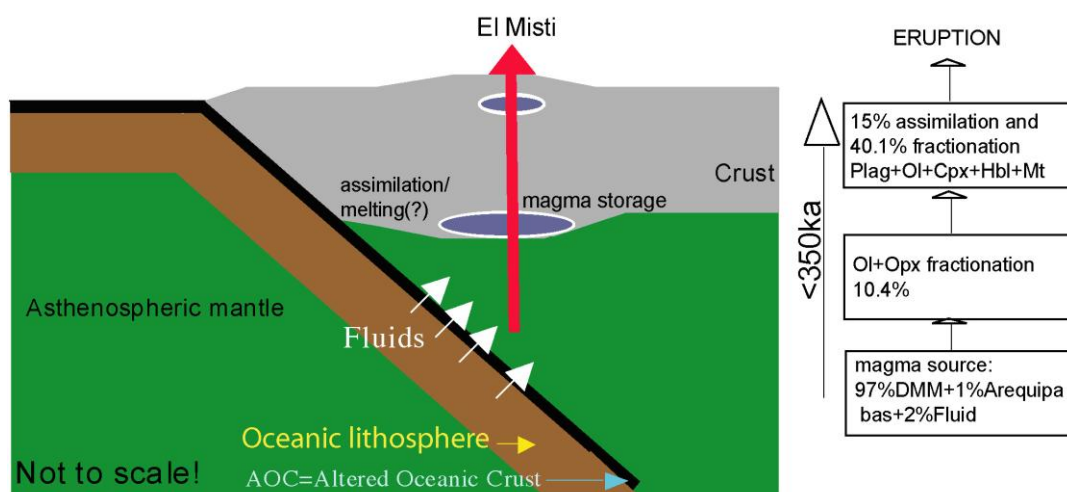


Fig. 4-18 Simplified schematic model for El Misti system according to U-Th data and some major and trace elements as presented in text.

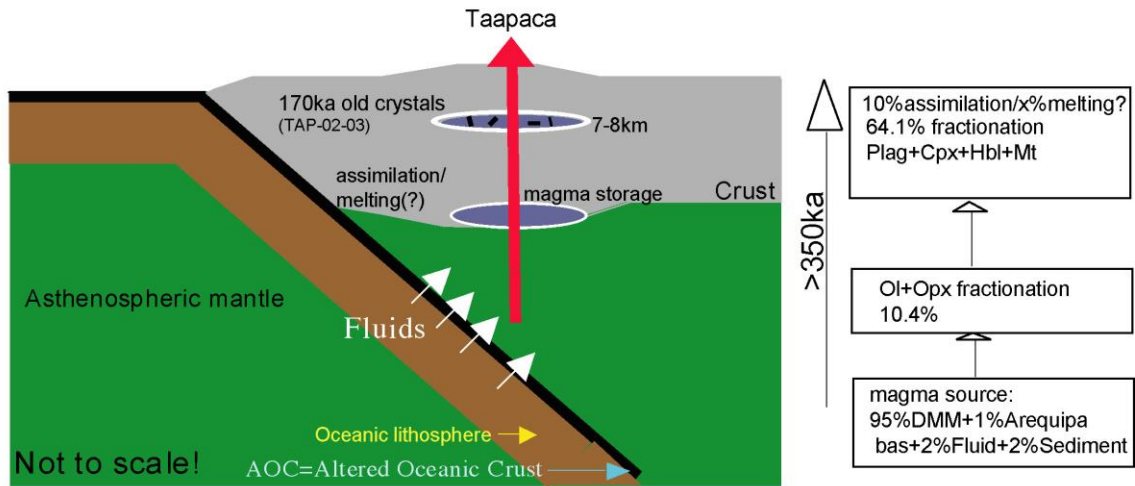


Fig. 4-19 Simplified schematic model for Taapaca Volcanic Complex according to U-Th data and major and trace elements as presented in text.

6 Appendix

6.1 Analytical techniques.

6.1.1 Sample preparation

Samples used in this study have been selected from a large set of collection from the field - work in the year of 2002 and in previous years (1987, 1999, 2000). These samples cover all stratigraphic units and compositions of the two volcanoes. Pyroclastic as well as lava flows were collected and included in the study. About 1-3 kg of most unaltered rocks for each sample was collected in the field to minimize contamination. Hand specimen was kept from all samples.

6.1.2 Whole rock powders

In the laboratory the samples were firstly crushed with a steel jaw crusher followed by a second step in a steel lined roller crusher into 1cm in diameter. 100g powders for bulk analyses were obtained from sample splits (by mechanical splitting device) pulverized in agate mill. This 100g were then ground to powder (65 μ m) in agate mills for about 30-40 min. The rest of the samples were washed and then sieved into fractions (>500 μ m, 500-250 μ m, 250-125 μ m, and <125 μ m) and used further for mineral separations.

6.1.3 Mineral separation

Between 10 and 100mg of the mineral separates (magnetite, amphibole, biotite, apatite, sphene) from 250-500 μ m and 125-250 μ m fractions were prepared for U-Th measurements by the Thermal Ionization Mass Spectrometer. The mineral concentrates have been prepared by Franz Electromagnet and then carefully picked under binocular for purity of the mineral fractions. Chosen grains of each fraction of magnetite, amphibole, biotite, sphene, apatite separates have been prepared (mounted in epoxy and highly polished) and checked (qualitative) by the electron microprobe.

6.2 XRF analyses.

Whole rock samples were analyzed by XRF on glass discs for major elements (Si, Ti, Al, Fe, Mn, Mg, Ca, Na, K, P) and trace elements (Nb, Zr, Y, Sr, Rb, Pb, Ga, Zn, Ni, Co, Cr, V, Ba, Sc). The measurements were carried out on a fully automated PHILIPS PW 1480 and data processing was controlled by the Philips X40 software package X-ray fluorescence spectrometer at the department of geochemistry at the Geowissenschaftliche Zentrum Göttingen (GZG). 700mg of powdered sample were thoroughly mixed with 4200mg Spectroflux 100 (Lithiumtetraborate [Li₂B₄O₇]) and melted in an automated Schoeps SGE-20 melting apparatus at 1000°C. The melt was held at the temp for 10 min to achieve a homogenous liquid which then was poured into a platinum mold. Fe₂O₃ was determined titrimetrically with KMnO₄ and the loss on ignition (LOI) be weight difference at heating to 1100°C. Analytical error for major elements are around 1% (except for Fe and Na, 2%; and LOI, ~10%) and for trace elements around 5%.

For the calibration of major and trace element determination about 50 reference materials were used (variety of international geochemical reference samples from the US Geological Survey, the International Working Group "Analytical standards of minerals, ores, and rocks", the National Research Council of Canada, the Geological Survey of Japan, the South African Bureau of Standards, the National Institute of Standards & Technology, etc).

6.3 ICP-MS analyzes.

Trace elements REE (La-Lu), HFSE (Nb, Ta, Zr, Hf), LILE (Rb, Sr, Ba, Cs) and others (Li, Sc, Cu, V, Cr, Co, Ni, Zn, Y, Pb, Th, U) were analyzed on ICP-MS Perkin Elmer SCIEX (Elan DRC II).

Sample for measurement were prepared by 100mg of powder samples weighted into Teflon beakers after Heinrichs & Hartmann (1990) and dissolved under pressure in a mixture of acids composed of 3ml HF, 3ml HClO₄, and 1ml HNO₃. After cessation of gas formation, the beakers were tightly closed and heated in a muffle oven at 200°C for 14 hours. After cooling to ambient temperatures, the beakers were opened and placed on a hot plate for evaporation at 180°C. Dried samples were re-dissolved in 2ml HNO₃ and put onto hot plate again. The second stage evaporation, 2ml HNO₃, 5ml de-ionised water and the internal standard were added to the samples. These solutions were rinsed onto 100 ml quartz glass flask and the remaining volume was filled with de-ionised water. The resulting solution contained the sample in a dilution 1:1000 in 2% HNO₃ with 20ppb Rh, Re, In as internal standard. It was kept in polyethylene bottles and measured within two days to minimize the risk of precipitation on interchange with the plastic container. For each fifteen samples a blank solution and a lab-intern and international standard were prepared. All reagents used were three times distilled to suppress blank values.

2σ error of the method is estimated to be <20% for Nb and Ta, <10% for Be, Cs, Cu, Hf, Li, Y, Pb, Rb, Tl, Th and U and ~5% for the rare earth elements.

6.4 Procedure for U-Th isotopes

U and Th isotope analyses have been determined following a modified procedure of Heumann et al., (2002).

The standard procedure for U-Th isotopes concerned:

- Chemical dissolution (Hf, HNO₃, HCL) of whole rocks and mineral separates (magnetite, amphibole, biotite, sphene, apatite)
- Isotope Dilution (²²⁹Th-spike, ²³⁶U-spike)
- Ion exchange (BioRad) column separation
- Measurement on Thermal Ionisation Mass Spectrometer-TIMS Finnigan MAT 262 RPQplus

During the preparations as well as at measurements significant difficulties related to:

- Complete dissolution of mineral separates
(from several mineral separates for Taapaca samples satisfying chemistry was achieved from only about half of prepared samples, however from all these prepared solutions mineral separates from only one sample Tap-02-03 got reliable results)
- Th isotopic composition of El Misti whole rocks
Th isotopic ratio of El Misti whole rock samples (²³⁰Th/²³²Th=400 000) was too high for a standard procedure and therefore a modified procedure was applied with double amount of material and 2ml columns to get enough ²³⁰Th for the measurements on the Mass Spectrometer.

➤ TIMS measurements

Problems with keeping stable signal especially for $^{230}\text{Th}/^{232}\text{Th}$ caused necessity for loading of 400-600 ng Th on the filament, while standard procedure after Heumann et al., 2002 concern 200ng

Th measurements were run in a static mode, measuring firstly $^{230}\text{Th}/^{229}\text{Th}$ (with difficult ^{230}Th) and than $^{229}\text{Th}/^{232}\text{Th}$ ratio.

U measurements were run by peak jumping mode (minimum of 1hour for a single measurement)

6.4.1 Chemical separation

Sample dissolution

Powdered whole rock samples (100mg for Taapaca samples and 200mg for El Misti samples) and mineral separates (10-100mg) were digested in cleaned PFA beaker by a 1:2 mixture of concentrated HNO_3 and 40% HF to which few drops of distilled HClO_4 were added to avoid the formation of insoluble fluorides. After two days on hot plate (140°C) solutions were evaporated to dryness, nitrated three times and subsequently dissolved in 6N HCl.

After cooling down, the samples were spiked for U and Th concentrations with ^{229}Th (~0.4 ml) spike and ^{236}U (~0.5ml) spike solutions and left overnight for equilibration.

Procedure for double amount of whole rock El Misti samples followed the procedure after Heumann et al., 2002 but with modified quantity of acids used for dissolution.

Chromatographic ion-exchange technique

The initial separation of Th and U involved two successive elutions on 0.5ml quartz columns containing AGIX8 anion exchange resin (200-400 mesh). After washing with 2ml 7N HNO_3 and collecting Th fraction in 2ml 6N HCl a clean U fraction was collected with 2ml H_2O . Th was farther purified second time on the same but cleaned 0.5ml columns by washing with 5ml 7N HNO_3 and collecting with 1ml 6N HCl. Both separated Th and U fractions were than dried down, nitrated with concentrated HNO_3 and picked up with 0.5ml 7N HNO_3 .

For El Misti whole rock samples 2ml size columns were used with adopted procedure presented above.

Clean fractions of U and Th have been loaded on the filament. Measuring technique contained the measurement on double Re ribbon filaments.

For samples from El Misti Volcano higher amount of clean fractions with average of 600ng for Th and 100 ng of U was loaded on the filaments. For Taapaca whole rocks 10-450 ng of Th and 40-140 ng of U clean fractions were loaded. For mineral separates various amount of U and Th due to different concentrations of U and Th in particular mineral phases were loaded on the filaments.

6.4.2 TIMS analyses

Samples chosen for whole rock and mineral separate analyzes have been measured at Thermal Ionization Mass Spectrometer equipped with RPQ (TIMS_{RPQ+}) at the Geowissenschaftliches Zentrum Göttingen (GZG). The measurements for whole rocks as well as mineral separates have been run together with Table Mountain Latite (TML) as a comparative standard. Total of 20 whole rock samples were analyzed for ^{238}U - ^{230}Th disequilibria. The external reproducibility of ± 0.69 for $^{238}\text{U}/^{234}\text{U}$ and ± 0.73 for $^{230}\text{Th}/^{232}\text{Th}$ (both 2σ) during the course of measurements is showed by repeated analyzes of an 112U-isotope solution (Cheng et al., 2000) and an in-house

$^{230}\text{Th}/^{232}\text{Th}$ -standart solution. Average composition of 174.753 for $^{230}\text{Th}/^{232}\text{Th}$ ratios were obtained for the in-house $^{230}\text{Th}/^{232}\text{Th}$ standard ($^{232}\text{Th}/^{230}\text{Th}=174.752$) and an average composition of 19.045 for $^{238}\text{U}/^{234}\text{U}$ ratios of the U112a-isotope solution ($^{238}\text{U}/^{234}\text{U}=19.044$). Sample isotope measurements by TIMS show an internal reproducibility for $^{238}\text{U}/^{234}\text{U}$ ratios of $\pm 0.5\%$ and for $^{230}\text{Th}/^{232}\text{Th}$ ratios of ± 1.2 (at the 2σ confidence level).

Isochrone calculation was done using last squares fitting of a straight line (York, 1969).

Tab. 6-1 Results for TML and in-house standard measurements for U-Th isotopes.

Sample	[Th] $\mu\text{g/g}$	[U] $\mu\text{g/g}$	($^{238}\text{U}/^{232}\text{Th}$)	($^{230}\text{Th}/^{232}\text{Th}$)	($^{230}\text{Th}/^{238}\text{U}$)	($^{234}\text{U}/^{238}\text{U}$)
572-4	6.98	2.26	0.981 \pm 8	0.998 \pm	1.017	-
572-5	7.02	2.26	0.974 \pm 9	0.995 \pm	1.021 \pm 9	-
573-3	29.97	10.60	1.073 \pm 9	1.013 \pm 11	0.944 \pm 13	1.002 \pm 19
573-4	29.94	10.51	1.065 \pm 6	1.007 \pm 8	0.945 \pm 10	1.001 \pm 16
573-5	29.87	10.49	1.066 \pm 6	1.00 \pm 8	0.938 \pm 10	0.980 \pm 14
388 (1)	27.99	10.81	1.172 \pm 13	-	-	1.005 \pm 12
388 (2)	30.35	10.07	1.007 \pm 86	1.041 \pm 20	1.034 \pm 90	-
388 (3)	-	-	-	-	-	-
388 (4)	31.86	10.52	1.002 \pm 5	1.017 \pm 7	1.015	1.034 \pm 8
388 -4	29.78	10.62	1.082 \pm 7	1.019 \pm 8	0.942 \pm 9	0.998 \pm 6
388 -5	29.05	-	-	1.031 \pm 7	-	-

6.5 Ar/Ar analyzes

Selected samples from Taapaca were measure by Ar/Ar method of dating at the Department of Geology & Geophysics, University of Wisconsin-Madison. Detailed information on the Ar/Ar procedure and method of dating is given in Singer and Pringle (1996).

6.6 Modelling

Tab. 6-2 Calculated composition of primary melts from olivine plus orthopyroxene fractionation models (see text for further explanation). Column from left to write: Nicolson andesite; olivine and orthopyroxene (Tatsumi and Ishizaka 1981); primary melt with Mg-# 68; primary melts with Mg-# 70; primary melts with Mg-# 72. The amount of olivine and orthopyroxene that is needed to arrive at primary conditions (Mg-#68 to 72) is listed in the lowermost lines. All Mg-# are for Fe=0,85 total Fe; *: Fe₂O₃ is calculated from the difference of FeO to FeO^{tot}.

	Nicolson Andesite	Olivin	Opx						
SiO ₂	52,98	40,25	56,5	52,48	52,34	52,19	52,16	51,94	51,68
TiO ₂	1,49			1,32	1,28	1,23	1,34	1,31	1,26
Al ₂ O ₃	16,61	0,00	1,28	14,89	14,41	13,86	15,06	14,66	14,17
Fe ₂ O ₃ *	1,46*			1,30*	1,26*	1,21*	1,32*	1,28*	1,24*
FeO	7,45	9,98	9,17	7,68	7,74	7,81	7,67	7,73	7,80
MnO	0,14	0,15	0,26	0,15	0,15	0,15	0,15	0,15	0,15
MgO	5,52	48,3	29,85	9,14	10,15	11,29	9,15	10,10	11,25
CaO	8,54			7,62	7,36	7,07	7,73	7,51	7,26
Na ₂ O	3,76			3,35	3,24	3,11	3,40	3,31	3,19
K ₂ O	1,85			1,65	1,60	1,53	1,68	1,63	1,58
P ₂ O ₅	0,35			0,31	0,30	0,29	0,32	0,31	0,30
Summe	100,15	98,68	97,06	99,90	99,83		99,97	99,92	
FeO ^{tot}	8,76	9,98	9,17	8,85	8,87	8,90	8,86	8,9	8,9
Mg-#	56,9	89,7	85,3	68,0	70,0	72,03	68,0	70,0	72,0
% Ol				5,4	6,9	8,6	7,1	9,0	11,3
% Opx				5,4	6,9	8,6	2,4	3,0	3,7

Tab. 6-3 Major, trace elements and isotopic composition of Arequipa Basement samples.

Arequipa basement	RCH-04-234	RCH-04-232	BAS_21	Charcani gneiss	041101M Mollendo	average
SiO ₂	65,25	65,45	67,87			66,19
TiO ₂	0,4	0,4	0,51			0,44
Al ₂ O ₃	17,93	16,51	15,58			16,67
Fe ₂ O ₃	3,81	4,89	4,14			4,28
FeO	0	0	0			0
MnO	0,12	0,1	0,07			0,10
MgO	1,9	1,94	1,89			1,91
CaO	4,91	4,96	3,48			4,45
Na ₂ O	3,85	3,41	3,66			3,64
K ₂ O	1,67	2,19	2,66			2,17
P ₂ O ₅	0,14	0,13	0,14			0,14
Summ	100,0	100,0	100,0			100,0
Rb	49	64	117	15		61,25
Sr	374	376	315	150		303,75
Ba	450	651	663			588
La	9,3	34,2	30,8		27,0	25,3
Ce	19,3	66,2	63,1		41,2	47,5
Nd	10,3	26,6	25,3	36	9,8	21,6
Sm	2,3	4,4	4,1		1,3	3,0
Eu	0,6	1	1,1		1,1	1,0
Gd	1,7	3,5	3,1		1,0	2,3
Dy	2,8	3	2,4		0,4	2,2
Er	1,2	1,7	1,3		0,3	1,1
Yb	1,4	1,9	1,1		0,4	1,2
Lu	0,2	0,3	0,2		0,1	0,2
Nb	7	7	9			7,7
Ta	0,5	0,5	0,2		0,6	0,4
Zr	81	109	161			117
Hf	1,3	1	1,9		1,26	1,37
Pb	11,8	9,7	12,6		18,1	13,05
Th	2,2	9,7	1,5		0,833	3,56
U	0,7	1,2	0,1		0,107	0,53
87Sr/86Sr	0,7056	0,7075	0,7303	0,74	0,746	0,72588
143Nd/144Nd	0,512747	0,512258	0,511463	0,5115		0,511992
206Pb/204Pb	18,43	17,94	17,12			17,83
207Pb/204Pb	15,62	15,58	15,59			15,60
208Pb/204Pb	38,42	38,81	38,20			38,47
18 O			6,3		10,6	8,45
(238U/232Th)	0,97	0,38	0,47	0,20		0,45
(230Th/232Th)	0,97	0,38	0,47	0,20		0,45

Tab. 6-4 Mineral/melt partition coefficient used for modeling (source: German Reservoir Database).

Kd (mineral/melt part coeff)	O1	Opx	Cpx	Gt	Mt	Amph	Plag
Rb	0,04	0,0006	0,011	0,0007	0,15	0,12	0,1
Sr	0,000033	0,0007	0,093	0,0008	0,11	0,5	2
Ba	0,0000055	0,013	0,00036	0,0000062	0,26	0,42	0,3
La	0,0004	0,002	0,056	0,01	0,098	0,17	0,27
Ce	0,01	0,003	0,098	0,03	0,11	0,26	0,2
Nd	0,0059	0,0068	0,23	0,087	0,14	0,44	0,014
Sm	0,0004	0,01	0,26	0,29	0,15	0,76	0,12
Eu	0,0016	0,013	0,474	0,32	0,1	0,88	0,07
Gd	0,01	0,016	0,3	0,498	0,14	0,86	0,05
Dy	0,007	0,022	0,33	3,17		0,78	0,17
Er	0,0256	0,08	0,4	3,6		0,68	0,019
Yb	0,0491	0,09	0,45	4,03	0,17	0,59	0,03
Lu	0,018	0,06	0,28	5,5		0,51	0,008
Nb	0,01	0,15	0,04	0,02	0,8	0,12	0,01
Zr	0,06	0,02	0,128	0,65	0,28	0,2	0,2
Hf	0,04	0,01	0,263	0,23		0,1	0,01
Pb	0,0003	0,0013	0,0075	0,0003		0,1	0,36
Th	0,0000062	0,00005	0,003	0,0014		0,11	0,07
U	0,0000078	0,00004	0,002	0,00588		0,15	0,08

7 Literature

Ablay G.J., 1997, Evolution of the Teide-Pico Viejo volcanic complex and magmatic system Tenerife, Canary Islands. PhD Thesis, University of Bristol.

Abley G.J., Carroll M.R., Palmer M.R., Marti J., Sparks R.S.J., 1998, Basanite-phonolite lineages of the Teide-Pico Viejo volcanic complex, Tenerife, Canary Islands: *Journal of Petrology*, v. 39, p. 905-936.

Aitcheson S.J., Harmon R.S., Moorbath S., Schneider A., Sole P., Soria E.E., Steele G., Swainbank I., Wörner G., 1995, Pb isotopes define basement domains of the Altiplano, Central Andes: *Geology*, v. 23, p. 555-558.

Allmendiger R.W., Jordan T.E., Kay S.M. and Isacks B., 1997, The evolution of the Altiplano-Puna plateau of the Central Andes: *Annual Reviews of Earth and Planetary Sciences*, v. 25, p. 139-174.

Allmendiger R.W., Figueroa D., Snyder D., Beer J., Mpodozis C., Isacks B.L., 1990, Foreland shortening and crustal balancing in the Andes at 30°S latitude: *Tectonics*, v. 9, p. 789-809.

Allégre C.J., 1968, ^{230}Th dating of volcanic rocks: a comment: *Earth and Planetary Science Letters*, v. 5, p. 209-210.

Allégre C.J., Coandominés M., 1976, Fine chronology of volcanic processes using ^{238}U - ^{230}Th systematics: *Earth and Planetary Science Letters*, v. 28, p. 395-406.

Allegré C.J., Dupré B., Lewin E., 1986, Thorium/Uranium ratio of the earth: *Chemical Geology*, v. 56, p. 219-227.

Arndt N.T., Goldstein S.L., 1989, An open boundary between lower continental crust and mantle: its role in crust formation and crustal recycling: *Tectonophysics*, v. 161, p. 201-112.

Ayers J., Dittmer S.K., Layne G.D., 1997, Partitioning of elements between peridotite and H_2O at 2.0-3.0 GPa and 900-1100°C, and implications to models of subduction zone processes: *Earth and Planet. Science Letters*, v. 4, p. 606-692.

Balburg H., Hevre F., 1997, Geodynamic evolution and tectonostratigraphic terranes of northwestern Argentina and Northern Chile: *Geolog. Soc. Am. Bull.*, v. 109, p. 869-884.

Banaszak m., 2007, Kristallisationsbedingungen und Barium-Zonierung von Sanidinen in Magma des Taapaca Vulkans, Nord Chile, Diploma Thesis, Georg-August Universität Göttingen.

Barazangi M., Isacks B., 1976, Spatial distribution of earthquakes and subduction of the Nazca plate beneath South America: *Geology*, v. 4, p. 606-692.

Barreiro B.A., Clark A.H., 1984, Lead isotopic evidence for evolutionary changes in magma crust interaction, Central Andes, Southern Peru: *Earth and Planetary Sci. Lett.*, v. 69, p. 30-42.

Beaumont C., Janieson R.A., Nguyen M.H. and Lee B., 2001, Himalayan tectonics explained by extrusion of a low viscosity crustal channel coupled to focused surface denudation: *Nature*, v. 414, p. 738-742.

Beck S.L., Zandt G., 2002, The nature of orogenic crust in the Central Andes: *J. Geophys. Res.*, v. 107doi:10.1029/2000JB000124.

Berlo K., Turner S., Blundy J., Hawkesworth C., 2004, The extent of U-series disequilibria produced during partial melting of the lower crust with implications for the formation of the Mount St. Helens dacites: *Contrib. Mineral. Petrol*, v. 148, p. 122-130.

Black S., Macdonald R., De Vivo B., Kilburn C.R.J., Rolandi F., 1998, U-series disequilibria in young (A.D. 1944) Vesuvius rocks: preliminary implications for magma residence times and volatile addition: *Journal of Volcanology and Geothermal Research*, v. 82, p. 97-111.

Black S., Macdonald R., Kelly M.R., 1997, Crustal origin for peralkaline rhyolites from Kenya: evidence from U-series disequilibria and Th-isotopes: *Journal of Petrology*, v. 38, p. 277-297.

Bohrson W.A., Reid M.R., 1998, Genesis of evolved ocean island magmas by deep-and shallow-level basement recycling, Socorro Island: *Journal of Petrology*, v. 39, p. 4.

Bosch M., Rodriguez I., 1992, North Venezuelan collisional crustal block; the boundary between the Caribbean and South American plates: *Journal of South American Earth Sciences*, v. 6, p. 133-143.

Bourdon B., Zindler A., Wörner G., 1994, Evolution of the Laacher See magma chamber: evidence from SIMS and TIMS measurements of U-Th disequilibria in minerals and glasses: *Earth and Planetary Science Letters*, v. 126, p. 75-90.

Bourdon B., Wörner G., Zindler A., 2000, U series evidence for crustal involvement and magma residence times in the petrogenesis of Parinacota volcano, Chile: *Contribution to Mineralogy and Petrology*, v. 139, p. 458-469.

Bourdon B., Henderson G.M., Lundstrom C.C., Turner S.P., 2003, Uranium-Series Geochemistry, Geochemical Society, Mineralogical Society of America.

Boyton W.V., 1984, Geochemistry of the rare earth elements: meteorite studies, in P. Henderson, ed., *Rare Earth Elements Geochemistry*: Amsterdam, Elsevier, p. 63-114.

Brennan J.M., Shaw H.F., Reyerson J.F., 1995, Experimental evidence for the origin in lead enrichment in convergent-margin magmas: *Nature*, v. 378, p. 54-56.

Börstrom K., Joensuu O., Valdes S., Charm W., Glaccum R., 1976, Geochemistry and origin of East Pacific sediments sampled during DSDP Leg 34, in Yeats R.S. et al., ed., *Initial Rep Deep Sea Drill Project*: Washington, p. 559-574.

Cahill T. and Isacks B.L., 1992, Seismicity and shape of the subducted Nazca plate: *J. Geophys. Res.*, v. 97, p. 17, 503-17, 529.

Capaldi G., Cortini M., Gasparini P., Pece R., 1976, Short lived radioactive disequilibria in freshly erupted volcanic rocks and their implications for the pre-eruption history of a magma: *J. Geoph Res.*, v. 81, p. 350-358.

Charlier B.L., Blake S., Wilson C.J.N., van Calstern P.W., 2000, Magma residence times at Taupo volcano: a zircon U-series study. In: Smith I.E., Davidson J., Gamble J.A., Price R.G., (eds) *State of the Arc 2000: Processes and Time Scales. Extended Abstracts.* Wellington: Royal Society of New Zealand., p. 32-35.

Cheng J.H., Edward R.L., Hoff J., Gallup C.D., Richards D.A. and Asmerom Y., 2000, The half-life of uranium-234 and thorium-230: *Chemical Geology*, v. 169, p. 17-33.

Cheng J.H., Edwards R.L., and Wasserburg G.J., 1992, Mass spectrometry and application to uranium-series disequilibrium. In: Ivanovich, M. and Harmon R., (eds) *Uranium series disequilibrium: Application to environmental problems.* p. 174-205, Clarendon Press, Oxford.

Clavero JE., Sparks RSE, Pringle MS., Polanco E., Gardeweg MC (2004) Evolution and volcanic hazard of Taapaca Volcanic Complex, Central Andes of Northern Chile. *J. Geol. Soc. London* 161, 603-618.

Claude-Ivanaj C., Bourdon B., Allegré CJ., 1998, Ra-Th-Sr isotope systematics in Grande Comore Island: A case study of plume-lithosphere interaction.: *Earth and Planet. Scienc. Lett.*, v. 164, p. 99-117.

Cobbing EL, Ozard JM., Snelling NJ., 1977, Reconnaissance geochronology of the crystalline basement rocks of the Coastal Cordillera of southern Peru: *Geol. Soc. Am. Bull.*, v. 88, p. 241-246.

Coira B., Davidson J., Mpodozis C., Ramos V., 1982, Tectonic and magmatic evolution of the Argentine Puna-model for changing subduction geometry: *International Geology Review*, v. 35, p. 677-720.

Condomines M., Tanguy J-C, Michaud V., 1995, Magma dynamics at Mt Etna: Constraints from U-Th-Ra-Pb radioactive disequilibria and Sr isotopes in historical lavas: *Earth and Planetary Science Letters*, v. 132, p. 25-41.

Condomines M., Hemond C., Allegré CJ., 1988, U-Th-Ra radioactive disequilibria and magmatic processes.: *Earth and Planet. Scienc. Lett.* v. 90, p. 243-262.

Condomines M., Gauthier P-J, Sigmarsson O., 2003, Timescales of Magma Chamber Processes and Dating of Young Volcanic Rocks.

Costa F., Chakraborty S., Dohmen R., 2003, Diffusion coupling between trace and major elements and a model for calculation of magma residence times using plagioclase: *Geochimica et Cosmochimica Acta*, v. 67, p. 2189-2200.

Dalmayrac B., Laubacher G., Mocco R., 1997, *Geology des Andes Peruviennes, Caracteres Genereaux de L'évolution géologique des Andes Peruviennes, Techniques de Lanuedoc*, 361 p.

Dalziel I.W.D., 1992, On the organization of American plates in the Neoproterozoic and the breakout of Laurentia: *GSA Today*, v. 2, p. 237, 240-241.

Dalziel I.W.D., 1993, Tectonic tracers and the origin of the Proto-Andean margin: XII Congreso Geológico Argentino y II Congreso de Exploración de Hidrocarburos Actas, v. III, p. 367-374.

Damm K.W., P. S., Harmon R.S., Todt W., Omaniri R., Niemeyer H., 1990, Pre-Mesozoic evolution of the Central Andes basement (19°-24°). In: Reutter K.J., Scheeuber E., and Wigger P.J. (eds). *Tectonic of the Southern Central Andes*. Springer Verlag, Berlin, p. 263-276.

Damm K.W., Pichowiak S., Harmon R.S., Todt W., 1986, Geochemie, Petrologie und Geochronologie der Plutonite und des metamorphen Grundgebirges in Nordchile: *Berliner Geowissenschaftliche Abhandlungen*, v. A/66, p. 73-146.

Davidson J.P., Harmon R.S., Wörner G., 1991, The source of the Central Andes magmas: some considerations: *Geolog. Soc. Am. Andean magmatism and its tectonics settings*, v. 265, p. 233-244.

Davidson J.P., McMillan N.J., Moorbath S., Wörner G., Harmon R.S., Lopez-Escobar L., 1990, The Nevados de Payachata volcanic region (18°S/69°W, N.Chile) II. Evidence for a widespread crustal involvement in Andean magmatism: *Contribution to Mineralogy and Petrology*, v. 105, p. 412-432.

Davidson J.P. and Tepley F.J. III, 1997, Recharge in volcanic systems; evidence from isotope profiles of phenocrysts: *Science*, v. 275, p. 826-29.

Davies G.R., Halliday A.N., Mahood G.A., Hall Ch.M., 1994, Isotopic constraints on the production rates, crystallisation histories and residence times of pre-caldera silicic magmas, Long Valley, California: *Earth and Planetary Science Letters*, v. 125, p. 17-37.

Davies JH., von Blackenburg F., 1995, Slab breakoff: A model of lithosphere detachment and its test in the magmatism and deformation of collisional orogens. *Earth and Planetary Science Letters* v. 129, p. 85-102.

De Silva S.L., 1989, Altiplano-Puna volcanic complex of the central Andes: *Geology*, v. 17, p. 1102-1106.

DeSilva S.L., Francis P.W., 1990, Potentially active volcanoes of Peru-Observations using Landsat Thematic Mapper and Space Shuttle imagery.: *Bull of Volcanology*, v. 52, p. 286-301.- 1991, *Volcanoes of the Central Andes*: Heidelberg, Springer- Verlag, p. 232.

Deer W.A., Howie R.A., Zussman J., 1982, *Rock forming Minerals-Orthosilicates*, Longman Group.

Deer W.A., Howie R.A., Zussman J., 1987, *Rock forming Minerals-Single Chain Silicates*, Longman Group.

Dufek J., Cooper K.M., 2005, $^{226}\text{Ra}/^{230}\text{Th}$ excess generated in the lower crust: implications for magma transport and storage timescales: *Geology*, v. 33, p. 833-836.

Edwards R., R.L., Cheng J.H., and Wasserburg G.J., 1986, ^{238}U - ^{234}U - ^{230}Th - ^{232}Th systematics and the precise measurement of time over the past 500 000 years: *Earth and Planetary Science Letters*, v. 81, p. 175-192.

Elliot T., Plank T., Zindler A., While W., Bourdon B., 1997, Element transport from slab to volcanic front at the Mariana arc: *J. Geophysical Research*, v. 102, p. 14991-15019.

Entenmann J., 1991, Magmatic evolution of the Nevados de Payachata complex and the petrogenesis of basaltic andesites in the Central Volcanic Zone of northern Chile., Mainz, 177 p.

Evans P., 1999, U-series disequilibrium study of the Longonot trachyte magma chamber, Kenya: PhD Thesis, The Open University, Milton Keynes.

Ewart A., Griffin W.L., 1994, Application of proton-microprobe data to trace-element partitioning in volcanic rocks, trace-element partitioning with application to magmatic processes: *Chemical Geology*, v. 117, p. 251-284.

Foley S.F., Barth M.G., Jenner G.A., 2000, Rutile/melt partition coefficients for trace elements and an assessment of the influence of rutile on the trace element characteristics of subduction zone magmas: *Geochimica Cosmochimica Acta*, v. 64, p. 7933-938.

Gansekki C.A., Mahood G.A., and McWilliams M.O., 1996, $^{40}\text{Ar}/^{39}\text{Ar}$ geochronology of rhyolites erupted following collapse of the Yellowstone caldera, Yellowstone Plateau volcanic field: implications for crustal contamination: *Earth and Planetary Science Letters*, v. 142, p. 91-107.

Garcia M., Herail G., Charrier R., 1996, The Cenozoic forearc evolution in Northern Chile. 3rd ISAG, St. Malo, France, Andean Geodynamics. Orstom Editions, Collection Colloques et Seminares, p. 359-362.

Garrison J., Davidson J., Reid M., Turner S., 2006, Source versus differentiation controls on U-series disequilibria: Insights from Cotopaxi Volcano, Ecuador: *Earth and Planetary Science Letters*, v. 244, p. 548-565.

Nichols G.T., Wyllie P.J., Stern C.R., 2002, Subduction zone melting of pelagic sediments constrained by melting experiments: *Nature* v.371, p. 785-788.

Gerlach D.C. and Grove T.L., 1982, Petrology of Medicine Lake Highland volcanics: characterisation of endmembers of magma mixing: *Contribution to Mineralogy and Petrology*, v. 80, p. 147-159.

Giese P., Scheuber E., Schilling F., Schmitz M., Wigger P., 1999, Crustal thickening processes in the Central Andes and the different natures of the Moho-discontinuity: *J. South Am. Earth Science*, v. 12, p. 201-220.

Gill J.B., Williams R.W., 1990, Th isotope and U-series studies of subduction-related volcanic rocks: *Geochimica et Cosmochimica Acta*, v. 54, p.1427-1441.

Gill J.B., Pyle D., and Williams R.W., 1990, Igneous rocks. In *Uranium Series Disequilibrium* (eds. M. Ivanovich and R.S. Harmon), 2nd edition, Oxford Univ. Press.

Ginibre C., Wörner G., Kronz A., 2002, Minor- and trace-element zoning in plagioclase: implications for magma chamber processes at Parinacota volcano, northern Chile: *Contribution to Mineralogy and Petrology*, v. 143, p. 300-315.

Goldstein S.J., Murrell M.T., and Janecky D.R., 1990, Th and U isotopic systematics of basalts from Juan de Fuca and Gorda ridges by mass spectrometry: *Earth and Planet. Sci. Lett*, v. 96, p. 134-146.

Goldstein S.J. and Stirling C.H., 2002, Techniques for measuring U-series Nuclides 1992-2002: *Reviews in Mineralogy and Geochemistry*, v. 52, p. 23-57.

Gorring M.L., Kay S.M., Zeitler P.K., Ramos V.A., Rubiolo D., Fernández M.I. and Panza J.L., 1997, Neogene Patagonian plateau lavas: continental magmas associated with ridge collision at the Chile Triple Junction: *Tectonics*, v. 16, p. 1-17.

Harmon R.S., Barreiro B.A., Moorbath S., Hoefs J., Francis P.W., Thorpe R.S., Déruelle B., MaHugh J., Viglino J.A., 1984, Regional O-, Sr- and Pb relationships in Late Cenozoic calc-alkaline lavas of the Andean Cordillera: *J. Geol. Soc. London*, v. 141, p. 803-822.

Hawkesworth C., T. S., Peate D., McDermott F., van Calsteren P., 1997a, Elemental U and Th variations in island arc rocks: implications from U-series isotopes: *Chemical Geology*, v. 139, p. 207-222.

Hawkesworth C., Blake S., Evans E., Hughes R., Macdonald R., Thomas L., Turner S., Zellmer G., 2000, The time scales of crystal fractionation in magma chambers - interpreting physical, isotopic and geochemical perspectives: *Journal of Petrology*, v. 41, p. 991-1006.

Heath E., Turner S.P., Macdonald R., Hawkesworth C.J., P.van Calsteren, 1998b, Long magma residence time at an island arc volcano (Soufriere, St. Vincent) in the Lesser Antilles: evidence from ^{238}U - ^{230}Th isochron dating: *Earth and Planetary Science Letters*, v. 160, p. 49-63.

Hervé F., Demant A., Ramos VA, Pankhurst R.J., Suárez M., 2000, The Southern Andes. In: *Tectonic evolution of South America* (Cordani UG; Milani E.J., Thomaz Filho A., Campos DA., editors): *International Geological Congress*, p. 605-634.

Heumann A., Davies G.R., Elliott T.R., Staudigel H., Freedman P., Kara A., 1995, Magma chamber residence times: a Sr-Th isotope study of high silica rhyolites in Kenya: *Terra Nova*, v. 7, p. 154.

Heumann A. and Davies G.D., 2002, U-Th disequilibrium and Rb-Sr age constraints on the magmatic evolution of peralkaline rhyolites from Kenya: *Journal of Petrology*, v. 43, p. 557-557.

Higgins M.D., 1996a, Crystal size distributions and other quantitative textural measurements in lavas and tuff from Egmont volcano (Mt. Taranaki), New Zealand: *Bulletin of Volcanology*, v. 58, p. 194-204.

Higgins M.D., 1996b, Magma dynamics beneath Kameni volcano, Thera, Greece, as revealed by crystal size and shape measurements: *Journal of Volcanology and Geothermal Research*, v. 70, p. 37-48.

Higgins M.D., 2000, Measurement of crystal size distributions: *American Mineralogist*, v. 85, p. 1105-1116.

Hildreth W. and Moorbath S., 1988, Crustal contributions to arc magmatism in the Andes of central Chile: *Contribution to Mineralogy and Petrology*, v. 98, p. 455-489.

Hole M.J., Saunders A.D., Marriner G.F., Tarney J., 1984, Subduction of pelagic sediments: implications for the origin of Ce-anomalous basalt from the Mariana Islands: *Journal of Geological Society*, v. 141, p. 453-472.

Huene R., Weinrebe W., Heeren F., 1999, Subduction erosion along the North Chile margin: *Geodynamics*, v. 27, p. 345-358.

Irving A.J., Frey F.A., 1978, Distribution of trace elements between garnet megacrysts and host volcanic liquids of kimberlitic to rhyolitic composition: *Geochim. Cosmochim. Acta*, v. 42, p. 771-787.

Isacks B.L., 1988, Uplift of the Central Andean plateau and bending of the Bolivian Orocline: *J. Geophys. Res.*, v. 93, p. 3211-3231.

Ivanovich M. and Harmon R.S., 1992, Uranium-series disequilibrium: Applications to Earth, Marine and Environmental Sciences: New York, Oxford Science Publications, Oxford University Press.

James D.E., 1982, A combined O, Sr, Nd, and Pb isotopic and trace element study of crustal contamination in central Andean lavas, I. Local geochemical variations: *Earth and Planetary Science Letters*, v. 57, p. 47-62.

James D.E., Sacks I.S., 1999, Cenozoic formation of the central Andes: a geophysical perspective in *Geology and Ore Deposits of the Central Andes*: Littleton, Society of Economic Geologists, p. 1-25.

Kay R.W., 1980, Volcanic arc magmas: implications of a melting-mixing model for element recycling in the crust-upper mantle system: *J. Geology*, v. 88, p. 497-522.

Kay S.M., Mpodozis C., Coira B., 1999, Neogene magmatism, tectonism and mineral deposits of the Central Andes (22°S to 33°S). In: *Geology of Ore Deposits of the Central Andes*: Soc. Econ. Geol. Spec. Pub., v. 7.

Keppler H., 1996, Constraints from partitioning experiments on the composition of subduction-zone fluids: *Nature*, v. 380, p. 237-240.

Kessel R., Schmidt M.W., Ulmer P., Pettke T., 2005, Trace element signature of subduction-zone fluids, melts and supercritical liquids at 120-180 km depth: *Nature*, v. 437, p. 724-727.

Kigoshi K., 1967, Ionium dating of igneous rocks: *Science*, v. 156, p. 932-934.

Kohlbach I. and Lohnert E., 1999, Geological Map of Taapaca Volcano and adjacent areas (North Chile) 1:25 000. Diploma Mapping Thesis, Georg-August Universität Göttingen.

LeMaitre R.W., 1989, A classification of igneous rocks and glossary of terms: Oxford, Blackwell.

Lezaun J., 1997, Geochronology of Andine basement and tertiary volcanics. MS Thesis (unpublished), University of Göttingen, p. 1-124.

Loewy S.L., Conelly J.N., Dalziel I.W.D., 2004, An Orphaned Basement Block: The Arequipa-Antofalla Basement of the Central Andean margin of South America: *Geol. Soc. Am. Bull.*, v. 116, p. 171-187.

Lohnert E., 1999, Chemical variations of a sanidine megacryst and its implications on the pre-eruptive evolution of the Taapaca volcano in North Chile: Electron Microprobe and Sr-isotope studies, Georg-August Universität Göttingen.

Lundstrom C. C., Hoernle K., Gill J., 2003, U-series disequilibria in volcanic rocks from the Canary Islands: Plume versus lithospheric melting: *Geochimica et Cosmochimica Acta*, v. 67, p. 4153-4177.

Malburg Kay S. and Mpodozis C., 2002, Magmatism as a probe to the Neogene shallow of the Nazca plate beneath the modern Chilean flat slab: *Journal of South American Earth Science*, v. 15, p. 39-59.

Mamani M.I., 2006, Variation in magma composition in time and space along the Central Andes (13°S-28°S). PhD Thesis, Georg-August Universität Göttingen, p. 122.

Manning C.E., 2004, The chemistry of subduction zone fluids: *Earth and Planet. Science Letters*, v. 223, p. 1-16.

Marsch B.D., 1988, Crystal size distribution (CSD) in rocks and the kinetics and dynamics of crystallisation. I: theory: *Contribution to Mineralogy and Petrology*, v. 99, p. 277-291.

McCulloch M.T. and Gamble J.A., 1991, Geochemical and geodynamical constraints on subduction zone magmatism: *Earth and Planet. Science Letters*, v. 102, p. 358-374.

McDemott F., and Hawkesworth C., 1991, Th, Pb, and Sr isotope variations in young island arc volcanics and oceanic sediments: *Earth and Planet. Sci. Lett.*, v. 104, p. 1-15.

McDermott F., Elliot T., van Clasteren P. and Hawkesworth C.J., 1993, Measurement of $^{230}\text{Th}/^{232}\text{Th}$ ratios in young volcanic rocks by single-sector thermal ionisation mass spectrometry: *Chemical Geology*, v. 103, p. 283-292.

- McKenzie D., 1985, ^{230}Th - ^{238}U disequilibrium and the melting processes beneath ridge axes: *Earth and Planet. Sci. Lett*, v. 72, p. 149-157.
- Miller D.M., Goldstein S.L., Langmuir C.H., 1994, Cerium/lead and lead isotope ratios in arc magmas and the enrichment of lead in the continents: *Nature*, v. 368, p. 514-520.
- Mitchell A.H. and Reading H.G., 1969, Continental margins, geosynclines and ocean floor spreading: *J. Geol.*, v. 77, p. 629-646.
- Mpodozis C., Ramos V.A., 1990, The Andes of Chile and Argentina. In *Geology of the Andes and its relation to hydrocarbon and mineral resources* (Ericksen, G.E.; Pinochet M.T.C.; Reinemund J.A.; editors). Circum Pacific Council for Energy and Mineral Resources, Earth Science Series, p. 59-90.
- Mukasa S.B. and Henry D.J., 1990, The San Nicolás batholith of coastal Peru: early Paleozoic continental arc or continental rift magmatism? *Journal of Geological Society*, v. 147, p. 27-39.
- Nakamura M., 1995, Continuous mixing of crystal mush and replenished magma in the ongoing Unzen eruption: *Geology*, v. 23, p. 807-810.
- Newman S., Finkel R.C., MacDougall J.D., 1984, Comparison of ^{230}Th - ^{238}U disequilibrium systematics in lavas from three hot spot regions: Hawaii, Prince Edward and Samoa: *Geochimica et Cosmochimica Acta*, v. 48.
- Norambuena E., Leffer-Griffin L., Mao A., Dixon T., Stein S., Sacks S., Ocola L., Ellis M., 1998, Space geodetic observations of Nazca-South America convergence across the Central Andes: *Science*, v. 279, p. 358-362.
- Nur A. and Ben-Avraham Z., 1982, Oceanic Plateaus, the fragmentation of continents and mountain building: *J. Geophysical Research*, v. 87, p. 3644-3662.
- Otman D.B., White W.M., Patchett J., 1989, The geochemistry of marine sediments, island arc magma genesis, and crust-mantle recycling: *Earth and Planetary Science Letters*, v. 94, p. 1-21.
- Oversby V.M. and Gast P.W., 1968, Lead isotope composition and uranium decay series disequilibrium in recent volcanic rocks: *Earth and Planetary Science Letters*, v. 5, p. 199-206.
- Pardo-Casas F. and Molnar F., 1987, Relative motion of the Nazca (Farallon) and South American plates from Late Cretaceous time: *Tectonics*, v. 6, p. 233-248.
- Parkinson I. J., Hammond S. J., James R. H., Rogers N. W., 2007, High-temperature lithium isotope fractionation: Insights from lithium isotope diffusion in magmatic systems: *Earth and Planetary Science Letters*, v. 257, p. 609-621.
- Paquereau-Lebti P., Thouret J.C., Wörner G. and Fornari M., 2006, Neogene and Quaternary ignimbrites in the area of Arequipa, Southern Peru: stratigraphical and petrological correlations: *Journal of Geothermal Research*, v. 154, p. 251-275.

- Peate D.P. and Hawkesworth Ch.J., 2005, U series disequilibria: Insights into mantle melting and the timescales of magma differentiation: *Reviews of Geophysics*, v. 43, p. RG1003, doi: 10.1029/2004RG000154.
- Pilger R.H., 1984, Cenozoic plate kinematics, subduction and magmatism: South American Andes: *Journal of Geodynamics*, v. 27.
- Plank T. and Langmuir C.H., 1993, Tracing trace elements from sediment input to volcanic output at subduction zones: *Nature*, v. 362, p. 739-746.
- Ramos V.A., 1988, Late Proterozoic-Early Paleozoic of South America - a collisional history: *Episodes*, v. 11, p. 168-174.
- Ramos V.A., 1999, Plate Tectonic Settings of the Andean Cordillera: *Episodes*, v. 22, p. 183-190.
- Ramos V.A. and Kay S.M., 1992, The Southern Patagonian plateau basalts: retroarc testimony of a ridge collision, Argentina. In: Olivier R.A., Vatin-Perignon N., Laubacher G., (eds) *Andean Geodynamics Symposium*, Grenoble, Tectonophysics, p. 261-282.
- Reagan M.K., Volpe A.M., Cashman K.V., 1992, ^{238}U and ^{232}Th -series chronology of phonolite fractionation at Mount Erebus, Antarctica: *Geochimica et Cosmochimica Acta*, v. 56, p. 1401-1407.
- Reid M.R, Coath C.D., Harrison M., McKeegan K.D., 1997, Prolonged residence times for the youngest rhyolites associated with Long Valley Caldera: ^{230}Th - ^{238}U ion microprobe dating of young zircons: *Earth and Planetary Science Letters*, v. 150, p. 27-39.
- Ruprecht P., 2004, Zoned plagioclase in lavas from El Misti volcano (S. Peru): Implications for changing regimes in the magma chamber: *Diploma Thesis*, Universität Göttingen, Germany.
- Ruprecht P. and Wegner W., 2003, *Stratigraphy of Rio Chili Canyon*, Georg-August University, Göttingen.
- Ruprecht P., Wörner G., 2007, Variable regimes in magma systems documented in plagioclase zoning patterns: El Misti stratovolcano and Andagua monogenetic cones: *Journal of Volcanology and Geothermal Research* 165, p. 142-162.
- Sadowski G.R. and Bettencourt J.B., 1996, Mesoproterozoic tectonic correlations between eastern Laurentia and the western border of the Amazon Craton: *Precambrian Research*, v. 76, p. 213-227.
- Shackleton R.M., Ries A.C., Coward M.P. and Cobbold P.R., 1979, Structure, metamorphism and geochronology of the Arequipa Massif of coastal Peru: *Journal of the Geological Society*, London., v. 136, p. 195-214.
- Sigmarsson O., Carn S., Carracedo J.C., 1998, Systematics of U-series nuclides in primitive lavas from the 1730-36 eruption on Lanzarote, Canary Islands, and implications for the role of garnet pyroxenites during oceanic basalt formation.: *Earth and Planet. Scienc. Lett.*, v. 163, p. 137-151.

Singer B.S. and Pringle M.S., 1996, Age and duration of the matuyama-Brunhes geomagnetic polarity reversal from $^{40}\text{Ar}/^{39}\text{Ar}$ incremental heating analyses of lavas: *Earth and Planetary Science Letters*, v. 139, p. 47-61.

Singer B.S., Cauvin A., and Roperch P., 1996, High precision $^{40}\text{Ar}/^{39}\text{Ar}$ dating of Tahiti lavas recording geomagnetic reversals in the later Matuyama Chron: *EOS, Transactions, AGU*, v. 77, p. 173.

Singer B.S., Wijbrans J.R., Nelson S.T., Pringle M.S., Feeley T.C., and Dungun M.A., 1998, Inherited argon in a Pleistocene andesite lava; $^{40}\text{Ar}/^{39}\text{Ar}$ incremental-heating and laser-fusion analyses of plagioclase: *Geology*, v. 26, p. 427-430.

Stalder R., Foley S.F., Brey G.P., Horn I., 1998, Mineral-aqueous fluid partitioning of trace elements at 900-1200°C and 3.0-5.7 GPa: new experimental data for garnet, clinopyroxene and rutile, and implications for mantle metasomatism: *Geochimica et Cosmochimica Acta*, v. 62, p. 1781-1801.

Stern C.R., 1991, Role of subduction erosion in the generation of Andean Magmas: *Geology*, v. 19, p. 78-81.

Stern C., Kilian R., 1996, Role of the subducted slab, mantle wedge and continental crust in the generation of adakites from the Andean Austral Volcanic Zone: *Contribution to Mineralogy and Petrology*. V. 123, p. 263-281.

Stern C., 2004, Active Andean volcanism: its geologic and tectonic setting: *Rev. geol. Chile*, v. 31, p. 161-206.

Stern R., 2006, Backbone of the Americas - Patagonia to Alaska-: 3-7 April 2006 Mendoza, Argentina.

Sun S-S and McDonough W.F., 1989, Chemical and isotopic systematics of ocean basalts: Implications for mantle compositions and processes, in Saunders A.D. and Norry M.J., ed, *Magmatism in the Ocean Basins*, v. 42, *Geol Soc London Spec. Publ*, p. 313-345.

Sébrier M. and Soler P., 1991, Tectonics and magmatism in the Peruvian Andes from Late Oligocene time to the present. In: Harmon R.S., and Rapela C.W., (eds) *Andean magmatism and its tectonic setting: Geological Society of America Special Paper*, v. 265, p. 259-276.

Tadeucci A., Broecker W.S., Thurber D., 1967, ^{230}Th dating of volcanic rocks: *Earth and Planetary Science Letters*, v. 3, p. 338-342.

Tatsumi Y., 1982, Origin of high-magnesian andesites in the Stouchi volcanic belt, southwest Japan, II. Melting phase relations at high pressures: *Earth and Planetary Science Letters*, v. 60, p. 305-317.

Tatsumi Y. and Ishizaka K., 1981, Existence of andesitic primary magma: An example from Southwest Japan: *Earth and Planetary Science Letters*, v. 53, p. 124-130.

Tatsumi Y., Sukuyama M., Fukuyama H., Kushiro I., 1983, Generation of arc basalt magmas and thermal structure of the mantle wedge in subduction zones: *Journal of Geophysical Research*, v. 88, p. 5815-5825.

Teutter K.J. and Wigger P.J., *Tectonics of the Southern Central Andes. Structure and evolution of an active continental margin*: Berlin, Springer.

Thornburg T. and Kulm L.D., 1987, Sedimentation in the Chile Trench: Depositional morphologies, lithofacies, and stratigraphy: *Geolog. Soc. Am. Bull*, v. 98, p. 33-52.

Thorpe R.S., 1982, *Andesites: Orogenic Andesites and Related Rocks*, 724 p.

Thouret J.C., 2005, The stratigraphy, depositional processes and environment of the late Pleistocene Pollalio-period deposits at Mount Hood Volcano, Oregon, USA: *Geomorphology*, v. 70, p. 12-32.

Thouret J.C., Finizola A., Fornari M., Legeley-Padovani A., Suni J., F. M., 2001, Geology of El Misti volcano near the city of Arequipa, Peru: *GSA Bull*, v. 113, p. 1593-1610.

Tilton G.R. and Barreiro B.A., 1980, Origin of lead in Andean calc-alkaline lavas, southern Peru: *Science*, v. 210, p. 1245-1247.

Tosdal R.M., 1996, The Amazon-Laurentian connection as viewed from the Middle Proterozoic rocks in the central Andes, western Bolivia and northern Chile: *Tectonics*, v. 15, p. 827-842.

Turner S. P., Bourdon B., Gill J., 2003, Insights into magma genesis at convergent margins from U-series isotopes. In: Turner SP (Ed.) *Uranium-Series Geochemistry. Reviews in Mineralogy and Geochemistry: Reviews in Mineralogy and Geochemistry*, v. 52, p. 255-316.

Turner S. P., George R.M.M., Jerram D. A., Carpenter N., Hawkesworth C. J., 2003c, Some case studies of plagioclase growth and residence times in island arc lavas from the Lesser Antilles and Tonga, and a model to reconcile apparently disparate age information: *Earth and Planetary Science Letters*, v. 214, p. 279-294.

Turner S. P., Hawkesworth C., van Calstren P., Heath E., Macdonald R., Black S., 1996, U-series isotopes and destructive plate margin magma genesis in the Lesser Antilles: *Earth and Planetary Science Letters*, v. 142, p. 191-207.

Turner S.P., 2002, On the time-scales of magmatism at island-arc volcanoes: *Philosophical Transactions of the Royal Society of America*, v. 360, p. 2853-2871.

Turner S.P. and Hawkesworth C., 1997, Constraints of flux rates and mantle dynamics beneath island arcs from Tonga-Kermadec lava geochemistry: *Nature*, v. 389, p. 568-573.

Unruh D.M. and Tatsumoto M., 1976, Lead isotopic compositions and uranium, thorium and lead concentrations in sediments and basalts from the Nazca plate, in Yeats R.S. et al., ed., *Initial Rep Deep Sea Drill Project 34*: Washington, US Govt Printing Office, p. 341-7.

Vigier N., Bourdon B., Joron J. L., Allégre C. J., 1999, U-decay series and trace element systematics in the 1978 eruption of Ardoukoba, Asal rift: timescales of magma crystallization: *Earth and Planetary Science Letters*, v. 174, p. 81-98.

Von Huene R., and Scholl DW., 1993, The return of sialic material to the mantle indicated by terrigenous material subducted at convergent margins: *Tectonophysics*, v. 219, p. 163-175.

Wasteneys H.A., Clark A.H., Farrar E., Langridge R.J., 1995, Grenvillian granulite-facies metamorphism in the Arequipa Massif, Peru: A Laurentia-Gondwana link: *Earth and Planetary Science Letters*, v. 132, p. 63-73.

Wegner W. and Ruprecht P., 2003, *Volcanic Geology and Valley History of Rio Chili Canyon, Arequipa (Southern Peru)*, Georg-August Universität Göttingen.

Whitman D., Isacks B., Kay S., 1996, Lithospheric structure and along-strike segmentation of the Central Andean Plateau: seismic Q, magmatism, flexure, topography and tectonics: *Tectonophysics*, v. 259, p. 29-40.

Widom E., Schmince H.-U., Gill J.B., 1992, Processes and timescales in the evolution of chemically zoned trachyte: Fogo A, Sao Miguel, Azores: *Contribution to Mineralogy and Petrology*, v. 111, p. 311-328.

Wilson M., 1989, *Igneous Petrogenesis. A global tectonic approach*.

Winter J.D., 2001, *An introduction to Igneous and Metamorphic Petrology*.

Workman RK. and Hart S.R., 2005, Major and trace element composition of the depleted MORB mantle (DMM): *Earth and Planetary Science Letters*, v. 231, p. 53-72.

Wörner G., Harmon R.S., Davidson J.D., Moorbath S., Turner T.L., McMillan N., Nye C., López-Escobar L., Moreno H., 1988, The Nevados de Payachata Volcanic Region 18°S/69°W, N.Chile I. Geological, geochemical and isotopic observations: *Bulletin of Volcanology*, v. 30, p. 287-303.

Wörner G., Lopez-Escobar L., Moorbath J., Horn S., Entenmann J., Harmon R.S., Davidson J.D., 1992, Variaciones Gequimicas, locales y regionales, en el arco volcánico Andino del Norte de Chile (17°30'-22°00'S). *revista Geológica de Chile.*, v. 19, p. 37-92.

Wörner G., Moorbath S., Harmon R.S., 1992, Andean cenozoic volcanics reflect basement isotopic domains: *Geology*, v. 20, p. 1103-1106.

Wörner G., Moorbath S., Entenmann J., Harmon R.S., Davidson J.D., López-Escobar L., 1994, Large geochemical variation along the central Arc of northern Chile (17.5-22°S), in S. E. Teutter K.J., Wigger P.J., (eds), ed., *Tectonics of the Southern Central Andes. Structure and evolution of an active continental margin*: Berlin, Springer, p. 77-92.

Wörner G., Hammerschmidt K., Hemjes-Kunst F., Lezaun J., Wilke H., 2000, Geochronology (⁴⁰Ar-³⁹Ar-, K-Ar-, and He-exposure-) ages of Cenozoic magmatic rocks from Northern

Chile(18°-22°S). Implications for magmatism and tectonic evolution of the central Andes, v. 27, p. 205-240.

Wörner G., Wegner W., Kiebalá A., Singer B., Heumann A., Kronz A., Hora J., (2004a), Evolution of Taapaca Volcano, N. Chile, evidence from major and trace elements, Sr-, Nd-, Pb-, and U-series isotopes, age dating and chemical zoning in sanidine megacrysts. IAVCEI conference Nov. 15-19, Pucon Chile.

York D., 1969, Least-squares fitting of a straight line: Canadian Journal of Physics, v. 44, p. 1079-1086.

Yu-Hsuan Chang, 2007, O-isotopes as Tracer for Assimilation Processes in Different Magmatic Regimes (El Misti, S.Peru and Taapaca, N.Chile), Georg-August Universität Göttingen.

Zellmer G. F., Hawkesworth C. J., Sparks R. S. J., Thomas L. E., Harford C., Loughlin S., 2003b, Geochemical evolution of the Soufriere Hills volcano, Monserrat, Lesser Antilles Volcanic Arc: Journal of Petrology, v. 44, p. 1349-1374.

Zellmer G.F., Annen C., Charlier B.L.A., George R.M.M., Turner S.P., Hawksworth C.J, 2005, Magma evolution and ascent at volcanic arcs: constraining petrogenetic processes through rates and chronologies: Journal of Volcanology and Geothermal Research, v. 140, p. 171-191.

Zellmer G.F., Blake S., Vance D., Hawkesworth C.J., Turner S., 1999, Plagioclase residence times at two island arc volcanoes (Kameni islands, Santorini, and Soufriere, St. Vincent) determined by Sr diffusion systematics: Contribution to Mineralogy and Petrology, v. 136, p. 345-357.

Acknowledgements

Many people helped and supported me directly and indirectly during the time of this PhD.

First I would like to thank my advisor Prof. Dr. Gerhard Wörner for giving me opportunity to make this PhD, for continuous help, for many fruitful discussions and patience.

I would like to thank Prof. Dr. B. Hansen for his interest in my work including his kind offer for corefferat.

Arnd Heumann I thank for introducing me to the TIMS machine and U-Th theory.

Great thanks I give to Gabi Mengel for help in the laboratory work and many very helpful suggestions in the laboratory but not only.

For support I thank sincerely Ilona Velder, who found a solution in trouble situation any time it was necessary.

I also thank to anyone from the Geochemistry Department: Dr. G. Hartman, Dr. K. Simon, I. Reuber, E. Schiffczyk, for help in preparations, analyses and discussions.

I sincerely wish to acknowledge collaboration and constructive discussions with Birgit Scheibner, Mirian Mamani, Andreas Kronz, Silke Triebold, Wenke Wegner, Philip Ruprecht, Janina Klaus, Svenja Rausch, Magda Banaszak, Yu-Hsuan Chang. I also thank Katja Janssen, Tania, Paweł Bardzik for their friendship and unusual experience, which made the time of this PhD very speciall.

Bardzo dziękuję Wojtkowi Dybalskiemu za niezastąpione dyskuje i pomoc szczególnie w końcowej fazie pisania tej pracy.

Największe podziękowania należą się moim Rodzicom oraz Asi, Domce i Arkowi. Jestem wdzięczna za to, że mimo odległości zawsze byli obecni, wspierali mnie i wierzyli we mnie. Na sam koniec dziękuję ciepło za wszystko Agnieszce, Grzegorzowi i Pawłowi.

Lebenslauf

Name Kiebala
Vorname Aneta
Geboren am 29-03-1977
In Rzeszów, Polen

Schulausbildung:

1984-1986 Grundschule Nr 4 Leżajsk, Polen
1986-1992 Grundschule, Boguchwała, Polen
1992-1996 St Konarski Gymnasium, Rzeszów, Polen
Abschluss: Allgemeine Hochschulreife-Abitur

Universität Ausbildung:

1996-2001 Jagiellonski Universität, Kraków, Polen
Fakultät Biologie und Geowissenschaften
Schwerpunkt: Geochemie und Mineralogie
Abschluss: Master of Science

October 2001 Beginn der Promotion an der Georg-August Universität Göttingen,
Deutschland
April 2008 Abschluss der vorliegenden Dissertation

Beruflicher Werdegang

October 2001-September 2007 Anstellung an der Georg-August Universität Göttingen als
Wissenschaftliche Mitarbeiterin

